بسم الله الرحمن الرحيم

BACHELOR OF SCIENCE IN ELECTRICAL AND ELECTRONIC ENGINEERING

STRAIN IMAGING TECHNIQUE BY 2D PLATE SMOOTHING SPLINE METHOD

A dissertation Submitted to the Department of Electrical and Electronic Engineering in Partial Fulfillment of the Requirements for the Degree of Bachelor of Science in Electrical and Electrical Engineering

SUBMITTED BY

MD. TARIQUL ISLAM (STUDENT ID: 082431)

MD. IMTIAZUL HAQUE (STUDENT ID: 082423)

SAFAYAT BIN HAKIM (STUDENT ID: 082401)

Department of Electrical and Electronic Engineering
Islamic University of Technology (IUT)
The Organization of the Islamic Cooperation (OIC)
Board Bazar, Gazipur-1704, Dhaka, Bangladesh
October, 2012

BACHELOR OF SCIENCE IN ELECTRICAL AND ELECTRONIC ENGINEERING

STRAIN IMAGING TECHNIQUE BY 2D PLATE SMOOTHING SPLINE METHOD

A dissertation Submitted to the Department of Electrical and Electronic Engineering in Partial Fulfillment of the Requirements for the Degree of Bachelor of Science in Electrical and Electrical Engineering

SUBMITTED BY

MD. TARIQUL ISLAM (STUDENT ID: 082431)

MD. IMTIAZUL HAQUE (STUDENT ID: 082423)

SAFAYAT BIN HAKIM (STUDENT ID: 082401)

SUPERVISOR

DR. KAZI KHAIRUL ISLAM

PROFESSOR

Department of Electrical and Electronic Engineering
Islamic University of Technology (IUT)
The Organization of the Islamic Cooperation (OIC)
Board Bazar, Gazipur-1704, Dhaka, Bangladesh

October, 2012

CERTIFICATE OF APPROVAL

The thesis titled "***Strain imaging technique by 2D plate smoothing spline method***" submitted by Md. Tariqul Islam, Md. Imtiazul Haque and Safayat Bin Hakim bearing Student No. 082431, 082423 & 082401 respectively of Academic Year 2011-2012 has been found as satisfactory and accepted as partial fulfillment of the requirement for the degree of Bachelor of Science in Electrical and Electronic Engineering on 16th October, 2012.

BOARD OF EXAMINERS

1. **Dr. Kazi Khairul Islam** — Supervisor
   Professor
   Department of Electrical and Electronic Engineering
   Islamic University of Technology (IUT)
   Board Bazar, Gazipur-1704, Bangladesh

2. **Dr. Md. Shahid Ullah** — Member
   Professor and Head
   Department of Electrical and Electronic Engineering
   Islamic University of Technology (IUT)
   Board Bazar, Gazipur-1704
   Dhaka, Bangladesh

3. **Dr. Md. Ashraful Haque** — Member
   Professor
   Department of Electrical and Electronic Engineering
   Islamic University of Technology (IUT)
   Board Bazar, Gazipur-1704
   Dhaka, Bangladesh

DECLARATION OF CANDIDATE

We declare that the work in this dissertation was carried out in accordance with the Regulations of the Islamic University of Technology (IUT). The work is original except where indicated by special reference in the text and no part of the dissertation has been submitted for any other degree. The dissertation has not been presented to any other University for examination either in the Bangladesh or overseas. Any views expressed in the dissertation are those of the author.

Md. Tariqul Islam
10/10/2012

(Signature & Date)

1. Md. Tariqul Islam
Student ID: 082431
Academic Year: 2011-2012

Md. Imtiazul Haque
10/10/2012

(Signature & Date)

2. Md. Imtiazul Haque
Student ID: 082423
Academic Year: 2011-2012

Safayat Hakim
10/10/2012

(Signature & Date)

3. Safayat Bin Haki
Student ID: 0824
Academic Year: 2011

DEDICATION

TO OUR BELOVED PARENTS

WHO ALWAYS PICKED US UP ON TIME

AND ENCOURAGED US TO CARRY ON OUR JOURNEY

TOWARDS THE VAST REALM OF KNOWLEDGE

ACKNOWLEDGEMENTS

First and foremost, our utmost gratitude to the omnipresent ALLAH, for answering our prayers for giving us the strength to plod on despite our constitution wanting to give up and throw in the towel, thank you so much ALLAH for giving us ability to overcome all the obstacles in the completion of this dissertation work! This thesis has been benefitted from the guidance of, and discussions with Dr. Kazi Khairul Islam in the Department of EEE at Islamic University of Technology, and from the support and enthusiasm of Dr. S. K. Alam in the Riverside Research Institute, NY, USA. We are indebted to both supervisors, as their discussions and continual support provided much encouragement over the course of this work. We are also thankful to Riverside Research Institute, NY, USA for providing various in vitro specimens and phantom simulation data required the analysis. We are also grateful to Dr. Md. Shahid Ullah, Professor & Head of the Department of EEE at Islamic University of Technology for his kind support and guidance.

Last but not the least; we are indebted to our parents for supporting us throughout all our studies at University, and also to our friends, relatives and well-wishers who have always supported us in every stage of our life.

TECHNICAL ABSTRACT

Medical imaging is vital to modern clinical practice, enabling clinicians to examine tissues inside the human body non-invasively. Its value depends on accuracy, resolution, and the imaged property (e.g., density). Various new scanning techniques are aimed at producing elasticity images related to mechanical properties (e.g., stiffness) to which conventional forms of ultrasound; X-ray and magnetic resonance imaging are insensitive. Elastography, palpography or strain imaging has been under development for almost two decades. Elasticity images are produced by estimating and analyzing quasi-static deformations that occur between the acquisitions of multiple ultrasound images. Likely applications include improved diagnosis of breast cancer (which often presents as a stiff lump), but the technique can be unreliable and difficult to perform. Practical imaging is based on freehand scanning, i.e., the ultrasound probe is moved manually over the surface of the tissue. This requires that elasticity images are calculated fast to provide a live display, and the images need to present meaningful elasticity data despite the poorly controlled properties of the deformations.

Robust strain estimation is important in elastography. Strain estimates derived from each estimated deformation provide a form of elasticity image. A method is devised for predicting the accuracy of each strain estimate, which is first applied for dynamic resolution selection: parameters are automatically modulated to produce images with fixed precision at variable resolution. However, a high signal-to-noise ratio (SNR_e) and contrast-to-noise ratio (CNR_e) are sometimes attained by sacrificing resolution. Currently several strain estimation algorithms have been developed e.g. Global uniform stretching (with gradient), Global uniform stretching (with least squares), Adaptive stretching etc. Amongst these Spline based strain estimation technique by Alam et al. is showing better performance than the other conventional strain estimators. This least-squares-based smoothing spline strain estimator can produce elastograms with high SNR_e and CNR_e without significant loss of resolution. This technique based on smoothing curve to a set of noisy observations, using a spline function on one dimensional data is developed on one dimensional data. Our target is to use 2D data and apply thin plate smoothing spline method to get better elastograms. In this thesis, we will show the performance parameters of 2D plate spline based elastograms such as SNR_e & CNR_e with the variation of strain & weight. Here, we will

also show comparison among the performance of various strain estimators to visualize the fact that Spline based strain estimator is more effective than the others.

Key words: Medical Imaging, Ultrasound, Elastography, Elasticity Imaging, Strain Imaging, RF Echo Signal, Spline, Phantom, Elastographic Signal-to-Noise Ratio (SNR_e), Elastographic Contrast-to-Noise Ratio (CNR_e)

TABLE OF CONTENTS

GLOSSARY

1D/2D/3D	"one-/two-/three-dimensions", "one-/two-/three dimensional"
ultrasound	pressure waves at high frequencies (≫ 20 kHz)
ultrasonic	relating to ultrasound
US	ultrasound system
transducer	any device converting signals between different physical bases (e.g. from ultrasonic pressure waves to electrical signals)
RF	radio frequency
insonification	transmission of ultrasound (into a region of tissue)
anechoic	not echogenic; does not give rise to echoes
hypoechoic	relatively weakly echogenic
isotropic	the same in all directions; direction-independent
anisotropic	not isotropic; direction-dependent
orthotropic	(anisotropic) having different properties defined along orthogonal directions
echogenic	gives rise to echo
echogenicity	the strength with which ultrasound is reflected by a region of tissue containing scatterers
heterogeneous	containing multiple regions with different properties
inhomogeneities	locations where physical properties change
scatters	small inhomogeneities that reflect ultrasound
ARFI	acoustic radiation force impulse
TDE	time delay estimation
artifact	a misleading image feature
ASE	adaptive strain estimation
B- Scan	a conventional ultrasound image; a 2D image showing the amplitude/ envelope of ultrasound signals
center frequency	the centroid of the frequency spectrum (of an ultrasound signal)
decorrelate	becomes less similar
decorrelation	reduced similarity (between pre- and post-deformation ultrasound signals)
displacements	change in position

strain	measures of deformation excluding translation and rotation based on spatial derivatives of displacement
SF	strain filter
speckle	random-looking, fine-grained amplitude variation caused by interference between signals from closely-spaced sources
in vivo	(scanning) of laboratory samples
in vitro	(scanning) of tissue in a living body
ex vivo	(scanning) of excised tissue
phantom	an object fabricated for testing ultrasound scanning
ROI	region of interest
FEM	finite element modeling
MRI	magnetic resonance imaging
real time	(computations) with real-world time constraints (such as needing to process ultrasound data as they are acquired)
off-line	not real time
PW	pulsed wave
HIFU	high intensity focused ultrasound
SNR_e	elastographic signal-to-noise ratio
CNR_e	elastographic contrast-to-noise ratio

LIST OF FIGURES

CHAPTER I

INTRODUCTION TO ULTRASOUND BASED ELASTICITY IMAGING

1.1 INTRODUCTION

Manual palpation is a universal technique which is being used over the centuries. Variation of tissue stiffness actually indicated towards the existence of abnormality or the symptoms of disease such as cancer. The idea that mechanical properties are related to pathology is not new: clinicians have employed manual palpation to feel for stiff lumps as long ago as 400 BC [1]. Even today palpation is the preliminary tool which is practiced by the physician to detect symptoms or disease [2]. Palpation is a routine physical examination where the clinician qualitatively assesses low-frequency tissue stiffness. During palpation, lumps that are discrete and differ from the surrounding tissue are identified for further diagnosis. Though these lumps may dislocate or feel fixed within the tissue, subtle finding are much more difficult to interpret. Specifically, in many tumor cases and despite the difference in stiffness, the small size of a pathological lesion and/or its non-superficial location impedes detection and evaluation by palpation.

Mechanical testing of the human tissues has drawbacks and most cases are not practical. Sometimes these methods go through some rigorous steps like testing the specimens under physical load conditions. A well-established method which can be used as an example in this case is biopsy. Usually these tests require cutting the specimens from larger tissues and from certain locations. It is an issue of concern that the mechanical tests are destructive to tissues and they only give information about that small portion not the whole organ [3]. Different imaging modalities (Ultrasound, Computed Tomography, and Magnetic Resonance Imaging) are available to detect tissue characteristics but diagnostic imaging does not provide any information about the tissue elastic properties.

The mechanical properties of soft tissue stiffness are largely dependent on composition (i.e., adipose, fibrin, collagen etc.) and their relative organization at both the microscopic and macroscopic scale [4]. Specifically, Krouskop et al. [5] demonstrated experimentally that glandular and fibrous tissues in normal breast tissue samples were stiffer than that of adipose tissue by approximately 8 and 20 dB, respectively. Therefore, it is this mechanical behavior dynamic range exhibited by these respective tissue building

blocks that constitutes the foundation and heterogeneity of normal tissue elasticity. It is expected that imaging parameters related to tissue stiffness will provide new information that is associated with tissue structure and/or pathology.

Recent improvements in imaging technology have allowed accurate, high resolution, in some cases quantitative visualization of the stiffness of relatively deep-lying structures. The rapid development of this technique has spawned clinical trials in many anatomical areas. These indicate that elastograms may differentiate between benign and malignant lesions, and distinguish between different types of malignancy, in some cases better than conventional B-mode ultrasound images [6].

1.2 ULTRASOUND

The use of ultrasound in the modern-day medical clinic has found a solid niche among the various methods for imaging the body. Ultrasound is defined as acoustic waves with frequencies above those that can detected by the ear, from about 20 kHz to several hundred MHz [7].The waves are generated by small acoustic transducers, which that are electrically driven and typically placed on the skin. The waves propagate into the tissue of the body where a portion is reflected from the myriad of interfaces between tissues with different acoustic properties.

1.3 MEDICAL ULTRASOUND

Ultrasound is widely used in several medical applications. It is possible to perform both diagnosis and therapeutic procedures, using ultrasound to guide interventional procedures (for instance biopsies or drainage of fluid collections). Sonographers are medical professionals who perform scans which are then typically interpreted by radiologists, physicians who specialize in the application and interpretation of a wide variety of medical imaging modalities, or by cardiologists in the case of cardiac ultrasonography (echocardiography). Sonographers typically use a hand-held probe (called a transducer) that is placed directly on and moved over the patient. Typical diagnostic sonographic scanners operate in the frequency range of 2 to 18 MHz, though frequencies up to 50–100 MHz have been used experimentally in a technique known as biomicroscopy in special regions, such as the anterior chamber of the eye. Ultrasound sources may be used to generate regional heating and mechanical changes in biological tissue, e.g. in occupational therapy, physical therapy and cancer treatment. However the use of ultrasound in the treatment of musculoskeletal conditions has fallen out of favor. Increasingly, clinicians (physicians and other healthcare professionals who provide direct patient care) are using ultrasound in

their office and hospital practices, for efficient, low-cost, dynamic diagnostic imaging that facilitates treatment planning while avoiding any radiation exposure.

Sonography (Ultrasound imaging) is effective for imaging soft tissues of the body. A detailed brief about ultrasound imaging will be given in the following chapters. Superficial structures such as muscles, tendons, testes, breast, thyroid and parathyroid glands, and the neonatal brain are imaged at a higher frequency (7–18 MHz), which provides better axial and lateral resolution. Deeper structures such as liver and kidney are imaged at a lower frequency 1–6 MHz with lower axial and lateral resolution but greater penetration.

1.4 SEVERAL MEDICAL IMAGING MODALITIES

Among the wide array of technologies in modern medicine, medical imaging is a major advancement. The ability to take pictures of the human body has many useful clinical applications. Different modalities of medical imaging have emerged over the years, each with their own advantages and disadvantages. For any patient who needs his or her body visualized, doctors select the most appropriate imaging studies in order to deliver the best care. Major medical imaging modalities are discussed below:

1.4.1 PROJECTION X-RAY (RADIOGRAPHY)

X-rays are waves that have a relatively high frequency along the electromagnetic spectrum. They are absorbed or transmitted by different body tissues in varying amounts, producing different shades of black and white on an x-ray image. In general, bone appears white, soft tissue appears gray, and air appears black [8].

The basic type of x-ray imaging is plain radiography. This involves an x-ray machine aimed at the patient's body with a recording plate positioned behind the region of interest. Once the machine delivers its radiation, the image is captured on the plate. This allows a physician to assess the bones for fractures, the abdomen for bowel obstruction, and the breasts for signs of cancer (mammography), among other applications.

Certain x-ray studies involve contrast dye to enhance the image, such as visualization of certain arteries (angiography) and the spinal cord (myelography) [8]. In such cases, x-ray is delivered as fluoroscopy, constantly delivering radiation to produce a real-time set of images similar to a video. This ensures that an optimal image can be taken.

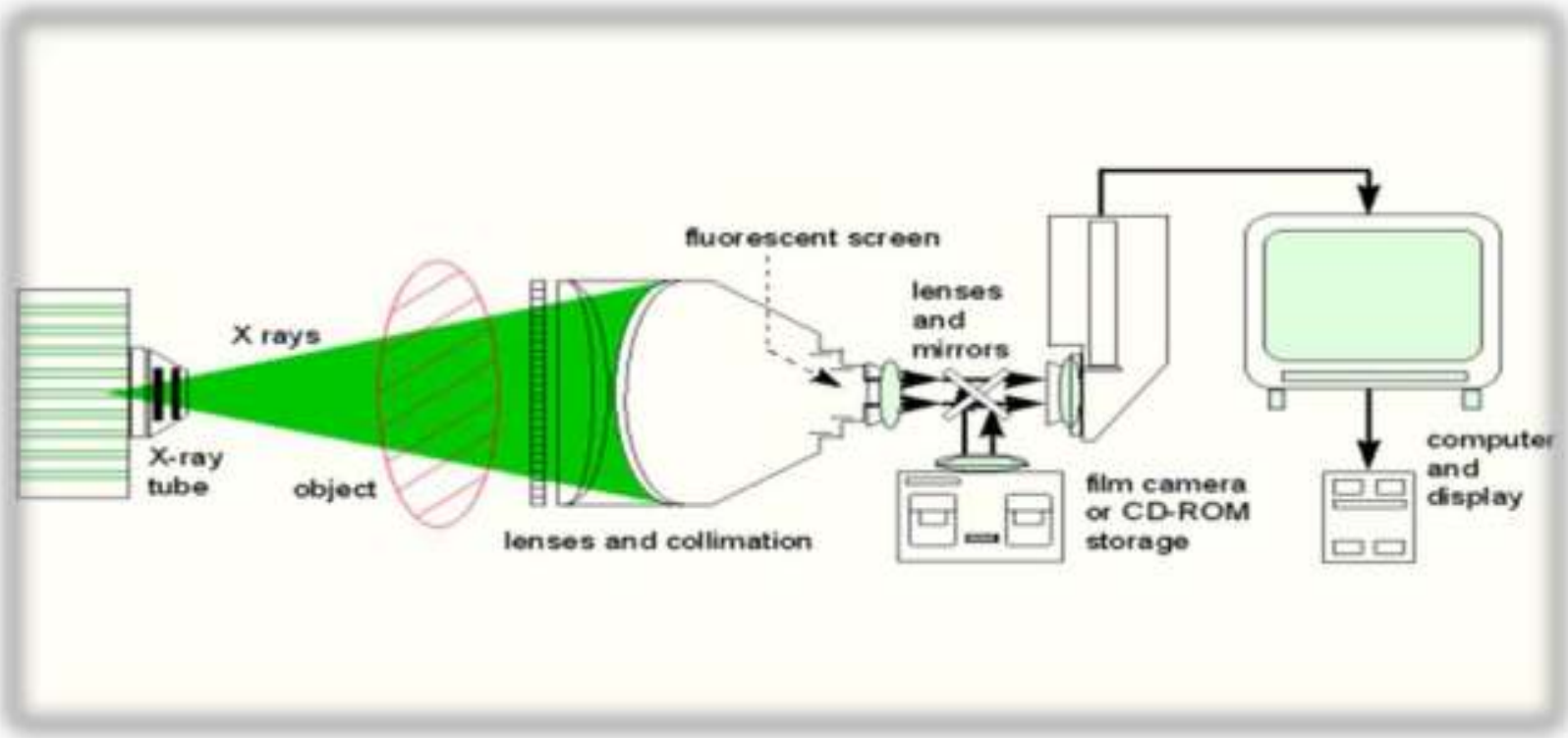

Figure 1.1: Principle of an X-ray system with image intensifier.

1.4.2 X-RAY COMPUTED TOMOGRAPHY (CT)

X-rays are also used in computed tomography (CT). This type of study involves a patient who lies on a sliding table of a CT scanner and moves slowly through a circular rim where x-rays are delivered in multiple directions. Collimated X-ray beam is used to image a patient in thin sections (thickness depends upon body part imaged) [9]. Detectors surround patient. A nearby computer combines the data of each x-ray shot and forms two-dimensional slices of the patient's body and generates image based on different densities available after beam has traversed patient. CT scans allow clinicians to assess parts of the body that are otherwise not visible on plain radiography.

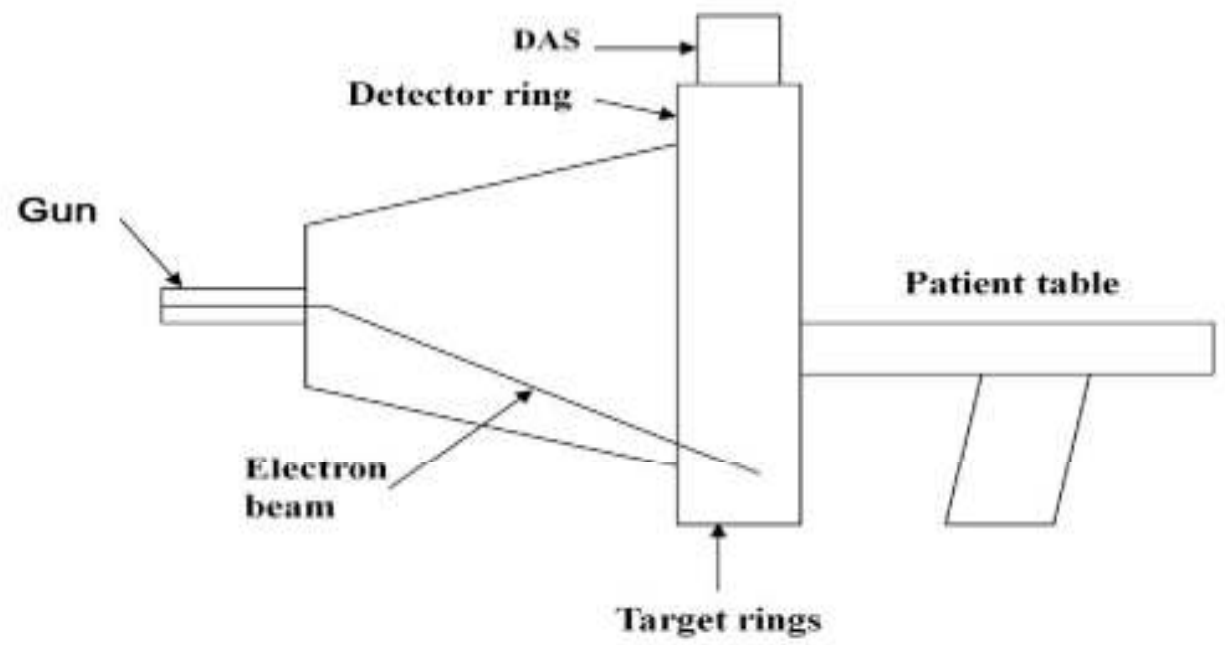

Figure 1.2: Fifth generation CT (Image data are acquired in as little as 50 msec).

1.4.3 ULTRASOUND IMAGING

Ultrasound imaging has gained popularity over the last half century for obtaining diagnostic medical images due to its safety and non-invasiveness. Three primary factors can be attributed to this development [10]. First of all, ultrasound imaging provides non-invasive visualization and identification of internal organs and soft tissue structures. Secondly, the biological effects of ultrasound radiation have been deemed negligible for the energy levels utilized in conventional examinations. Thirdly, it is cost-effective which is always considered as an attractive parameter in today's medical imaging network for both the patient and clinician alike. Basically, these factors have led ultrasound medical imaging to be adopted widely in clinical settings.

Before utilizing any medical imaging modality, a signal must be propagated through the body from an external source. As soon as the inherent biological information is encoded within this propagating signal, it is measured and recorded, and this information is analyzed and displayed for visualization. The propagating signals are actually pressure waves which are produced with the help of piezoelectric materials that is transducers, which essentially convert an electrical signal into its equivalent mechanical vibration/oscillation or vice-versa.

A mechanical vibration is induced in a piezoelectric element (or set of elements) by applying an electrical pulse signal. That vibration is conducted across the transducer-tissue interface (given proper acoustical coupling) and eventually takes the form of an ultrasonic pulse while penetrating through the tissue elements. A fraction of the incident pulses energy is redirected in the form of an echo signal because of the local spatial fluctuations in tissue acoustical impedance while that pulse propagates in tissue. The impingement of the backscattered echoes on the piezoelectric elements of the transducer yield mechanical forces which generate deformations and that deformations are converted into proportional voltage signals by the transducer. The transit time of the echo signals are proportional to the distance traveled (assuming a constant speed of sound). Therefore, the transit time is measured and the echo amplitudes are recorded as a function of depth and are commonly referred to as an A-line (where 'A' stands for amplitude).For every transducer element (or combination of elements), these A-lines are sequentially recorded and once this is done, a sonogram is generated which is nothing but a 2D B-mode (where 'B' stands for brightness) gray-scale image (Figure 1.3).

Figure 1.3: Sonogram of a typical human liver, which depicts the relative homogenous echo intensity within the parenchyma.

The frequency of the propagating pulse and the resolution of an ultrasound image are directly related to each other. Typically, ultrasound imaging systems operate at frequencies ranging from 3 to 15 MHz from a clinical point of view. Utilization of high frequency transducer results in better and increased resolution of the sonogram (both axially and laterally) but at the same time, propagation depth is limited by the attenuation effects as these signal types are more vulnerable to attenuation. Thus, the fundamental tradeoff encountered in ultrasonic imaging: resolution versus penetration depth.

In an Overall point of view, ultrasound is an attractive imaging modality for the reasons mentioned above, and due to the relative ease at which engineering modifications can be carried out and assessed; it is indeed a suitable platform for elasticity-related research initiatives.

1.4.4 MAGNETIC RESONANCE IMAGING (MRI)

Magnetic resonance imaging (MRI), unlike x-ray imaging, does not use radiation. Instead, MRI works based on magnetic waves and the spin of protons. MRI exploits the existence of induced nuclear magnetism in the patient. Magnets with an odd number of photons or neutrons possess a weak but observable nuclear magnetic moment. Most commonly photons (H) are imaged, although (13C, Phosphorous (P) sodium (Na) and Fluorine (F) are also of significant interest. The nuclear moments are normally randomly oriented, but they align when placed in a strong magnetic field (typically 0.2-1.5 T). The NMR signal from a human is due predominantly to water protons. Since these protons exist in identical magnetic environments, they all resonate at the same frequency. Hence the NMR signal is simply proportional to the volume of the water. The key innovation for MRI is to impose spatial variation

on the magnetic field to distinguish spins by their location. Applying a magnetic field gradient causes each region of the volume to oscillate at a distinct frequency. The primary contrast mechanisms exploit relaxation of the magnetization is T_1 and T_2 [11].

Spin-lattice relaxation T_1: The exponential rate constant describing the decay of the z component of magnetization towards the equilibrium magnetization. Typical values in the body are between 300 and 3000 msec.

Spin-Spin relaxation T_2: The exponential rate contrast describing the decay of the transverse components of magnetization (M_x and M_y).

Compared with CT, images on MRI have more detail, which can be useful for analyzing soft tissue that is harder to look at on CT. MR Images provide excellent contrast between various forms of soft tissues. For patients who have no ferromagnetic foreign bodies within them, MRI scanning appears to be perfectly safe and can be repeated as often as necessary without danger. The NMR signal is also not blocked by air like US and there is no need for radioactive tracers as in the case of nuclear medicine scanning. Typical imaging studies range from 1 to 10 minutes but new fast imaging techniques acquire images in less than 50 msec.

1.4.5 HARMONIC IMAGING

Harmonic imaging can involve injection of contrast agent with the appropriate micro-bubbles and then scanning the region of interest at a given transmit frequency and tuning the receiver to listen at twice that value. For example, transmit at 3 MHz and receive at 6 MHz. The result is that the backscattered echoes from resonant bubbles contain harmonics.

Harmonic imaging can be performed in B mode and Doppler mode [12]. Not all micro-bubble contrast agents are suitable for harmonic imaging – the bubble size is important, as is the surrounding shell, which must be flexible to allow resonance to occur.

The strongest echoes recorded will be those from the regions where there is contrast like the blood vessels. Echoes from the tissues surrounding the vessels, being composed of the fundamental frequency rather than the second harmonic, produce a much lower response in the receiver and therefore have a reduced brightness in the display (in comparison to their appearance in a standard B mode imaging)

The returning increased frequency harmonic signal has to travel one direction only, towards the probe. The advantages of high frequency imaging and the one-way travel effect are reduced reverberation, beam aberration, and side lobes plus improved resolution and cystic clearing [13].

- Improved axial resolution due to higher frequencies
- Better lateral resolution due to narrower beams
- Decreased noise from side lobes improves signal-to-noise ratios and reduces artifacts
- Improved range penetration
- Better contrast resolution
- Harmonic imaging can be particularly useful for depicting cystic lesions and those containing echogenic tissues such as fat, calcium, or air
- In patients with a body mass index of 30 or more, harmonic imaging can lead to better lesion visibility and confidence of diagnosis
- Improved imaging of the liver, gallbladder, pancreas, pelvis, kidneys, and retroperitoneal lymph nodes
- Additionally patients who were imaged poorly with fundamental frequency ultrasound could be examined by second harmonic imaging.

Disadvantage of less penetration, more shadowing and could confuse with respect to possible calculi.

1.4.6 NUCLEAR IMAGING

Nuclear imaging looks at physiological processes rather than at anatomical structures. Nuclear imaging is unique in that the means of visualization are not external waves delivered to the body. Rather, electromagnetic waves are emitted from within. In nuclear imaging, short-lived radiopharmaceuticals (radioactive drugs that emit gamma rays and that are attracted to the organ of interest) are injected into a patient's bloodstream (in amounts of picomolar concentrations thus not having any effect on the process being studied) [14]. The half-life of these materials is between few minutes to weeks. The time course of the process being studied and the radiation dose to the target are considered. The nuclear camera then, in effect, takes a time-exposure "photograph" of the pharmaceutical as it enters and concentrates in these tissues or organs. By tracing this blood flow activity, the resulting nuclear medicine image tells physicians about the biological activity of the organ or the vascular system that nourishes it.

This type of imaging is also unique in that nuclear medicine physicians, not radiologists, are the ones who interpret nuclear imaging studies. Nuclear Medicine has a wide variety of uses, including the diagnosis of cancer, studying heart disease, circulatory problems, detecting kidney malfunction, activity of the thyroid gland and other abnormalities in veins, tissues and organs [15].

1.4.7 REAL TIME STRAIN IMAGING

Strain Imaging (SI), also called "tactile imaging", "stress imaging", or "computerized palpation" is a new modality of medical diagnostics that is based on visualizing the sense of touch. In real time SI,

the internal structures of an organ are visualized by measuring the pattern of mechanical stresses on its surface. SI closely mimics manual palpation, since the ultrasonic probe with a pressure sensor array mounted on its face acts similar to human fingers during clinical examination, slightly compressing soft tissue by the probe i.e. different regions with different hardness are compressed differently the local strain is computed and displayed real time strain imaging computes and displays the local strain with more than 30 frames per second the strain is computed by the determination of local displacements between two consecutive images. Mechanical properties of tissues, i.e. Young's modulus and viscosity, are highly sensitive to tissue structural changes accompanying various physiological and pathological processes [16]. A change in Young's modulus of tissue during the development of a tumor could reach thousands of percent.

1.5 ULTRASOUNDBASED ELASTICITY IMAGING

The growing interest in tissue elasticity imaging alternately known as Elastography, has been on the rise over the last two decades and many research initiatives have been devoted in this regard. Among those, some methods have focused on quantitatively measuring physical parameters, such as Young's moduli, whereas others have attempted to render an image that qualitatively relates to the tissue stiffness distribution. The development of new imaging methodologies and approaches for estimating the elastic properties of soft tissue in order to differentiate between normal and morbid tissue structures. An important distinction of ultrasound-based elasticity imaging systems is that tissue echogenicity and stiffness, assigned to the Bulk and shear moduli distributions, respectively, are disjoint. Figure 1.4 illustrates the variation of the shear and bulk moduli for various materials and body tissues [17].

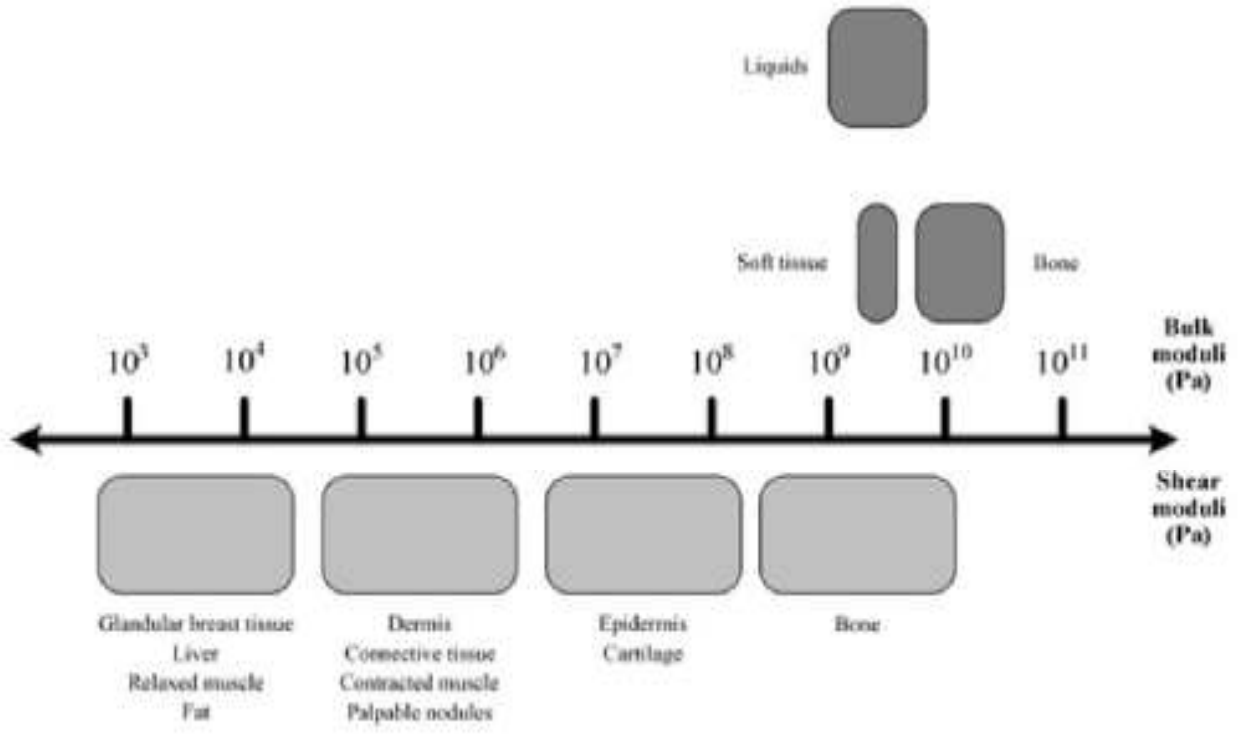

Figure 1.4: Summary of the relative shear and bulk moduli variation for several materials and biological tissue types (adapted from Sarvazyan et al. 1998).

It should be noted from the figure that the Bulk moduli show limited dynamic range whereas Shear moduli exhibit wide dynamic range, which spans several orders of magnitude for the various biological materials and tissues. From Fig. 1.4, it can be deduced that though there may exist a relatively limited spatial fluctuation in the underlying Bulk moduli (which determines ultrasonic wave propagation and scattering) for given tissue volume, the shear modulus (and thus the elastic properties) may exhibit considerably significant spatial fluctuations. It is this large dynamic range in the elastic properties that motivates clinicians to use palpation for tissue analysis and forces research into elasticity imaging.

All the approaches and methodologies which exist today for ultrasound based tissue elasticity imaging, they share the following basic elements:

1. Tissue is perturbed by an external mechanical force.
2. Local tissue motion is measured
3. Some elasticity parameters are measured.

Direct estimation and imaging of tissue elasticity properties is beyond the capability of any known modality. Therefore, a prerequisite condition for all tissue elasticity imaging is to employ a mechanical force to stimulate tissue motion. Moreover, the mechanical sources can be classified based on the spatial characteristics of the tissue excitation. In External methods, a compressive is applied on the skin surface or on the subcutaneous tissue surface to distort the tissue structures. These external sources can be further classified by the temporal characteristics of the mechanical source: static (or quasi-static) methods and dynamic methods. On the contrary, internal methods employ mechanical force internally and directly on the tissue region of interest. These mechanical sources can either be biological in nature (such as cardiovascular pulsation) or manually induced using approaches such as the radiation force of focused ultrasound.

1.6 ELASTICITY IMAGING: AN ALTERNATE APPROACH OF BIOPSY

The internal complex system of a human body produces harmless abnormal growths or swelling under skin which is simply known as "tumor". A tumor doesn't necessarily indicate any fear unless it is not malignant i.e. benign, though most of our hearts skips a beat just by hearing the name "tumor". But if the tumor turns out to be a malignant one, then it is cancerous and tending to invade the normal surrounding tissue. So when it seems to be a breast lump and becomes very difficult for a doctor to palpate its harmless, the next available option is biopsy. Actually biopsy is a procedure to extract the

tissue from a questionable tumor and determine whether the tumor is benign or malignant. It is an invasive process and there's a lot of anxiety involved under the best of circumstances. It also causes considerable stress to patients. The overall cost for this procedure may vary between $2,000 and $3,000 depending on the how much of the tissue is extracted and the method adopted to extract the tissue [18]. Overall, it's a lengthy process where several weeks may take for the pathological report to come back. A newer ongoing study in the field of biomedical engineering shows that the twist on the traditional ultrasound technique of using RF signals and mechanical properties of tissue i.e. Elastography is proving valuable to create an image of what's going on inside of a human body, can distinguish if a growth is malignant or benign instantaneously. In this paper, we have already discussed that harmless tumors are a lot softer than cancerous tumors. In the case of a breast tumor, a benign one is anywhere from 5 to 100 times more elastic than a malignant one. By adopting the advantage of this characteristic, elastography quickly diagnoses breast cancer without the use of a needle or a scalpel. It's kind of alike mechanical palpation guided to the next stage: tremendously dependable, digital, and unaffected by the depth of the tumor. As part of the ongoing research, 179 patients underwent both the process of biopsy and elastography. The research team got 184 elastograms and performed biopsies on all solid lesions. Of 134 biopsies, 56 brought out as cancerous ones [19]. Elastography decently distinguished 98 percent of lesions that had malignant findings on biopsy, and 82 percent of lesions that turned out to be benign. Again, in another analysis of 115 breast masses that were urged for biopsy, ultrasound elastography was 79% precise in identifying the cancerous ones. Elastography is completely a non-invasive procedure and its cost may be $100 to $200 [20]. Also, since it's possible to analyze the results on the spot for the doctor, diagnosing a tumor as malignant or benign can happen in one visit. And there's no need to take another appointment for a patient to get the results after a week or two of sleepless nights. So, the employment of elastography as an appurtenant to routine breast ultrasound safely lessens the number of biopsies of benign lesions and offers the potential to map tumors more incisively.

1.7 REVIEW OF PREVIOUS WORK

Extensive research in the elastography field over the past twenty years has shown applications in tissue mimicking phantoms as well as biological tissues. Activity in the field utilizes a variety of techniques to validate the methods clinically. Elastography in general can be divided into Ultrasound Elastography (USE) and MR Elastography (MRE), each of which uses different methods of applying the stress.

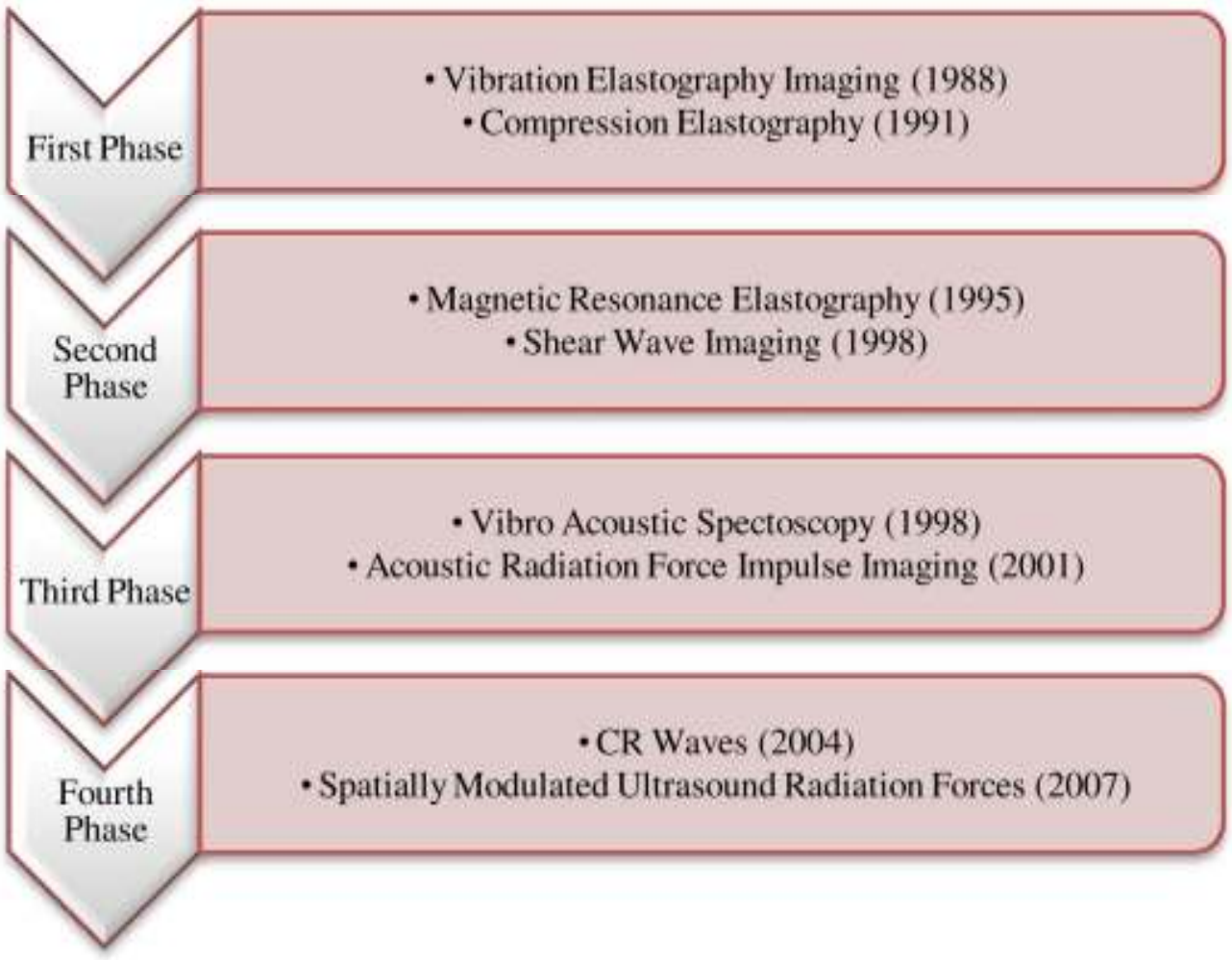

Figure 1.5: Twenty year timeline of the evolution of elastographic imaging, showing some of the major categories of approaches.

Behavior of the human body surface subjected to sound fields or mechanical vibration was first studied by Oestreicher et al. [21]. Dickinson et al. used the correlation coefficient between successive A-scans to measure the amplitude and frequency of tissue motion [22]. They set up a correlation parameter to measure the changes of the interrogated region between two successive A-scans. Birnholz et al. tried to qualitatively determine the stiffness of fetal lung by evaluating ultrasound B-scans, where one can see the compression of lung due to cardiac pulsations [23]. Krouskop et al (1987) reported one of the first quantitative measurements of tissue elasticity using gated pulsed Doppler [24]. A single A-line pulsed Doppler instrument was used in their experiments to measure actual tissue flow at points of interest under external vibrations.

Dr. Robert Lerner, a radiologist at the University of Rochester, was intrigued by the ability of palpation to detect some prostate cancers that were undetectable by ultrasound. After some experimentation, Lerner et al. developed and presented preliminary work on vibration amplitude sonoelastography (sonoelasticity imaging) [25].

Compression elastography introduced in 1991 by Ophir et al compression elastography utilizes a comparison of ultrasound B-scan RF information from tissue before and after a modest compression [26]. The concept can be explained by invoking the stress–strain relations under a simple uniaxial (one dimensional) displacement. Compression elastography thus produces images of relative strain which are

simple to interpret so long as the applied stress is relatively uniform. The advantage of the technique is that the ultrasound scanning transducer, handheld in most applications, can be used to produce a localized compression near the region of interest in the breast and other applications, particularly in more superficial targets of interest.

In USE, a shear wave is generated by the radiation force produced by an amplitude modulated beam of focused ultrasound. These waves are detected with Ultrasound and acquired data are used to calculate the elastic properties of tissues. A detailed assessment of the progress and challenges in the ultrasound elastography field has been discussed in a paper presented by Parker et al. [27].

MRI (Magnetic Resonance Imaging) is more expensive than diagnostic ultrasound, but it can measure all three spatial components of the induced tissue displacement with high accuracy and precision, and thus is more suited for quantitative elastography. In MRE the induced tissue motion is measured using either the saturation tagging or the phase-contrast method [28]. MRE visualizes the mechanical properties within soft tissues by employing either a quasi-static or dynamic mechanical source MR Elastography (MRE) is based on the phase contrast method developed for imaging blood flow and diffusion in MRI [29, 30]. The first MRE method was presented by Lewa [31] where the MR phase changes were used to measure the viscoelastic properties [32]. Plewes and colleagues proposed an MRE method that utilizes a phase-contrast imaging sequence to estimate the spatial strain incurred when the tissue or phantom under investigation is deformed quasi-statically. Muthupillai et al proposed a dynamic approach to MRE based on the phase contrast imaging method.

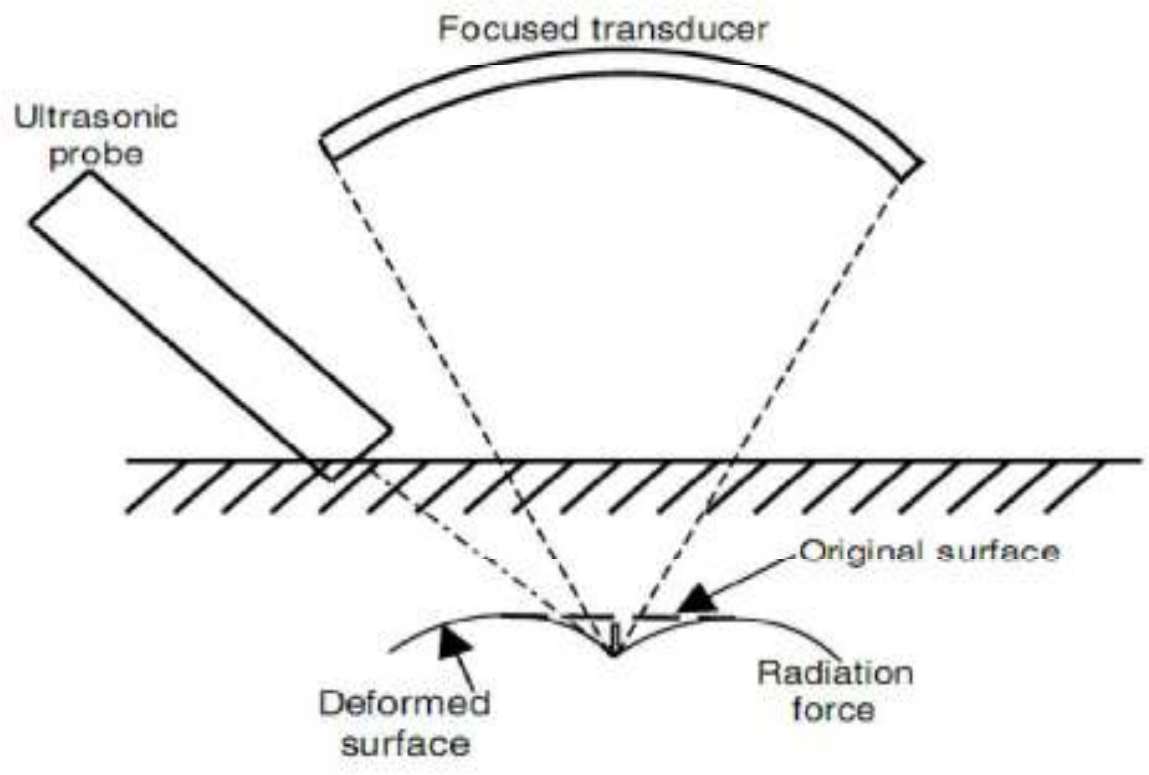

Fig: 1.6 Schematic representation of the early work by Sugimoto to measure the displacement of a specimen's surface under radiation force

As an ultrasound beam propagates through an absorbing medium, the energy transfer results in a second-order effect that produces a force proportional to local intensity and absorption, which is termed radiation force. Sugimoto et al devised laboratory system that applied radiation force to a tissue sample, while measuring the resulting displacement with an ultrasonic probe. The displacement versus time relaxation curve was fit to a multi-exponential function as a model of the mechanical properties.

The use of acoustic radiation force (ARF) as an imaging modality was introduced by Nightingale et al. [33]. The advantages of ARFI (and the other radiation force based techniques) stem from the fact that anywhere an imaging system can focus; a pushing pulse of radiation force can be applied. Optical systems can be configured to track tissue motion in real time. In particular, optical coherence tomography (OCT) is directly analogous to ultrasound imaging in that a speckle image of a 2D plane can be produced at high frame rates. Compression elastography by OCT was introduced by Schmitt using a free-space Michelson interferometer and utilizing speckle tracking to determine displacements and then calculate strain [34]. In thermo-acoustic imaging, a short impulse of electromagnetic energy or laser energy is distributed throughout tissue, and differential absorption creates a thermal expansion waves which are detected and utilized in a reconstruction.

1.8 CURRENT RESEARCH IN ELASTOGRAPHY AND ITS FUTURE

Current research in Elasticity imaging is focusing mainly to make it more practicable in real time. The emphasis of much of the research has been on optimizing the measurement precision so that high quality quantitative data can be obtained. The 2D system incorporates an algorithm for tracking axial displacements between consecutive frames of ultrasound data. Pressure is applied to the tissue subject through the scanning probe, and this causes small deformations between frames. 3D Elastography is able to provide more valuable and accurate strain information. When we take into account the strain information in axial, lateral and elevational then the process is a 3D process.

Development and experimentation focuses on dynamic high frequency ultrasound of the musculoskeletal system. The near future will bring an expanding set of techniques; some integrated into scanners and others as stand-alone devices, with an expanding set of clinical diagnoses that benefit from an assessment of the biomechanical properties of tissues.

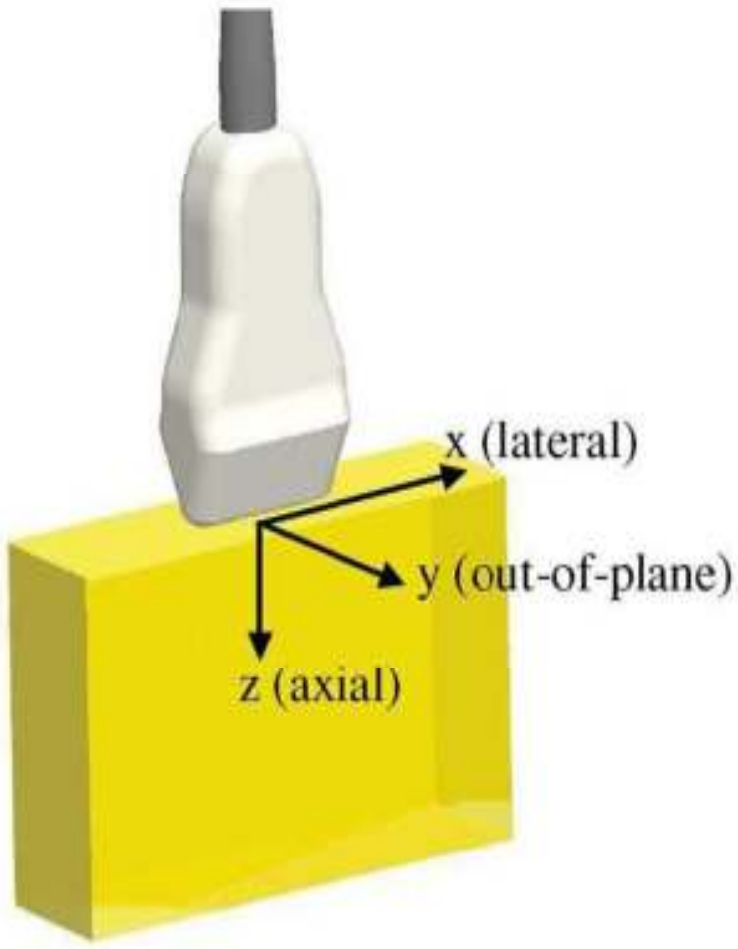

Figure: 1.7 Explanation of the movement of transducer in different directions

Another important direction for the field is the development of advanced estimators that go beyond relative stiffness and Young's modulus. Specifically, viscosity, anisotropy, nonlinearity, dispersion and their changes with disease have only recently been estimated and there is enormous opportunity for devising accurate estimation techniques and applying them to developmental models of major diseases. The opportunity is great; however the challenges are also great, particularly since the study of elastographic imaging and the biomechanics of normal and diseased tissue is highly multidisciplinary, covering classical mechanics, wave propagation, biomechanics, imaging, digital signal processing, radiology and pathology plus other specialties. Progress will require highly interactive teams covering a broad range of expertise.

1.9 CHAPTER SUMMARY

In this chapter, we have discussed about how ultrasound based elasticity imaging can be of immense importance to reveal significant information about soft tissue's pathology. Manual palpation and relationship between ultrasound based elasticity imaging has been incorporated. However, difficulties faced in assessing mechanical properties of soft tissues have been pointed out and how the modern technological advancements have pave the way for acquiring better and high quality elastogram have also been discussed. The role of Medical ultrasound in imaging tissue properties along with their imaging

modalities have been incorporated in a concise manner. The relative advantageous prospects of ultrasound based tissue elasticity imaging over other conventional modalities such as: MRI, CT Scan, Radiography etc. have been discussed too. Besides, how elastography as an ultrasound imaging technique can play its role as an alternative approach to Biopsy have also been incorporated in this chapter. Brief reviews of extensive research work in the elastographic field over the last 20 years have also been included. Last of all, ongoing research work and future prospective of Elastography as an ultrasound based imaging are also-incorporated.

CHAPTER II

FUNDAMENTALS OF TISSUE ELASTICITY

2.1 INTRODUCTION

Mechanical properties of biological soft tissues are nonlinear, viscoelastic and anisotropic [35], in nature which generally presents a unique set of challenges to test and model those properties. Therefore combing all these factors in mind, a general deduction can be given about the tissue that is tissue does not stick to the definition of an elastic material. Because, to be an elastic material there should be a one-to-one correspondence between states of stress and strain. So, overall simplification to the modeling framework must be developed in order to employ elastography as a clinical tool for quantifying these soft tissue mechanical properties.

Tissue samples having nonlinear elastic properties possess a stress-strain relationship that can be described as following an exponential function or a close approximation to such [36]. For a large range of deformations, this type of non-linear response occurs but if the deformation is limited (i.e., strains less than 10 %), then the strain-strain relationship of human tissue does in fact exhibit a linear response which is experimentally analyzed by both Krouskop et. al [37]and Mridha and Ödman [38]. Therefore, for small strains; these results imply that the effects of nonlinearity in homogeneous tissue are negligible. However, with the application of strain in heterogeneous tissue, the local strain distribution (i.e., relative contrast) will vary significantly. In addition to that, since the elastic modulus in tissue spans several orders of magnitude, this increases the importance of linearity in the stress-strain relationship.

An important point to be noted that, the elastic modulus for a given material can be worked out mathematically as the first-order derivative of the stress-strain relationship (function) [39]. Therefore, tissue modulus will exhibit nonlinearity if the stress-strain relationship is nonlinear and a deflection from theory of linear elasticity happens. As a result, dependency between strain and stress measurements will occur and thus, a better definition of tissue elasticity properties can be given if they are conditioned at a given applied strain or stress level [40]. But, an additional level of complexity arises when attempting to quantify and correlate results of clinical elastography as described by Fung et al. [36].

Viscoelastic properties are of practical importance in case of biological soft tissues and their mechanical measurements. The strain is not only a function of stress, but also the strain rate [35] in case

of a viscoelastic material. It has been shown that, for small low frequency compressions in muscles, the steady states are established in a few milliseconds [41] implying that phase shift does not manifest (or is minimal) in the cyclic stress-strain relationship, a common indicator of a viscoelasticity [34]. In a general sense, small strains coupled with low frequency compressions, viscoelastic component of a soft tissue mechanical model can be disregarded [37].

Anisotropic properties are generally exhibited by most biological tissues [40]. Even the most general form requires a large number of terms to describe the mechanical properties if anisotropic tissues are considered within a mathematical framework. This complexity reduces to a great extent if our assumption is that tissue is isotropic and then only two independent constants are needed which are termed as the Lamé constants.

An introduction of the stress-strain relationship and the equations of elasticity will be provided in the sections to follow. Moreover, we will discuss the principle concerns regarding elasticity imaging in tissue from a mechanics standpoint, and then introduce some of the simplifying assumptions that are commonly employed in order to reduce the complexity of the problem.

2.2 THEORY OF ELASTICITY

All structural materials inherently possess the property of elasticity to some extent more or less i.e. within a specific limit, if an external force is applied on any structure, deformation is produced and when this force is removed, deformation vanishes and the structure resumes its initial state. Perfect elastic body does not exist in real world as with the application of force, any structure does not come back to its initial shape without pertaining a minimum amount of deformation in it when the force is removed. Stress is the external force to be applied and another is strain which is the resulting deformation due to stress.

Let the cross-sectional area of a tendon be A and let the force acting on the tendon be F. The stress in the tendon would be then,

$$\gamma = F/A$$

Deformation of a structure that can be related to stresses is described by strain. Take a string of an initial length L_0. If it is stretched to a length L, then strain would be:

$$S = \frac{L - L_0}{L_0}$$

2.3 STRESS-STRAIN RELATIONSHIPS AND EQUATIONS OF ELASTICITY

When a compressive force or mechanical loading is applied on a deformable material such as biological soft tissue, deformation takes place and stresses develop within that body. In general, induced stress levels depend not only on the final state of deformation, but also on the history and rate of the applied loading, temperature etc. and the deformed body usually does not return to the its exact original configuration upon removing the load[34]. But, if the deformation is adiabatic (i.e., no heat is gained or lost) as well as infinitesimal, an acceptable assumption would be that the stress and strain are independent of the loading rate and history, and the removal of compressive force does not cause the material does return to its initial configuration. Such a deformation is termed elastic and the theory of elasticity can be employed to study the motion [39].

The stress in an elastic body can be expressed as a function of the strain only if it is dependent on deformation and can be expressed as:

$$\phi_{ij} = S_{ij}(\epsilon_{kl}) \quad \text{.....(2.1)}$$

Where ϕ_{ij} and ϵ_{kl} denote the second-order stress and strain tensors, respectively.

Above equation can be expanded into a Taylor's series expansion about $\epsilon_{kl} = 0$ yields:

$$\phi_{ij} = S_{ij}(0) + \frac{\partial S_{ij}(0)}{\partial \epsilon_{kl}}\epsilon_{kl} + \frac{1}{2!}\frac{\partial^2 S_{ij}(0)}{\partial \epsilon_{kl}\partial \epsilon_{mn}}\epsilon_{kl}\epsilon_{mn} + \frac{1}{3!}\frac{\partial^3 S_{ij}(0)}{\partial \epsilon_{kl}\partial \epsilon_{mn}\partial \epsilon_{op}}\epsilon_{kl}\epsilon_{mn}\epsilon_{op} + \text{.....(2.2)}$$

Higher-order nonlinear terms of eqn (2.2) can be neglected assuming that the deformation is linear elastic:

$$\phi_{ij} = Z_{ij} + A_{ijkl} \quad \text{.....(2.3)}$$

where, $Z_{ij} = S_{ij}(0)$ and $A_{ijkl} = \frac{\partial S_{ij}(0)}{\partial \epsilon_{kl}}$ are constants. A close inspection to eqn (2.3) and (2.3) reveals that Z_{ij} represents the state of stress at $\epsilon_{kl} = 0$, namely, the initial stress. The initial stress can be neglected in the context of linear elastic deformation and consequently, eqn (2.3) can be simplified to:

$$\phi_{ij} = A_{ijkl}\epsilon_{kl} \quad \text{.....(2.4)}$$

where eqn (2.4) is called the generalized Hooke's law or Hookean Equation. The proportionality of the stress and strain is related by eqn (2.4), which states that each of the components of the state of stress at a point is a linear function of the components of the state of strain at that point. As per notation, the subscripts i, j, k and l vary between 1 and 3 in a 3D space and where the first subscript denotes the direction of the axis to which the surface element is perpendicular and the second subscript denotes the direction of the component. For example, ϵ_{12} is the component of the strain tensor in the X_2 direction acting on the surface perpendicular to the X_1 axis.

The strain tensor introduced in eqn (2.4) is defined as:

$$\epsilon_{kl} = \frac{1}{2}\left(\frac{\partial \zeta_k}{\partial x_l} + \frac{\partial \zeta_l}{\partial x_k}\right) \quad \text{(2.5)}$$

where ζ_k is the displacement component in the k^{th} direction and x_l is the final position in the 1^{th} direction of the displaced material point. It should be noted here that eqn (2.5) is commonly referred to as Cauchy's infinitesimal strain tensor (Fung et al. 1973). In matrix form, eqn (2.4) can be expressed as:

$$\begin{pmatrix} \phi_{11} \\ \phi_{22} \\ \phi_{33} \\ \phi_{23} \\ \phi_{31} \\ \phi_{12} \\ \phi_{32} \\ \phi_{13} \\ \phi_{21} \end{pmatrix} = \begin{bmatrix} A_{1111} & A_{1122} & A_{1133} & A_{1123} & A_{1131} & A_{1112} & A_{1132} & A_{1113} & A_{1121} \\ A_{2211} & A_{2222} & A_{2233} & A_{2223} & A_{2231} & A_{2212} & A_{2232} & A_{2213} & A_{2221} \\ A_{3311} & A_{3322} & A_{3333} & A_{3323} & A_{3331} & A_{3312} & A_{3332} & A_{3313} & A_{3321} \\ A_{2311} & A_{2322} & A_{2333} & A_{2323} & A_{2331} & A_{2312} & A_{2332} & A_{2313} & A_{2321} \\ A_{3111} & A_{3122} & A_{3133} & A_{3123} & A_{3131} & A_{3112} & A_{3132} & A_{3113} & A_{3121} \\ A_{1211} & A_{1222} & A_{1233} & A_{1223} & A_{1231} & A_{1212} & A_{1232} & A_{1213} & A_{1221} \\ A_{3211} & A_{3222} & A_{3233} & A_{3223} & A_{3231} & A_{3212} & A_{3232} & A_{3213} & A_{3221} \\ A_{1311} & A_{1322} & A_{1333} & A_{1323} & A_{1331} & A_{1312} & A_{1332} & A_{1313} & A_{1321} \\ A_{2111} & A_{2122} & A_{2133} & A_{2123} & A_{2131} & A_{2112} & A_{2132} & A_{2113} & A_{2121} \end{bmatrix} \begin{pmatrix} \epsilon_{11} \\ \epsilon_{22} \\ \epsilon_{33} \\ \epsilon_{23} \\ \epsilon_{31} \\ \epsilon_{12} \\ \epsilon_{32} \\ \epsilon_{13} \\ \epsilon_{21} \end{pmatrix} \quad \text{.....(2.6)}$$

where A_{ijkl} are termed the elastic constants and define the properties of the material point under stress (Saada et al. 1993). A quick look on eqn (2.6) reveals that A_{ijkl} is a fourth-order tensor that relates the stresses in any plane to the strain in any plane through a set of 81 elastic constants. However, assuming symmetry in the stress-strain relationship, i.e., $\phi_{ij} = \phi_{ji}$ and $\epsilon_{kl} = \epsilon_{lk}$ then:

$$A_{ijkl} = A_{jikl} = A_{ijlk} \quad \text{(2.7)}$$

And the number of independent elastic constants reduces from 81 to 36. The stress-strain relationship can thus be expressed as:

$$\begin{pmatrix} \phi_{11} \\ \phi_{22} \\ \phi_{33} \\ \phi_{23} \\ \phi_{13} \\ \phi_{12} \end{pmatrix} = \begin{bmatrix} A_{11} & A_{12} & A_{13} & A_{14} & A_{15} & A_{16} \\ A_{21} & A_{22} & A_{23} & A_{24} & A_{25} & A_{26} \\ A_{31} & A_{32} & A_{33} & A_{34} & A_{35} & A_{36} \\ A_{41} & A_{42} & A_{43} & A_{44} & A_{45} & A_{46} \\ A_{51} & A_{52} & A_{53} & A_{54} & A_{55} & A_{56} \\ A_{61} & A_{62} & A_{63} & A_{64} & A_{65} & A_{66} \end{bmatrix} \begin{pmatrix} \epsilon_{11} \\ \epsilon_{22} \\ \epsilon_{33} \\ 2\epsilon_{23} \\ 2\epsilon_{13} \\ 2\epsilon_{12} \end{pmatrix} \quad \ldots\ldots\ldots (2.8)$$

Furthermore, if the material under consideration is orthotropic (i.e., there are three planes of symmetry orthogonal to one another), then the stress-strain relationship is given as:

$$\begin{pmatrix} \phi_{11} \\ \phi_{22} \\ \phi_{33} \\ \phi_{23} \\ \phi_{13} \\ \phi_{12} \end{pmatrix} = \begin{bmatrix} A_{11} & A_{12} & A_{13} & 0 & 0 & 0 \\ A_{21} & A_{22} & A_{23} & 0 & 0 & 0 \\ A_{31} & A_{32} & A_{33} & 0 & 0 & 0 \\ 0 & 0 & 0 & A_{44} & 0 & 0 \\ 0 & 0 & 0 & 0 & A_{55} & 0 \\ 0 & 0 & 0 & 0 & 0 & A_{66} \end{bmatrix} \begin{pmatrix} \epsilon_{11} \\ \epsilon_{22} \\ \epsilon_{33} \\ 2\epsilon_{23} \\ 2\epsilon_{13} \\ 2\epsilon_{12} \end{pmatrix} \quad \ldots\ldots\ldots (2.9)$$

From eqn (2.9), it is inferred that for a linear elastic orthotropic material, the number of elastic constants is 12. If the total work done in a cyclic process of deforming and undeforming a material is zero (i.e., the process is completely reversible), then there exists a strain energy function such that $A_{ijkl} = A_{klij}$ and the number of constants further reduces from 12 to 9. If the material is isotropic (i.e., the material properties are independent of the coordinate system), then the number of independent elastic constants reduces to 2 and the stress-strain relationship reduces to the form:

$$\begin{pmatrix} \phi_{11} \\ \phi_{22} \\ \phi_{33} \\ \phi_{23} \\ \phi_{13} \\ \phi_{12} \end{pmatrix} = \begin{bmatrix} \alpha+2\eta & \alpha & \alpha & 0 & 0 & 0 \\ \alpha & \alpha+2\eta & \alpha & 0 & 0 & 0 \\ \alpha & \alpha & \alpha+2\eta & 0 & 0 & 0 \\ 0 & 0 & 0 & \eta & 0 & 0 \\ 0 & 0 & 0 & 0 & \eta & 0 \\ 0 & 0 & 0 & 0 & 0 & \eta \end{bmatrix} \begin{pmatrix} \epsilon_{11} \\ \epsilon_{22} \\ \epsilon_{33} \\ 2\epsilon_{23} \\ 2\epsilon_{13} \\ 2\epsilon_{12} \end{pmatrix} \quad \ldots\ldots\ldots (2.10)$$

where α and η are the Lamé constants. In terms of the Lamé constants, Hooke's law for an elastic material is given by (Saada et al. 1993):

$$\phi_{ij} = \alpha\delta_{ij}\epsilon_{kk} + 2\eta\epsilon_{ij} \quad \text{..... (2.11)}$$

with the inverted form written as:

$$2\eta\epsilon_{ij} = \phi_{ij} - \frac{\alpha}{3\alpha + 2\eta}\delta_{ij}\epsilon_{kk} \quad \text{..... (2.12)}$$

It should be noted that the term δ_{ij} appearing in eqns (2.11) and (2.12) is known as Kronecker's delta, which is unity when $i = j$ and zero otherwise.

Usually, Young's modulus and Poison's ration are the most common notations which are used to describe the elastic properties of materials since the Lamé constants are mathematically deduced and their physical meaning are difficult to interpret. With a simple contraction deformation experiment performed on an elastic isotropic material, the relationship between both the Young's modulus and Poisson's ratio and the Lamé constants can be deduced. For this example, a state of simple uniaxial compression is characterized by:

$$\phi_{11} = \phi_0, \phi_{22} = \phi_{33} = \phi_{12} = \phi_{23} = \phi_{31} = 0$$

where ϕ_0 is the uniformly applied compressive stress and the terms ϕ_{ij} $(i \neq j)$ denote the shearing stresses. Substituting this state of stress into eqn (2.12) yields:

$$2\eta\epsilon_{ij} = \phi_{11} - \frac{\alpha}{3\alpha + 2\eta}\phi_{11} = \frac{2(\alpha + \eta)}{3\alpha + 2\eta}\phi_0$$

By introducing the notation:

$$E = \frac{\phi_0}{\epsilon_{11}} = \frac{\eta(3\alpha + 2\eta)}{\alpha + \eta} \quad \text{..... (2.13)}$$

Therefore, the constant E can be quantified as a measure of rigidity for the material subjecting unidirectional compressive deformation, and is called the Young's modulus or the modulus of elasticity.

It is noted from the generalized Hooke's law that a simple contraction produces strains in the two transverse directions (i.e. ϵ_{22} and ϵ_{33}) even though there are no stresses applied in those directions. From eqns (2.12) and (2.13), we have:

$$\epsilon_{22} = \epsilon_{33} = -\frac{\alpha}{2\eta(3\alpha + 2\eta)}\phi_{11} = -\frac{\alpha}{2(\alpha + \eta)}\epsilon_{11}$$

where the negative sign implies expansions in the respective transverse directions. By introducing the notation:

$$\gamma = -\frac{\epsilon_{22}}{\epsilon_{11}} = -\frac{\epsilon_{33}}{\epsilon_{11}} = \frac{\alpha}{2(\alpha + \eta)} \quad \text{.....(2.14)}$$

then the constant γ is called the Poisson's ratio which quantifies the measure of the transverse (or lateral) strain due to axial strain for a material under compression.

Similarly, for the same elastic isotropic material subjected to simple shear of λ_0 in the $X_1 - X_2$ plane, then the corresponding stress tensors can be described as follows:

$$\phi_{12} = \lambda_0, \phi_{11} = \phi_{22} = \phi_{33} = \phi_{23} = \phi_{31} = 0$$

Upon substitution of this state of stress into eqn (2.11) yields:

$$\phi_{12} = \lambda_0 = 2\eta\epsilon_{12} = \eta\nu_{12} \quad \text{.....(2.15)}$$

where ν_{12} is the shearing strain. By introducing the notation:

$$G = \frac{\lambda_0}{\nu_{12}} = \eta \quad \text{..... (2.16)}$$

then the constant G can be interpreted as a measure of rigidity of the material in a unidirectional shear deformation, and is called the shear modulus. Furthermore, the shear modulus can be described as a function of E and γ as:

$$G = \frac{E}{2(1+\gamma)} \quad \text{..... (2.17)}$$

The bulk modulus (K) of a material is related to the fractional change in volume (V) that occurs under the application of a uniform surface pressure (i.e., $\phi_{11} = \phi_{22} = \phi_{33} = P$) and is defined as:

$$K = \frac{P}{dV/V} \quad \text{.....(2.18)}$$

The fractional change in volume for a cube of unity dimension is given by:

$$\frac{dV}{V} = (1+\epsilon_{11})(1+\epsilon_{22})(1+\epsilon_{33}) - 1 = \epsilon_{11} + \epsilon_{22} + \epsilon_{33} = \epsilon_{ii} \quad \text{..... (2.19)}$$

From eqns (2.18), (2.19) and (2.11), the bulk modulus can be expressed in terms of E and γ as follows:

$$K = \frac{E}{3(1-2\gamma)} \quad \text{.....(2.20)}$$

In the above example, a simple contraction experiment was described to introduce E and γ. It is important to note that the Young's modulus and Poisson's ratio in tension are the same as in compression [42]

Young's modulus measurements for soft biological tissues are found to be on the order of KPa [43]. The accurate measurement of lateral strain component is difficult in actual practice and therefore, Poisson's ratio of 0.495is taken as an assumption. As per convention, water is incompressible with a Poisson's ratio of 0.5 and soft tissue can be considered nearly incompressible due to the fact that it is mostly composed of water and resembles the value as stated above.

We consistently use E and γ for elastographic purpose to describe the elastic properties of tissues in lieu of the Lamé constants. In addition to that, the lateral, axial and elevational directions are represented by the x-axis, y-axis, and z-axis of Cartesian coordinate system respectively. This convention leads to the following set of governing elasticity equations [42]:

$$\epsilon_{xx} = \frac{1}{E}\{\phi_{xx} = \gamma(\phi_{yy} + \phi_{zz})\} \quad \text{.....(2.21)}$$

$$\epsilon_{yy} = \frac{1}{E}\{\phi_{yy} = \gamma(\phi_{xx} + \phi_{zz})\} \quad \text{..... (2.22)}$$

$$\epsilon_{zz} = \frac{1}{E}\{\phi_{zz} = \gamma(\phi_{xx} + \phi_{yy})\} \quad \text{..... (2.23)}$$

An examination of eqns (2.21) to (2.23) reveals the fact that the strain in any direction is dependent on the stress in all directions and the local values of the Poisson's ration as well as on Young's Modulus.

Eqns (2.21) to (2.23) also correspond to the mechanical properties measured at a point in a linear elastic isotropic homogeneous material. The heterogeneous nature of tissue materials compel us to determine the strain distribution in a material within some external boundary conditions (i.e., the magnitude and direction of the compressive force) and the local elastic properties. Therefore, an application of small global compressive deformation on a heterogeneous material may yield high localized strains in the softer regions and low localized strains in the stiffer regions.

2.4 TENSOR

The geometric objects which describe linear relations between scalars & vectors are known as Tensors. Such relations may include the different vector operations and linear maps. In fact, vectors and scalars are themselves tensors too in nature. A tensor can be represented as a multi-dimensional array of numerical values. The order (also degree or rank) of a tensor is the dimensionality of the array needed to represent it, or equivalently, the number of indices needed to label a component of that array.

Under the action of applied forces, solid bodies exhibit deformation to some extent, i.e. they change in shape and volume [44].The applied force is termed as Stress and the resulting deformation is termed as Strain. The classical example of the use of tensors in physics has to do with stress in a material object. Stress has the units of force-per-unit-area, or nt/m^2. It seems clear, therefore, that (stress) × (area) should equal (force); i.e., the stress-area product should be associated with the applied forces that are producing the stress. We know that force is a vector. We also know that area can be represented as a vector by associating it with a direction, i.e., the differential area dS is a vector with magnitude dS and direction normal to the area element, pointing outward from the convex side. Thus, the stress in the equation (force) = (stress) × (area) must be either a scalar or a tensor [45]. If stress were a scalar, then a single denominate number should suffice to represent the stress at any point within a material. But an immediate problem arises in that there are two different types of stress: tensile stress (normal force) and shear stress (tangential force). How can a single denominate number represent both? Additionally, stresses have directional properties more like "vector times vector" (or dyad) than simply "vector." We must conclude that stress is a tensor – it is, in fact, another tensor of rank 2 – and that the force must be an inner product of stress and area.

2.5 FACTORS THAT INFLUENCE THE STRAIN DISTRIBUTION

Mapping of the local axial strain distributions for a material undergoing a quasi-static deformation is the prime objective of elastography. So, a discussion of some of the factors which influence this process is a must. The stresses on the boundaries in the lateral and elevational directions become zero upon application of a uniaxial stress on a homogeneous material. But, generally tissue materials are heterogeneous (i.e., spatially varying modulus distribution) as discussed before and due to variations in the both the internal and external boundary conditions the stresses are not uniaxial and uniform too. Moreover, the Poisson's ratio is not consistently constant throughout the material either. Therefore, a deviation occurs in the local axial strain distribution which was supposed to be consistent with the description of eqn (2.22).

Usually, based on the mechanical factors (a) the tissue properties such as the modulus distribution, Poisson's ratio, internal boundary conditions (i.e., the connectivity of the tissue components), and (b) controlling factors such as the magnitude and direction of the external boundary conditions. To characterize the mechanical properties in soft tissues, the applied strain at the boundaries is typically used [36].

2.5.1 MODULUS DISTRIBUTION

For non-uniform modulus distributions, the stress and strain distributions in tissue are inherently three dimensional even when a uniform stress is applied at the boundaries. This concept is illustrated in Fig. 2.1 [36] where the cross-sectional modulus (Fig 2.1a), stress (Fig. 2.1b) and strain distributions (Fig 2.1c) are shown for a stiff cylindrical inclusion embedded in a softer homogenous matrix. At the upper boundary, a uniform compression is applied whereas both the upper and lower boundaries are specified as being free slip conditions for this example. As illustrated in Fig. 2.1b, the stress distribution around the inclusion is not uniform. From Fig. 2.1, we see that despite uniform stress and strain levels within the inclusion, there are distinct stress and strain concentrations located about the lesion-matrix interface. These concentrations are attributed to both the inclusion geometry and modulus contrast [46]. Also, a butterfly-like shadowing pattern along the cross diagonal axis is there which is attributed to the geometry of the inclusion. Interestingly, some researchers have suggested exploiting these distinct patterns to detect tumors and cancers [47]. This similarity between the tissue stiffness (i.e., modulus distribution) and corresponding strain distribution is of interest in elastographic imaging due to the fact that strain is traditionally used as a surrogate for the underlying tissue modulus distribution [49].

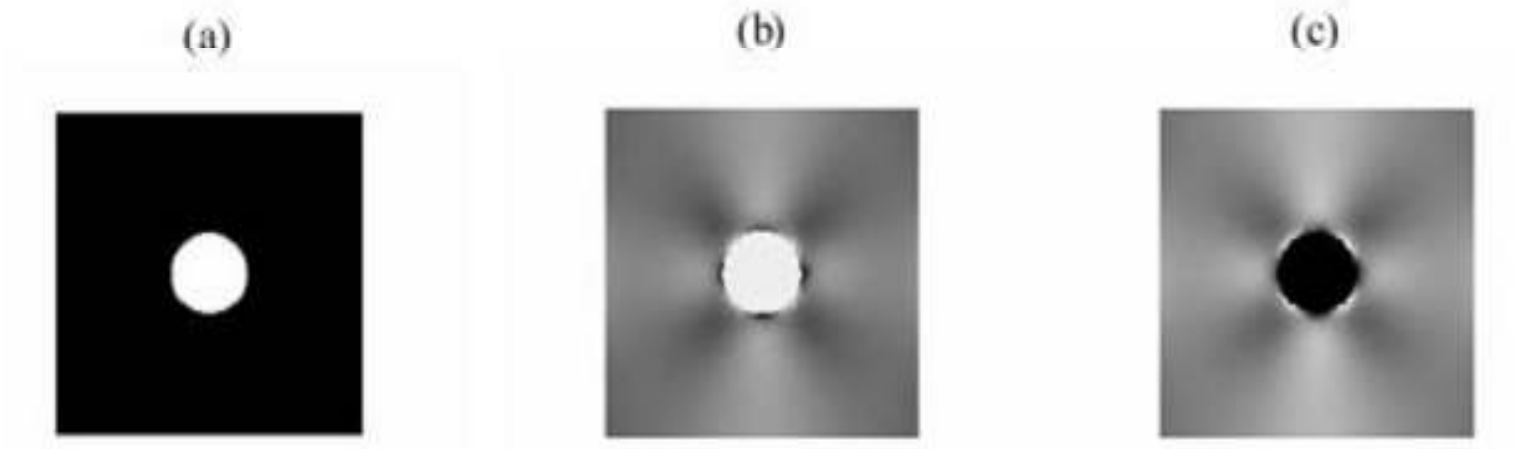

Figure 2.1: (a) Modulus, (b) Stress and (c) Strain images of an embedded circular inclusion three times stiffer than the surrounding matrix. Note that for each respective image, light and dark regions correspond to high stress and high strain, respectively. The numerical simulations were performed using FEMLAB (Comsol Inc., Burlington, MA, USA).

2.5.2 POISSON'S RATIO

The strain in any direction is strictly dependent on the local values of the Young's modulus and Poisson's ratio and the stress in all directions as evident from the relationships described by eqns (2.21) to (2.23). In case of mechanical modeling, we assume a Poisson's ration of 0.495 typically. Besides, Young's modulus in soft tissues is on the order of 10^4 [37], it is speculated that the local stress and modulus distributions will dominate over the local strain distributions with a slight dependence on Poisson's ratio's variations. The axial strain distribution (measured through the center of a material with an inclusion three times stiffer than the surrounding background) as a function of depth for three different Poisson's ratio values of 0.495, 0.497 and 0.499 respectively is depicted in Figure 2.2 [48]. It is to be noted that, no observable changes are observed in the strain distributions as the Poisson's ratio deviates from the desired value of soft tissue and.

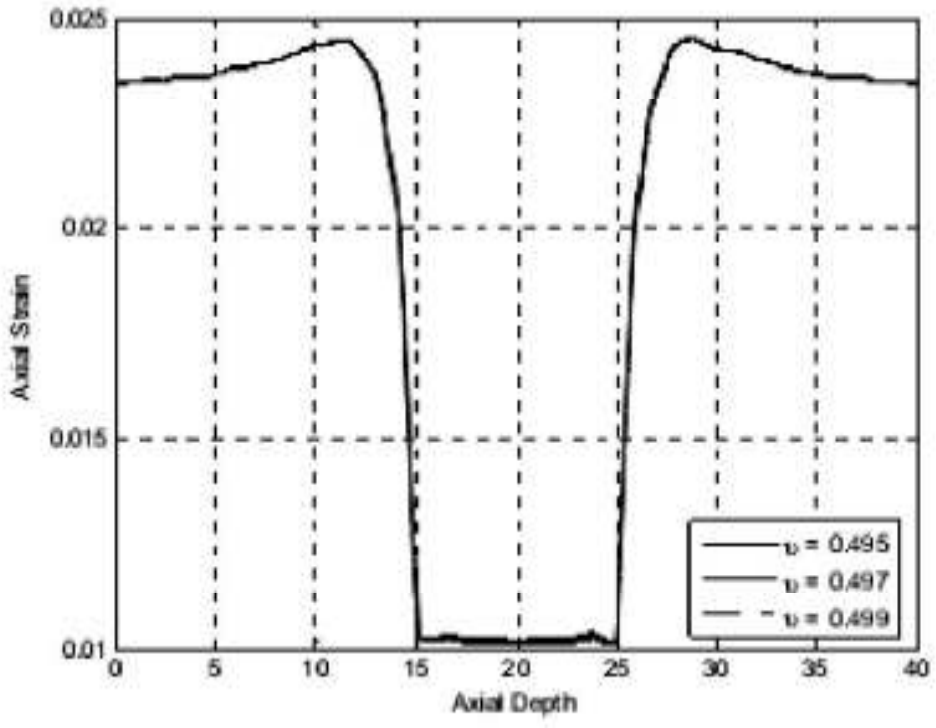

Figure 2.2 Axial strain as a function of depth measured through the center of a material composed of an inclusion (10 mm in diameter and centered at a depth of 20 mm) three times stiffer than the surrounding background and for the following Poisson's ratios: 0.495, 0.497, and 0.499. A strain of 2 % was applied to produce the deformation. (Kenneth Leon Hoyt, Spectral Strain Estimation Techniques for Tissue Elasticity Imaging, 2005)

2.6 MECHANICAL PROPERTIES OF TISSUE

Before adoption of any biomedical applications, the precise knowledge regarding the mechanical properties of tissues is an essential requirement. In elastography, elasticity data of soft tissues carries a significant role to get accurate diagnostics of the infected region. In many cases, a relationship exists between the presence of pathology and the palpable elastic properties of the tissue (e.g. breast, prostate, liver etc.).Many breast and prostate cancers are routinely detected by palpation. Such cancers may or may not be seen by ultrasonic imaging. Detection by palpation is limited to relatively large, proximal hard nodules. The diversity of mechanical properties encountered in soft biological tissues is huge. Soft organic tissues are in general characterized by very complex mechanical behavior. They show non-linear, anisotropic, viscoelastic and in some cases also viscoplastic behavior. They often have a layered or an even more complicated structure. The mechanical properties are inhomogeneous, i.e. they depend on the position in the material. The perfusion of the organs and their constituting tissues also plays an important role regarding the elastic properties. There are mainly two sources of elasticity in soft biological tissues. The first source of elasticity is due to changes of internal energy whereas the second one is due to changes

of entropy. Change of entropy occurs in tissues whenever changes of orientation or waviness of fibers during loading or unloading occur.

2.7 CHAPTER SUMMARY

Testing and modeling the mechanical properties of biological soft tissues is indeed a challenging work since many of them are nonlinear, viscoelastic and anisotropic. In elastography, our prime concern is to estimate the mechanical properties of soft tissue for applied strain levels of less than 10 %. Soft tissue can generally be conjectured to be linear elastic and the theory of elasticity, the generalized Hooke's law (eqn (2.4)) can be realized and can be utilized to study the underlying stress-strain relationship as long as this deformation range is maintained and (assuming that the compressive force is quasi-static). Isotropic nature of tissue enables us to describe the elastic properties (eqn (2.11)) in terms of only two independent constants. These two constants are the Lamé constants, or their technical derivatives, the Young's modulus (eqn (2.13)) and Poisson's ratio (eqn (2.14)).It was introduced and shown that for a uniformly applied surface deformation, the strain distribution in a heterogeneous material gives a relative depiction of the modulus distribution and corresponding elastic properties were explored based on these. Factors that influence the strain distribution in elastography were also introduced and discussed.

CHAPTER III

FUNDAMENTAL CONCEPTS IN ELASTOGRAPHY

3.1 INTRODUCTION

Elastography is well established in the literature as a strain imaging technique. In conjunction with existing ultrasound imaging, elastography can be employed to investigate the mechanical properties of soft tissue, namely the strain distribution or relative deformation. Throughout the last decade, elastography has been shown to be an effective imaging modality for differentiating cancerous from benign masses in the breast [50], identifying tumors in the prostate [51], monitoring both HIFU [52]and RF ablation [53] in tissue, intravascular-based assessment of vessel wall compliance and pathology and estimating cardiac motion and mechanical function [54].

In general, conventional elastography relies on the accurate estimation of displacements between windowed radio-frequency (RF) echo signals before and after tissue motion (in the form of an external or internal compression) is induced [55]. These displacement estimates are related to tissue strain via a gradient operator as applied to successive axial displacement estimates. Though these coherent methods are precise in extracting tissue strain information, they have been shown to be extremely sensitive to decorrelation (noise) sources [56]. Due to innate noise amplification properties of the gradient operator at small window sizes and/or large window overlaps, gradient-based coherent strain estimators have a fundamental limitation with regards to image spatial resolution.

Unlike coherent (temporal) strain estimation techniques, incoherent (spectral) methods do not need the phase information to estimate tissue motion. Moreover, noise amplifying gradient computation is not included in these coherent methods. Although these spectral elastographic techniques may be less accurate than the coherent methods, owing to the fact they do not use the signal phase information, they have been shown to be more robust [57]. Strain imaging in high noise environments, such as freehand-based scanning applications and intravascular imaging; this robustness is of immense significance.

3.2 PRINCIPAL OF ELASTOGRAPHY

Let's consider a system which is the concatenation of 3 springs with 3 different spring constants K1, K2 & K3 respectively. The amount of force needed to extend or contract a spring by unit length is known as spring constant. In our case, K1 and K2 is less than K3, i.e. middle spring is more rigid than the other two springs. Therefore, with the application of same force per unit area (i.e. stress) to compress this system won't result in same displacement or deformation (i.e. strain) because of the difference in rigidity of these springs. The middle one will be less deformed than the other two. In other words, it is less elastic than the other two springs which will deform more than the rigid spring because of their more elasticity.

The same analogy can be drawn to human tissues. Generally, human tissues have varying elasticity properties from mechanical standpoint of view. Tissues having higher elastic moduli will deform more than the tissues having less elastic moduli. In Elastography, by employing cross-correlation function we can measure the strain/deformation of tissues before & after the application of stress. Hence tissues' elastic moduli can be determined which then can be used to analyze and detect any unusual growth in human body.

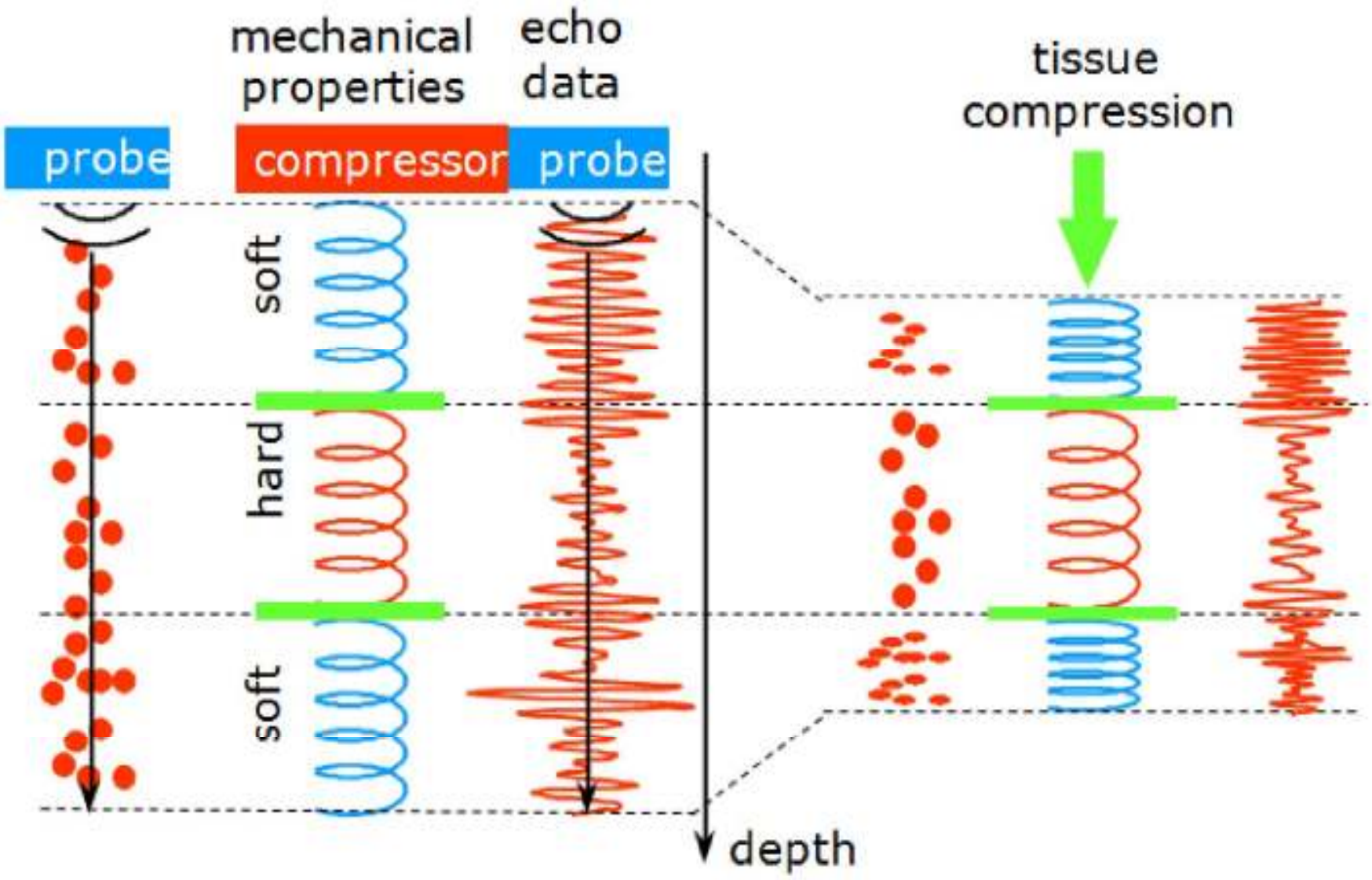

Figure 3.1: Schematic and conceptual argument used to explain the strain images produced by early compression systems (Ophir et al. 1991).

Generally, value of Poisson's ratio for tissues lies in between 0.49 and 0.499, that means tissue is nearly incompressible (Liquid – incompressible medium has 0.5). This fact can be used to establish a simple result that the shear and the Young's moduli of tissue are associated by a scaling factor of three, i.e. $E = 3G$. The bulk moduli K of most soft tissues vary by less than 15% from that of water, even though the shear modulus varies over a large range. Therefore, shear(G) and Young's(E) moduli, having the broadest dynamic range, are the most pertinent elasticity parameters to measure and are probably the most intimately related with what is felt in palpation.

Biological tissues change shape easily when compressed because of the presence of high water content but the volume is conserved. Therefore, $K >> G$, $\eta \sim 0.5$ and $E = 3G$.

3.3TYPE OF EXCITATION

3.3.1 STATIC METHODS

Since 1940s, radio frequency (RF) signals have been used to measure object motion and the development of Radar and Sonar. The use of ultrasound to measure soft tissue deformations dates back to the early 1980's. Specifically, it was shown by both Dickinson &Hill [58] and Wilson & Robinson [59] that tissue motion could be estimated using ultrasound from information embedded in radio frequency (RF) echo A-lines. It was demonstrated by them that, ultrasonic techniques could provide (one-dimensional (1D)) descriptions of soft tissue elasticity parameters. In these methods, hepatic tissue deformation was resultant of mechanical forces inherent to the natural cardiac activity. These conditions were assumed quasi-static since the resultant tissue deformations were small (less than 0.1 mm) and of low velocity (less than 2 Hz) as compared to the measurement time. A two-dimensional (2D) deformation imaging method was introduced by Mai and Insana [60] by using the same conceptual approach. The A-scan and M-mode analyses of endogenous tissue motion proposed20 years ago have been replaced by improved two-dimensional (2D) analyses [61] that take advantage of advancements in ultrasonic technology.

In 1991, Ophir and coworkers [62] introduced an ultrasound-based technique, termed elastography, for imaging soft tissue strain profiles (i.e. relative deformation) owing to a quasi-static compressive force. In this particular approach, tissue strain is considered as a replacement for tissue stiffness, a low tissue strain region implies high stiffness and vice-versa. Current elastographic techniques are generalized as being either coherent or incoherent in their approach. Regarding the former, axial tissue

motion is estimated (numerically) as the peak position of a cross-correlation function applied to congruent pre- and post-compressed RF echo data segments [63]. Phase value corresponding to the zero lag correlation function [64] can be used to estimate the axial tissue motion (i.e. time shifts). Subsample approximation is usually applied in order to improve accuracy [65] as these displacements are from a discrete valued correlation function. By processing all pre- & post-compressed A-line pairs, displacement estimates are acquired as a function of tissue depth & it is repeated until all the pre- & post echo line pairs are obtained. Eventually, the strain images (known as Elastograms) are formed by taking the gradient of the axial displacements estimates [65]. Figure (3.2) below depicts the elastographic data acquisition procedure for an externally applied compression. To ensure a uniform stress distribution within the tissue, a compression plate is fitted with an ultrasound transducer generally (66). In case of internally applied excitation, cross correlation based techniques are proven to be useful for tracking the tissue motion (such as vessel wall displacement) [67].

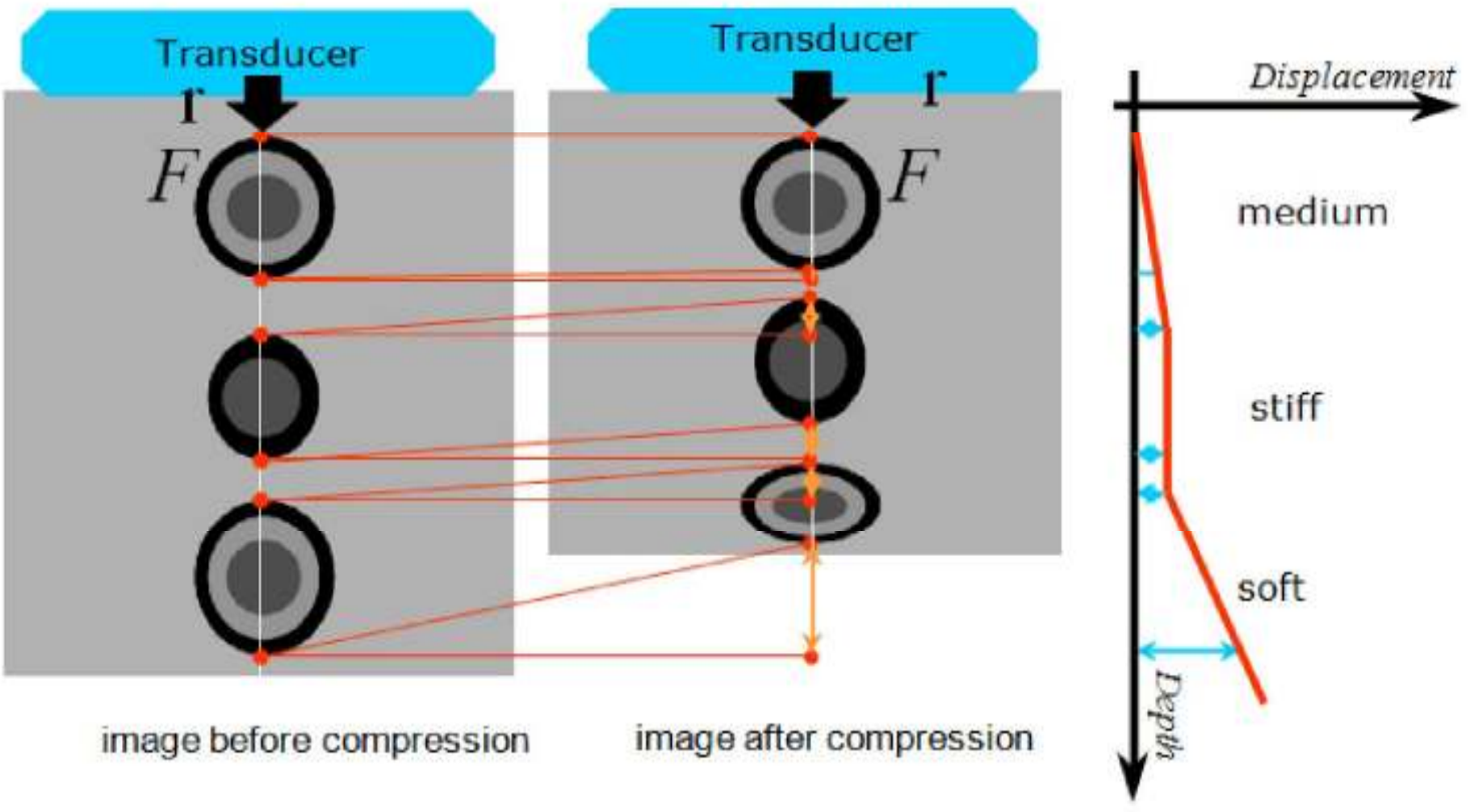

Figure 3.2: Conceptual illustration of the elastographic process denoting the pre- and post-compressed tissue states. The post-compressed state is induced using an externally applied axial compression using the transducer footprint and a compressor plate.

Due to the applied compression, physical deformation of the tissue occurs which in turn gives rise to additional signal distortions & that is why this elastographic technique of measuring (relative) tissue motion cannot be deemed as a pure displacement (time-delay) estimation problem. In addition to that,

after applying the compression, tissue scatterers experience a 3D motion pattern, and thus decorrelation [68] results in as this undesired movement of scatterers in and out of the ultrasound beam. Decorrelation is defined as a full loss of full correlation between pre- and post-compressed gated signal segments. Other factors such as: intra-window axial motion [69], electronic noise& phase jitter further intensify this decorrelation effect. In other words, decorrelation is one of the prime inhibiting factors in strain estimation and imaging [63].

Besides coherent strain estimation methods discussed above, there exists elastographic techniques which do not rely on the use of phase information to compute tissue strain& they are characterized as incoherent strain estimation. Use of baseband signals to compute tissue strain [70] has been proposed by some research groups & this is a time-domain based approach. Alternatively, several strain estimation techniques have been introduced that are Fourier analysis-based[71],in which tissue motion-related changes in mean scatterer spacing (due to ultrasonic scatterers spaced at quasi-regular intervals) were estimated from regularities in the spectral peaks. Additionally, spectral domain methods utilizing either the centroid shift [72], or spectral cross-correlation function [73], have been introduced as alternative methods to estimate tissue strain. The latter two methods have been shown to be direct estimators of tissue strain and are thus devoid of any noise amplifying gradient operator such as this case for the coherent-based elastographic approaches. In general, all these spectral techniques are based on the Fourier scaling principle which states that a scale change in the time-domain corresponds to an inversely related scale change in the frequency domain [74]. A flowchart illustrating both the coherent and incoherent elastographic techniques is provided in Figure 3.3.

The generalized approach to elastographic imaging involves estimating and displaying either some tissue mechanical parameter or motion property owing to the application of some mechanical force. Intuitively, the tissue modulus would appear to be the most relevant mechanical parameter of interest when considering elasticity imaging due to its quantitative significance.

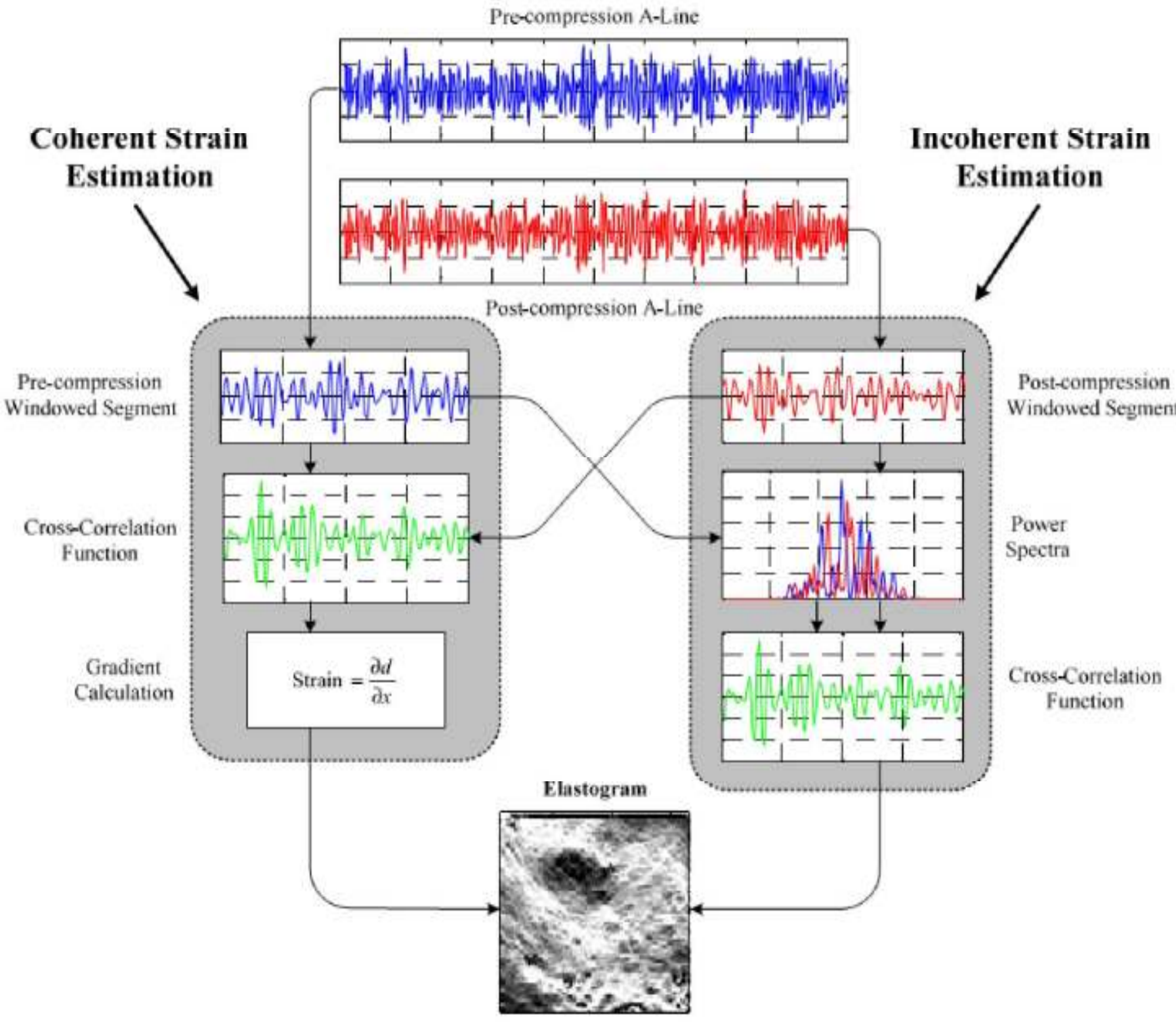

Figure 3.3: A flowchart illustrating the basic concepts and signal processing strategies for both the coherent and incoherent elastographic methods. (Kenneth Leon Hoyt, Spectral Strain Estimation Techniques for Tissue Elasticity Imaging, 2005)

3.3.2 DYNAMIC METHODS

Krouskop & his associates performed the measurements of the mechanical properties of soft tissue using ultrasound& this is one of the earlier documented reports detailing the noninvasive measurements. What they did was under external vibrations; actual tissue flow was measured by implementing a single A-line pulsed Doppler instrument in conjunction with a low frequency mechanical vibrator at points of interest. With the help of conventional Doppler techniques [75], the velocity information was extracted, positional derivatives were measured & consequently a relationship between tissue modulus & a system of linear equations were developed. In spite of having the capability of measuring tissue stiffness (modulus) in a very small region (i.e. 0.5 by 0.5 mm), it paved the ground work

for future research initiatives of this type. Using the same approach of an externally applied sinusoidal mechanical force, Sonoelastographic technique was conceived at the University of Rochester for measuring soft tissue elasticity [76]. A monochromatic mechanical perturbation (typically 30 to 1100 Hz)is coupled to the body surface to induce oscillations within the tissue and the underlying motion is detected simultaneously using Doppler ultrasound. The Doppler shift of an ultrasonic wave scattered from a spatially oscillating object (scatterer volume) is given by a Fourier-Bessel series of equally spaced harmonics above and below the Doppler carrier frequency [77]. In the end, sonoelastography implicates estimating the modulation coefficient from the backscattered RF data which consequently has been shown to be a function of vibrational amplitude [76]. The results are shown in a format resembling mainstream Doppler color flow mapping and are named as sonoelasticity images. The fundamental idea implicit in this technique is that hard tissues react differently to an applied mechanical oscillation than do normal tissues [78].

Yamakoshi et al. (1990) inaugurated a dynamic elasticity imaging system for assessing and exposing both vibrational amplitude and phase distributions of internal tissue excitations. This approach is correspondent to the sonoelastographic method. This approach allowed for visualization of the low frequency vibration whereas the low-frequency wave velocities were measured as a parameter for tissue delineation.

Primary results using sonoelastography depicted substantial variations in shear wave vibrational velocities for cm-sized regions of altered stiffness [80]. Detectability later shown to be increasing with vibration frequency although the penetration of higher vibration frequencies (in the kHz range) [81] was inhibited by loss mechanisms. A major limitation of the sonoelastographic technique is that it enhances attenuation (as compared to methods that utilize longitudinal acoustical wave propagation such as the elastography) due to the requirement of induction and subsequent propagation of shear (transverse) acoustical waves. But, one of advantages of this method is that the mass density and shear modulus of the linear-elastic medium in which shear wave propagates are directly related. Therefore, by measuring the propagation velocity of the shear waves and density; the shear modulus (a quantifiable tissue elastic parameter) can be determined but provided that the tissue under investigation is homogeneous and isotropic.

Use of acoustic radiation forces to induce localized internal vibrations in conjunction with tissue motion tracking is one of the examples of the more recent elasticity imaging techniques to appear in the literature. Acoustic radiation force is generally a physical process related with the propagation of acoustic waves through a dissipative medium (e.g., soft tissue). The transfer of momentum from the propagating

wave to the tissue causes this internally applied force to occur. Initially implemented using focused ultrasound for acoustical streaming purposes [80], the principles of acoustical radiation force were later shown by several different research groups to be viable for imaging applications as well.

Known as remote palpation, short-duration acoustic forces (typically less than 1.0 ms) are used in acoustic radiation force impulse (ARFI) imaging to yield localized displacements in tissue which are tracked using ultrasonic correlation-based methods. As shown by Sarvazyan and his associates [81], once the acoustical radiation force is applied and subsequently withdrawn from a region of interest, shear waves disseminate away from the initially displaced tissue. In most elasticity imaging techniques, generally the displacement magnitude owing to spreading shear waves is inversely proportional to local tissue rigorousness. A single ultrasound transducer is typically used in ARFI based-imaging systems to both transmit the radiation force and to receive RF echo frame data. Then, tissue displacement is calculated using typical cross-correlation elastographic techniques (and thus this method is inherently prone to decorrelation processes). Due to the localized nature of the constrictive force employed to stimulate tissue motion, initial results using ARFI imaging has been found to be promising.

Vibro-acoustography [82], which has similarity with ARFI imaging except that it employs dynamic excitation such as acoustic radiation forces to exert a low-frequency (normally kHz) localized stress field within or on the surface of a tissue structure. Dynamic internal excitation is produced from focused continuous-wave ultrasound beams propagating with offset center frequencies. The radiation force is generated from the interference between the two beams and subsequently tissue oscillation becomes equal to the offset. A hydrophone detects an acoustic emission from vibrating tissue. The resultant emission can be measured by scanning the focal point about a tissue region of interest at each point and utilized to generate an image.

3.4 ELASTOGRAMS AND ARTIFACTS

In elastographic process and method, our ultimate goal is to generate elastographic image i.e. elastograms. The data from the two RF pre- and post-compression lines undergo processing, and an elastogram ultimately appears on the monitor. There are two types of elastograms: gray scale and color. The hard and soft areas (i.e. areas of high and low elasticity, respectively) appear in the gray-scale elastogram as dark and bright, respectively. In a color elastogram of a general device, increasing tissue hardness appears, in ascending order, as red, yellow, green, and blue (Fig. 3.4). These colors represent the relative hardness of the tissues in the elastogram.

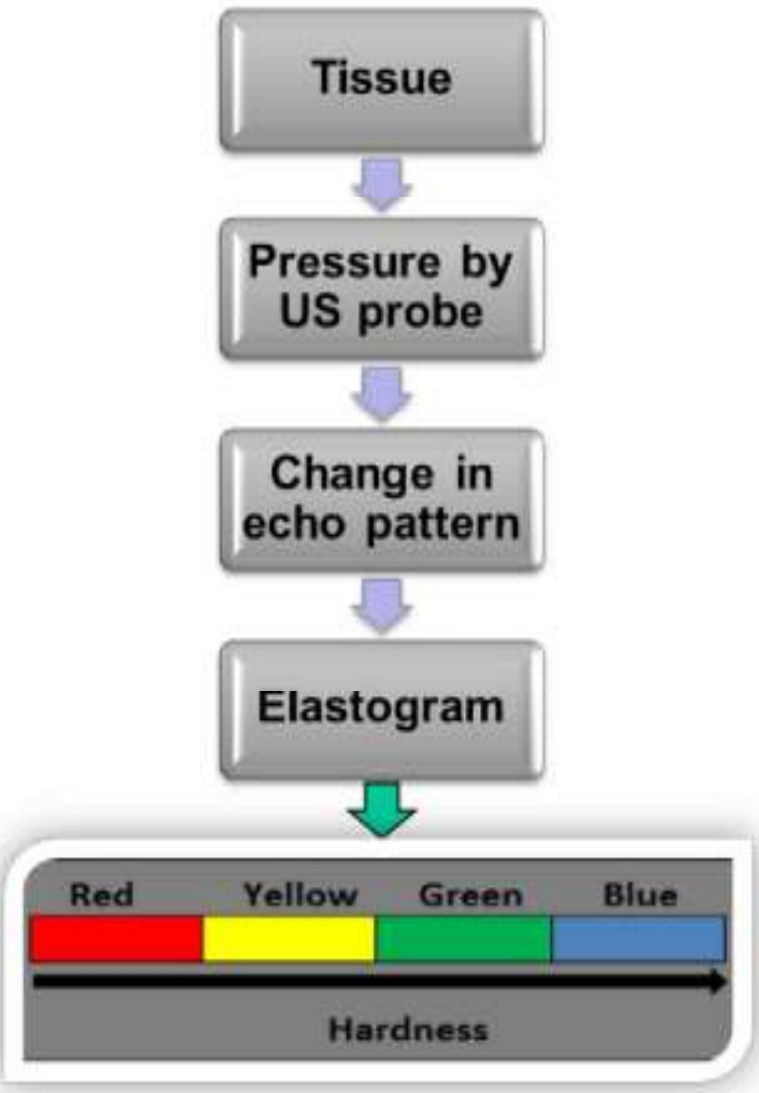

Figure 3.4: An overall elastographic process in block diagram to generate elastograms.

3.5 RADIO FREQUENCY ECHO SIGNALS

Radio frequency (RF) is a rate of oscillation in the range of about 3 KHz to 300 GHz, which corresponds to the frequency of radio waves, and the alternating currents which carry radio signals. In medical imaging, RF signal is the unprocessed electrical signal coming from the ultrasound scanner's probe. It thus contains all the information on the propagation of the acoustic waves and their intersections with the scanned tissue [83]. Ultrasound data usually can be acquired in one of two formats: either an envelope signal (normal) or the raw RF signal (less common). There are two reasons for preferring RF data:

1. RF data contains more information than the signal envelope.

2. Most search techniques use phase information from the RF signal as the search criterion, and the fact that the average phase change is known (it depends on the probe center frequency) is assistive for gradient-based search methods.

In order to get high accuracy measurements, the RF signal is used instead of the signal envelope. The difference between the two signals is shown in Figure-3.5:

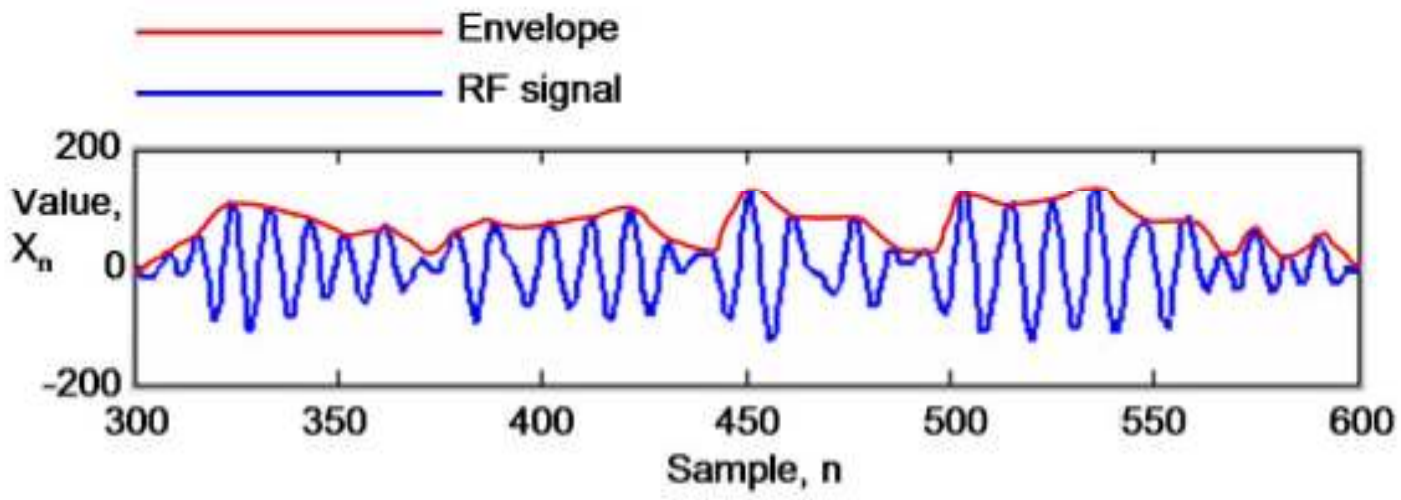

Figure 3.5: Elastography requires the raw RF signal. It has a varying frequency, so it contains considerably more information than the signal envelope.

To produce a RF signal, a piezoelectric crystal has an alternating current applied across it. The piezoelectric crystal grows and shrinks depending on the voltage run through it. Running an alternating current through it causes it to vibrate at a high speed and to produce an RF signal. This conversion of electrical energy to mechanical energy is known as the piezoelectric effect. The RF signal then bounces back off the object under investigation, which is known as RF echo signal. The RF signal hits the piezoelectric crystal and then has the reverse effect - causing the mechanical energy produced from the sound vibrating the crystal to be converted into electrical energy. By measuring the time between when the RF signal was sent and RF echo signal was received, the amplitude of the signal and the pitch of the signal, a computer can produce images, calculate depths and calculate speeds.

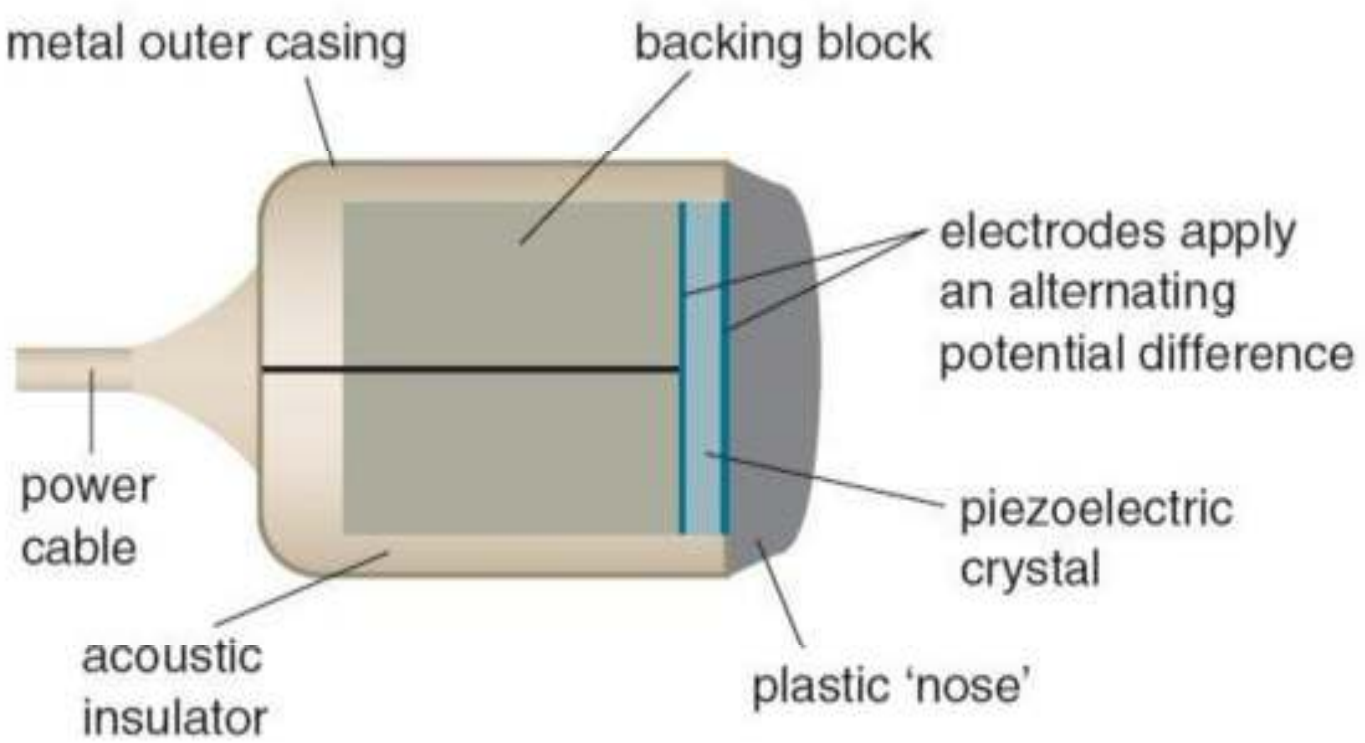

Figure 3.6: Generation of RF signal using a Transducer

Radio frequency (RF) energy has been used in medical treatments for over 75 years [84], generally for minimally invasive surgeries, using radiofrequency ablation and cryoablation, including the treatment

of sleep apnea [85] and also to create an image of some part of the inside of the body, such as the stomach, liver, heart, tendons, muscles, joints and blood vessels. These frequencies generally range between 1-50 MHz.

3.6 CORRELATION

It is frequently necessary to be able to quantify the degree of interdependence of one process upon another, or to establish the similarity between one set of data and another. In other words, the correlation between the processes or data is sought. The process of correlation occupies a significant importance in any signal processing tool. Applications are found in ultrasound image processing for estimating time delay in which data from pre and post-compression RF lines is compared. It is also used in the correlation detectors, as an integral part of the ordinary least squares estimation technique, in the computation of the average power in waveforms, and in many other fields, such as, for example, climatology.

3.6.1 CROSS-CORRELATION

Consider how two data sequences, each consisting of simultaneously sampled values taken form the two corresponding waveforms, might be compared. If the two waveforms varied similarly point for point, then a measure of their correlation might be obtained by taking the sum of the products of the corresponding pairs of points. This proposal becomes more convincing when the sum of the products will tend towards a vanishingly small random number as the number of pairs of points is increased. This is because all numbers, positive and negative, are equally likely to occur so that the product pairs tend to be self-cancelling on summation. By contrast, the existence of a finite sum will indicate a degree of correlation [86]. A negative sum will indicate negative correlation, which is an increase in one variable is associated with a decrease in the other variable. The cross-correlation $r_{12}(n)$ between two data sequences $x_1(n)$ and $x_2(n)$ each containing N data might therefore be written as:

$$r_{12}(n) = \sum_{n=0}^{N-1} x_1(n)\, x_2(n)$$

This definition of cross-correlation, however, produces a result which depends on the number of sampling points taken. This is corrected for my normalizing the result to the number of points by diving by N . Alternatively, this may be regarded as averaging the sum of products. Thus, an improved definition is:

$$r_{12}(n) = \frac{1}{N} \sum_{n=0}^{N-1} x_1(n)\, x_2(n)$$

In Elastographic technique, cross-correlation is an inevitable part since it gives the measurement of Time-delay estimation.

3.6.2 AUTO-CORRELATION

Autocorrelation refers to the correlation of a time series with its own past and future values. It is also sometimes called "lagged correlation" or "serial correlation", which refers to the correlation between members of a series of numbers arranged in time. Positive autocorrelation might be considered a specific form of "persistence", a tendency for a system to remain in the same state from one observation to the next. For example, the likelihood of tomorrow being rainy is greater if today is rainy than if today is dry. Geophysical time series are frequently auto correlated because of inertia or carryover processes in the physical system. For example, the slowly evolving and moving low pressure systems in the atmosphere might impart persistence to daily rainfall. Or the slow drainage of groundwater reserves might impart correlation to successive annual flows of a river. Or stored photosynthates might impart correlation to successive annual values of tree-ring indices. Autocorrelation complicates the application of statistical tests by reducing the number of independent observations. Autocorrelation can also complicate the identification of significant covariance or correlation between time series (e.g., precipitation with a tree-ring series). Autocorrelation can be exploited for predictions: an auto correlated time series is predictable, probabilistically, because future values depend on current and past values. Three tools for assessing the autocorrelation of a time series are (1) the time series plot, (2) the lagged scatterplot, and (3) the autocorrelation function.

3.6.3 DECORRELATION

Decorrelation is a general term for any process that is used to reduce autocorrelation within a signal, or cross-correlation within a set of signals, while preserving other aspects of the signal. The concept of Elastography relies on the estimation of strain for an applied tissue compression. Time delays between gated pre-compression and post-compression echo signals gives a measurement of strain. Utilizing the information about the location of the peak of cross-correlation function between gated pre-compression and post-compression echo signals enable us to compute the time delay estimates. Therefore, accurate estimation of time delays is a prerequisite condition for generating good quality elastogram. A main source of Time Delay estimation (TDE) error in elasticity imaging is the decorrelation of the echo

signal as a result of tissue compression (decorrelation noise) [87]. It is commonly described in terms of the correlation coefficient [88]. Decorrelation degrades the performance of Time Delay Estimation (TDE).

3.7 EXPLANATION OF THE DATA WINDOW

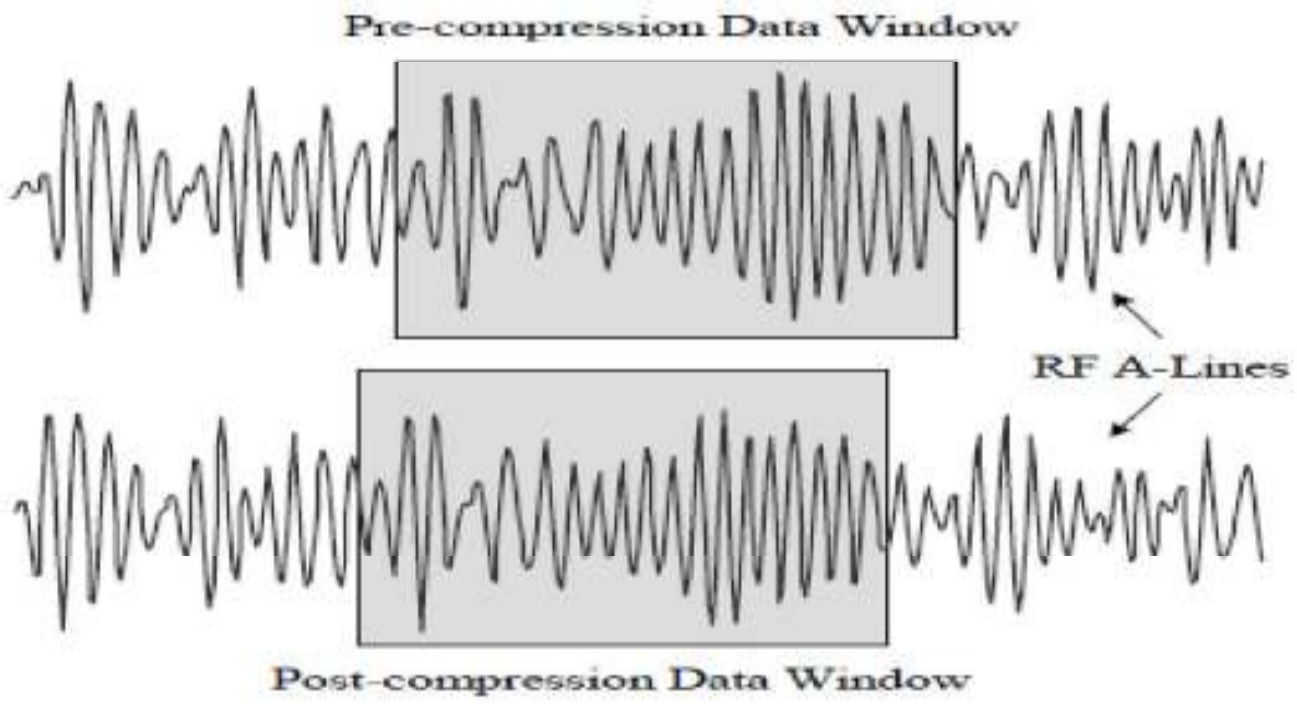

Fig 3.7: Small rectangular data windows over the pre-compression and the post-compression signal.

We often need to truncate data in diverse situations from numerical computations to filter design. For example, if we need to compute numerically the Fourier transform of some signal, say $e^{-t}u(t)$ on a computer, we will have to truncate the signal $e^{-t}u(t)$ beyond a sufficiently large value of t(typically five time constants and above). The reason is that in numerical computations, we have to deal with data of finite duration. Similarly, the impulse response h(t) of an ideal lowpass filter is noncausal, and approaches zero asymptotically as $|t| \to \infty$. For a practical design, we may want to truncate h(t) beyond a sufficiently large value of |t| to make h(t) causal. In signal sampling, to eliminate aliasing, we need to truncate the signal spectrum beyond the half sampling frequency Fs/2, using an anti-aliasing filter. Truncation operation may be regarded as multiplying a signal of a large width by a window function of a smaller (finite) width. Simple truncation amounts to using a rectangular window $W_R(t)$ in which we assign unit weight to all the data within the window width ($|t| \leq T/2$), and assign zero weight to all the data lying outside the window ($|t| > T/2$). It is also possible to use a window in which the weight assigned to the data within the window may not be constant.

Truncation operation may be regarded as multiplying a signal of a large width by a window function of a smaller (finite) width. Simple truncation amounts to using a rectangular window $W_R(t)$ (Fig. 3.7) in which we assign unit weight to all the data within the window width ($|t| \leq T/2$), and assign zero weight to all the data lying outside the window ($|t| > T/2$). It is also possible to use a window in which the weight assigned to the data within the window may not be constant.

3.8 TIME DELAY ESTIMATION FOR AXIAL DISPLACEMENT

Time delay estimation (TDE) is the process of determining the relative time shift between a reference signal and delayed signal. Time delays are generally estimated from the location of the peak of the cross-correlation function between the pre- and post-compression echo signals. The TDE lies at the core of many modern signal-processing algorithms. In medical ultrasound, TDE is used in blood flow estimation, phase aberration correction, motion compensation for synthetic receive aperture imaging, tissue elasticity estimation, radiation force imaging, and a number of other algorithms. Because of its central significance, TDE accuracy, precision, and computational cost are of critical importance to these and numerous other algorithms.

In elastography, TDE is a very important parameter. Two radio frequency (RF) ultrasound frames are acquired pre- and post-deformation. Some indication of the tissue elasticity is provided by the axial strain, which is usually retrieved in two steps: time delay estimation, by calculating time shift between pre-deformation RF data windows with post-deformation windows; and strain estimation, by differentiating the displacement field. Here displacement estimation in spatial domain is equivalent to time delay estimate in time domain.

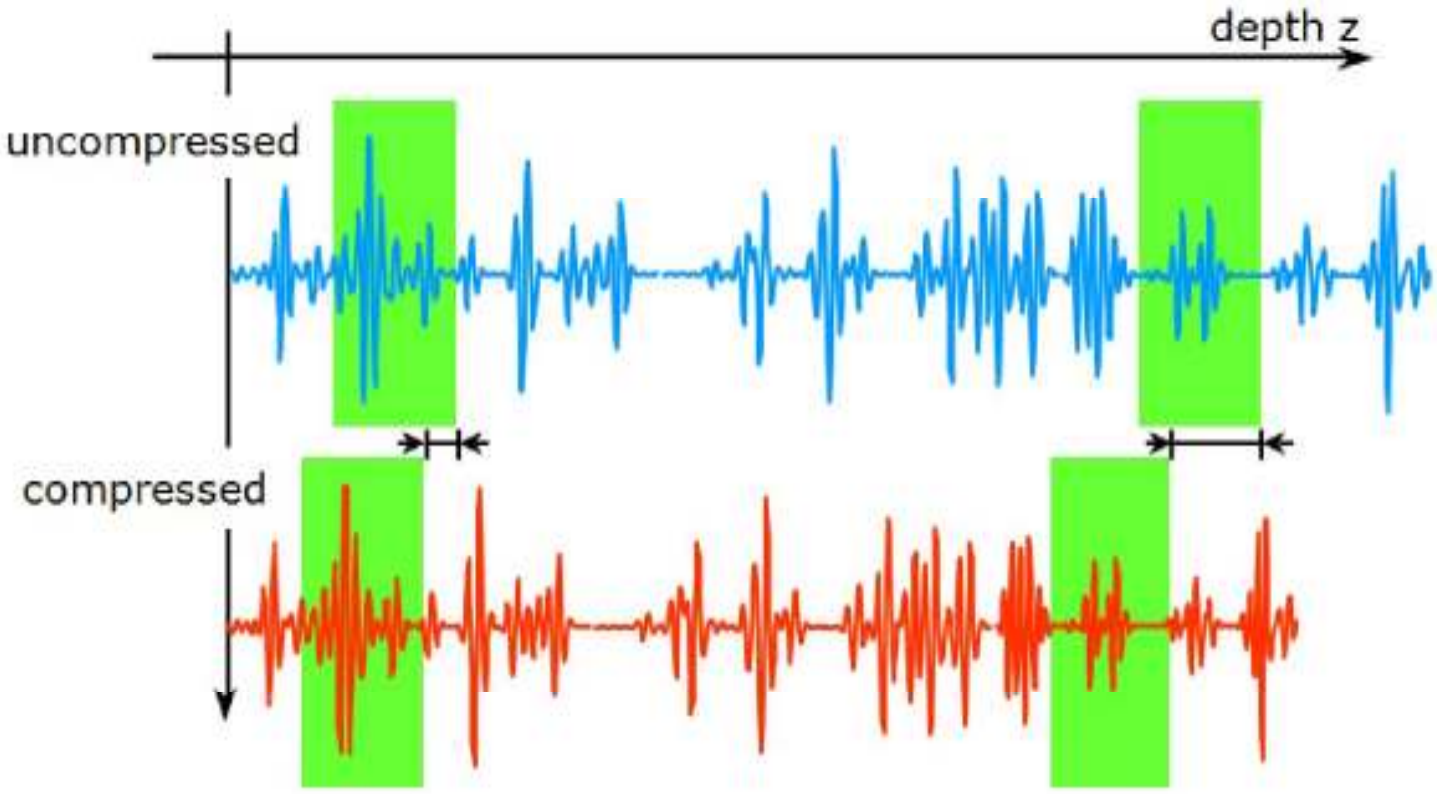

Figure 3.8: Time delay between Pre & post-compressed A lines in elastography.

The quality of elastograms is highly dependent on the quality of the TDE procedure. TDE in elastography is mainly corrupted by two factors [89]. First, random noise introduces errors in the TDE. Second, tissue needs to be compressed to produce elastograms. The very same compression of the tissue distorts the post-compression signal such that it is no longer an exact delayed version of the pre-compression signal. This decorrelation increases with increasing strain and is independent of the signal-to-noise ratio in the echo signals. Any phenomenon (such as lateral and elevational motions) that degrades the precision of the time delay estimates will also degrade the strain estimates, thus introducing additional noise into the elastogram. Echo signal decorrelation is one of the major limiting factors in strain estimation and imaging. For small strains, it has been shown that temporal compression of the pre-compression signal by the appropriate factor can almost entirely compensate for such axial decorrelation in a mechanically homogeneous medium [90]. When the post-compression echo signal is stretched, it in effect realigns all the scatterers within the correlation window. Global uniform stretching was found to be a very efficient displacement estimator for low contrast targets with significant improvement of SNR_e. However, in high contrast targets, there will be significant over-stretching in the areas of low strains, which by itself can significantly degrade elastograms in these areas. For these situations, an adaptive axial stretching algorithm may be necessary [91]. Axial stretching is mandatory in the presence of large strains; otherwise the elastograms become so noisy that they are practically useless. Axial stretching also enhances the dynamic range of elastography. It must be remembered that axial stretching can only recover most of the decorrelation suffered due to scatterer motion in the axial direction; decorrelation due to lateral and elevational motions, as well as other sources of decorrelation, cannot be compensated this way. Konofagou and Ophir have demonstrated that decorrelation due to lateral motion may be compensated

with high accuracy by using a phase sensitive signal interpolation technique [92]. This technique, when applied alternately with axial stretching, was shown to result in large improvements in elastographic image quality.

3.9 DISPLACEMENT ESTIMATION FROM TDE

Displacement estimation, a key step in the evaluation of tissue elasticity by quasi-static strain imaging, can easily be estimated from the previously mentioned TDE procedure. A time delay between the pre- and post-compressed echo signals arise from the spatial shift of the compressed tissue. Assuming the speed of sound in the soft tissue constant, the spatial shift is proportional to the time shift. Hence, delay estimate in time domain is equivalent to displacement estimation in spatial domain. From the axial gradient of this tissue displacement estimation, tissue strain is then calculated to generate elastograms. The speed and accuracy of the strain imaging system depends heavily on the displacement estimation algorithm in the first step. An efficient approach may incorporate a tracking strategy whereby each estimate is initially obtained from its neighbors' displacements and then refined through a localized search. This increases the accuracy and reduces the computational expense compared with exhaustive search. Robust tracking ensures that displacement estimates can be found by searching over small ranges without introducing large errors, location estimation corrects a well-known amplitude modulation artifact, and a "weighted phase separation" framework illuminates the scope for optimizing the speed and accuracy of deformation estimators.

Among several techniques for displacement estimation, correlation maximization was the first to be proposed by Ophir et al, 1991 [93] and remains the most widely used. The pre-deformation RF frame is divided into an axial–lateral grid of small windows, which are associated with corresponding windows in the post-deformation frame by searching for the highest correlation match. Tissue displacement is then given by the shift between the pre- and post-deformation windows. Efforts have been made to adapt the correlation algorithm to provide subsample accuracy by Céspedes et al., 1995 [94]. Moreover, standard correlations, and its variants such as the sum of absolute differences and the sum of squared differences, have been integrated with multi-level or multi-scale schemes to improve the estimation stability by Chaturvedi et al., 1998; Yeung et al., 1998; Pellot-Barakat et al., 2004; Shi and Varghese, 2007. As an alternative to exhaustive search, Zhu and Hall (2002) proposed a tracking strategy that takes the displacement in each row of the grid as an initial guess for the next row. This allows a smaller search range and hence a reduction in the computational expense [95].

3.10 SRAIN IMAING FROM ESTIMATED TISSUE DISPLACEMENT

After the displacement estimation using the above mentioned cross-correlation matching between the pre- and post-deformation windows, it is required to estimate the strain so that strain image or elastogram can be generated. The equation to calculate strain from displacement (time delay) is,

$$Strain = \frac{GradientofTissueDisplacement}{InitialSeparationBetweentheWindowedSegments}$$

Here, in MATLAB the gradient of the time delay has been calculated using the built in function "gradient". Initial separation between the windowed segments is nothing but the window shift used during the estimation. A detail of strain imaging techniques and parameters related to it will be discussed in Chapter-4.

As stated in the previous chapters, a stiffer tissue element will generally experience less strain than a softer one. Depending on these strain values, the area of lesion and the area of normal tissue region are separated from which the ultimate strain image is generated. MATLAB built in function "imagesc" is used to generate the gray scale strain image from the calculated strain values.

3.11 DIFFERENT ELASTOGRAPHIC METHOD

3.11.1 2D ELASTOGRAPHY

The 2D techniques that are considered to work by detecting only the axial component of tissue strain. The strain is being estimated by comparing the RF A-lines in two frames of ultrasound data. In each frame a different pressure is applied through the probe, and it gives rise to deformation of the tissue. Fig. 3.9 demonstrates how a small deformation can provide information about elastic properties. The algorithm's main job is to track the deformation so that estimates can be made of the strain field at regular points throughout the tissue. This is done using methods based on the complex cross-correlation function (CCC) acting on the data across the two frames. Several possible implementations are investigated, because the details determine both the accuracy of the estimates, and the computational cost.

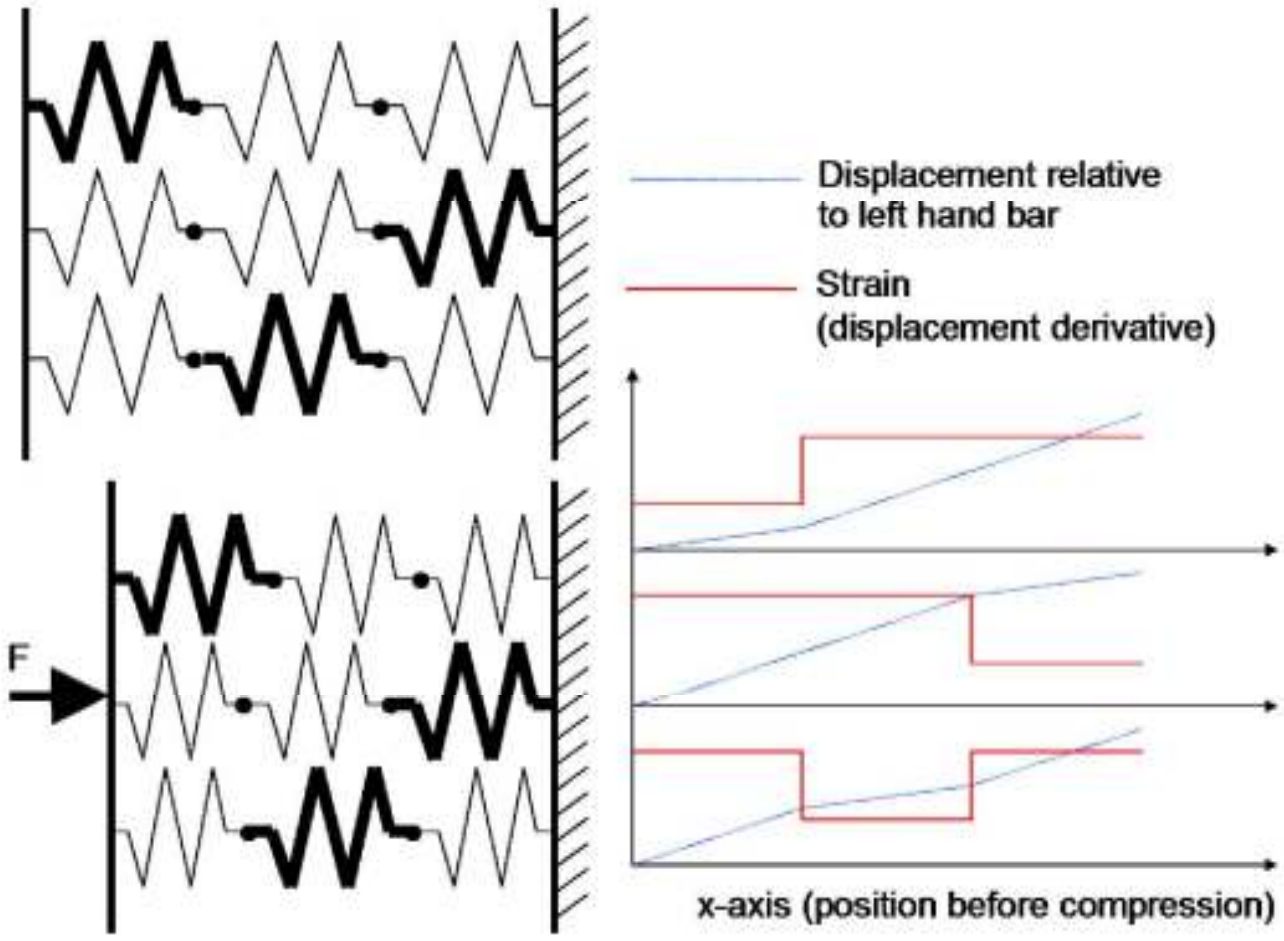

Figure 3.9: When a force is applied through the probe, assuming that the deformation is purely axial, the strain can be measured by tracking the displacement throughout the structure. The bold and light springs represent high and low stiffness respectively.

3.11.2 3D ELASTOGRAPHY

Movement in non-axial directions for 3D elastography can be conducted slowly enough to allow good axial strain estimation. This is because ultrasound has far lower resolution in the elevational and lateral directions. The quality of the elastograms is already sufficient to produce useful 3D visualizations. While ultrasound data is being acquired, the system also records probe position measurements. Frames of ultrasound data are acquired at >30 Hz and scans are approximately 10s in duration [96]. In this time, the operator slowly sweeps the probe across the subject's surface in the elevational direction, typically covering about 3 cm, trying also to incorporate some axial movement, while avoiding moving at all in the lateral direction. The techniques that have been tried are sketched in Fig. 3.10.

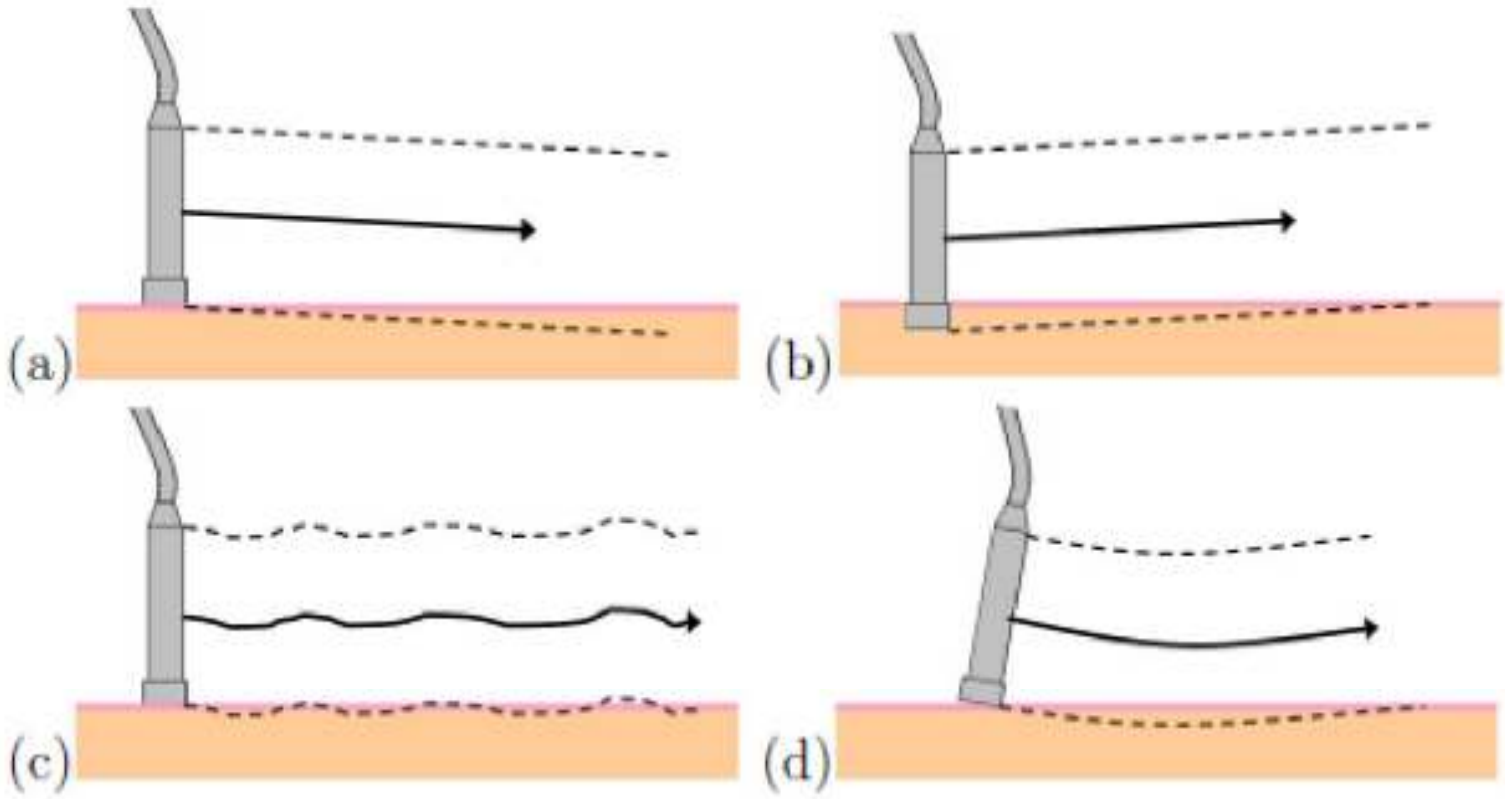

Figure 3.10: Scanning techniques. The user moves the probe elevationally and axially, while avoiding lateral movement. (a) The probe is lightly pressed into the tissue while it is swept across the surface. (b) The probe is initially pressed into the tissue, and is removed gradually during the sweep. (c) The user does not deliberately apply pressure; compression is the result of slight vertical vibration of the probe, or movement from within the subject (in the case of live subjects). (d) The user moves the probe steadily in a shallow arc over the tissue, involving initial compression and later decompression.

Once the data has been processed, it is straightforward to write it in a format that can be used by Stradx. As before, elastography was carried out on successive pairs of data frames. Elastogram data was recorded in *.sxi format, *.sx files were written to contain all the configuration information, and for every elastogram the position sensor data of the second frame in the pair was copied across. These files were the 3D elastograms, and they were inspected using the existing Stradx 3D visualization tools [97]. A "review" window allows the user to browse through the 2D elastograms that have been generated. From the review window it is possible to define the plane of a "reslice", so the data is displayed on a new plane slicing through the 3D data set. From the reslice window a third surface can be defined, called the "manifold", which displays the data on a third slice through the 3D data set. A fourth window, the "outline", presents all of these surfaces in their 3D context, and it can give a good indication of the shape of a 3D object.

3.11.3 MAGNETIC RESONANCE ELASTOGRAPHY (MRE)

Magnetic Resonance Elastography is an imaging technique for non-invasively assessing the elasticity properties of biological tissues using MRI (Magnetic Resonance Imaging) [98]. Although

major contributions to elastography were initially made by the ultrasound community, the advantages of MRE have only recently been recognized. Initial studies demonstrated that this novel imaging technique has the potential to probe biological tissues effectively. MRE can provide estimates of the mechanical properties of tissues, such as shear modulus or Young's modulus. For example, a small lesion of less than 1 cm in diameter and with stiffness only three times that of the background was detected in vivo in human subjects. MRE involves discrete application of external compression and simultaneous acquisition of time-sequential MR images followed by off-line processing of acquired data to estimate the motion experienced by the tissue [99]. While there are many possible applications of MRE, breast cancer detection and classification is currently the most common use. MRE has further potential as a diagnostic tool in such diseases as strokes, hyperthyroidism, disuse atrophy, or paralysis. The technical task of MRE generally consists of the application of a deformation force, followed by tracking the tissue deformation (motion analysis).

Static Magnetic Resonance Elastography (MRE) is a modality of elastography that uses Magnetic Resonance Imaging (MRI) principles for data acquisition from a biological sample under external loading. An estimation of the mechanical deformation of the loaded sample from its Magnetic Resonance (MR) images constitutes a key component of the static MRE. Efforts in this area of research have mainly been focused on developing data acquisition protocols and motion estimation algorithms for producing high quality elastography images.

3.11.4 ENDOSCOPIC ULTRASONOGRAPHIC ELASTOGRAPHY (EUS)

EUS is an endoscopic technique that allows detailed imaging of the pancreas and gastrointestinal wall layers. Hypothetically, elastography may provide an important adjunct to imaging as it allows "palpation" of inaccessible organs and even collection of quantitative information on the degree of hardness. In addition to providing imaging of tumors and enhancing TNM staging, EUS also provides guidance for fine needle aspiration (FNA) and biopsies of undiagnosed masses and lymph nodes (LN) suspicious for malignant invasion, providing further diagnostic and staging information [100].

As with traditional color Doppler imaging, EUS tissue elasticity imaging is performed with conventional EUS probes and does not require additional instrumentation either for measuring pressure or producing vibrations. The vibrations and compressions are provided physiologically by vascular pulsation and respiratory motion. The calculation of tissue elasticity distribution is performed in real- time and the examination results are represented in color superimposed over the conventional B-mode image.

3.11.5 FREEHAND ULTRASOUND ELASTOGRAPHY

High quality quasi-static freehand 2D ultrasound strain imaging is currently possible in real time [101], by comparing radio-frequency (RF) data from sequential ultrasound images during a slight deformation of the tissue due to contact pressure from the ultrasound probe. It has recently been shown that it is possible to produce stable, high quality strain data over a wide range of freehand motions of the probe [102]. The approach has considerable benefits over other techniques in that no additional equipment is required to induce the required stress field in the tissue: the clinician simply moves a normal ultrasound probe over the anatomy. This potentially makes the technique simpler to use as well as easier to implement.

3.11.6 ACOUSTIC RADIATION FORCE BASED ELASTOGRAPHY

Conventional diagnostic ultrasound images portray differences in the acoustic properties of soft tissues, whereas ultrasound-based elasticity images portray differences in the elastic properties of soft tissues (i.e. stiffness, viscosity). The benefit of elasticity imaging lies in the fact that many soft tissues can share similar ultrasonic echogenicities, but may have different mechanical properties that can be used to clearly visualize normal anatomy and delineate pathological lesions. Acoustic radiation force-based elasticity imaging methods use acoustic radiation force to transiently deform soft tissues. Acoustic radiation force results from a transfer of momentum from the propagating ultrasonic wave to the tissue through which it is propagating owing to absorption and scattering mechanisms. The dynamic displacement response of those tissues is measured ultrasonically and is used to estimate the tissue's mechanical properties. Both qualitative images and quantitative elasticity metrics can be reconstructed from these measured data, providing complimentary information to both diagnose and longitudinally monitor disease progression. Recently, acoustic radiation force-based elasticity imaging techniques have moved from the laboratory to the clinical setting, where clinicians are beginning to characterize tissue stiffness as a diagnostic metric, and commercial implementations of radiation force based ultrasonic elasticity imaging have been approached in two general categories: (i) those that provide qualitative images of relative differences in tissue stiffness, similar to external compression strain imaging, cardiac strain imaging [103] and intravascular ultrasound (IVUS) palpography and (ii) those that provide quantitative estimates of the underlying elastic modulus of tissue, as is done with MR elastography [104].

3.11.7 HIGH FREQUENCY ULTRASOUND ELASTOGRAPHY (HFUS)

Skin diseases such as psoriasis and scleroderma—as well as skin burnings, skin aging, and changes of the epidermal hydration—cause changes in skin elasticity. For this reason, tactile investigations are routinely performed during dermatological examinations, but the results strongly depend on the individual sense and experience of the physician. Presently, available tools for the

measurement of elastic skin properties are based on applying external mechanical deformations (traction, torsion, suction, etc.) and analyzing the resulting displacement of only the skin surface using optical measurements techniques. Lack of depth information as well as the limited spatial resolution, the latter being a result of limited measurements each performed at a single point at the skin surface, are the major drawbacks of the currently available techniques. High-frequency ultrasound (HFUS), however, is a valuable tool to image the morphology of small organs such as skin and eye in depth noninvasively with high resolution. Different attempts already have been made to assess elastic properties of the skin applying HFUS. Diridollou et al. used 20 MHz ultrasound for skin imaging accompanied by the application of suction to the skin surface [105]. The skin surface, the border between the dermis and the subcutaneous fat, and the border between the subcutaneous fat and the muscle were detected and changes in skin layers thickness were quantified and analyzed. Furthermore, the results of measurements along a single line were fitted to an analytical, elastic membrane model to determine intrinsic mechanical parameters of the skin [106]. A similar measurement technique was applied by Hendriks et al., measuring the deformation of the dermis based on ultrasound images. Results of these analyses were fitted to a finite element model. Pan et al. [107] acquired echo signals with a 40 MHz ultrasound biomicroscope while stretching the skin surface transversely. Applied stress and intensity changes in ultrasound images were analyzed. Furthermore, ultrasound attenuation and backscattering coefficients were measured and correlated with elastic skin properties.

In dermatology, HFUS in the 20MHz range and above is already being advantageously applied for noninvasive and high-resolution imaging of skin morphology and allows preoperative measurements of the tumor thickness as well as the progression and treatment of many skin diseases [108]. Capability to furnish spatially resolved information on the elastic behavior of the tissue, additional to the morphological one, that may enhance the noninvasive evaluation of the skin in vivo, is among the major desirable characteristics of a HFUS imaging system.

3.11.8 OPTICAL COHERENCE ELASTOGRAPHY (OCE)

Optical coherence elastography (OCE) is a novel elastography technology used to determine tissue biomechanical properties utilizing the in vivo imaging modality optical coherence tomography (OCT). The relationship between OCT and OCE is analogous to ultrasound sonography and elastography. With the inherent advantages of OCT, such as high resolution, non-invasive and real-time imaging, and millimeter-scale penetration depth in tissue, OCE techniques are unique for measuring or imaging biomechanical properties at the micron-scale tissue level, the cellular level, and even the molecular level.

OCE techniques have also been widely applied in different fields for biomechanical property measurements. For example, OCT has been investigated for intravascular imaging as a counterpart to intravascular ultrasound imaging, but offering higher spatial resolution. Intravascular OCE is studied to exploit prior information about arterial wall biomechanics to produce robust estimates of tissue velocity and strain [109]. OCE is also studied as a method for assessing the biomechanical properties of atherosclerotic plaques in which tissue phantoms and aorta are examined in vitro to quantify speckle modulation and measure the displacement and strain maps [110]. An OCE system is used for tissue elasticity reconstruction and distribution results from four representative tissue block models in intravascular imaging. OCE is also applied to measure the biomechanical properties of engineered and developing tissues as well. Spatially distributed mechanical displacements and strains are mapped in a representative model of a developing engineered tissue as cells began to proliferate and attach within a 3D collagen matrix. Displacements are quantified by a cross-correlation algorithm on pre- and post-compression images, from which OCE is able to differentiate changes in strain over time, which corresponded with cell proliferation and matrix deposition as confirmed with histological observations. OCE is also performed in the complex developing tissue of the Xenopus laevis (African frog) tadpole [111].

3.12 PERFORMANCE PARAMETER OF ELASTOGRAM

3.12.1 ELASTOGRAPHIC CONTRAST-TO-NOISE RATIO (CNRe)

In tissue strain imaging CNR_e is an important quantity which is important for identifying the existence of a specific lesion. Actually contrast resolution is hard to define as it has a considerable impact depends on the human observer as much as the quality of the actual image Detectability of lesions is possible by studying the noise and contrast properties of a given sample. Our goal lies in maximization of the detectability of a lesion of a given size by increasing contrast, while suppressing the noise. Actually the vital issue in elastography lies in strain estimation which is related to noise. This strain estimation noise is unfortunately coupled nonlinearly with strain. This makes the increase the strain contrast also increases the noise artifacts. Equation (5) appropriately expresses the CNR_e,

$$CNR_e = \frac{2(m_{\hat{\varepsilon}_l} - m_{\hat{\varepsilon}_b})^2}{\sigma^2_{\hat{\varepsilon}_l} + \sigma^2_{\hat{\varepsilon}_b}} \quad \ldots\ldots\ldots\ldots\ldots\ldots\ldots\ldots\ldots\ldots\ldots\ldots\ldots\ldots\ldots\ldots\ldots\ldots (3.1)$$

where $m_{\hat{\varepsilon}_l}$, $\sigma_{\hat{\varepsilon}_l}$, $m_{\hat{\varepsilon}_b}$ and $\sigma_{\hat{\varepsilon}_b}$ are mean and standard deviation of strain in the lesion and background respectively.

3.12.2 ELASTOGRAPHIC SIGNAL-TO-NOISE RATIO (CNRe)

The signal-to-noise ratio expressed as SNR_e in brief is an important parameter related to sensitivity of strain estimation. The elastographic signal-to-noise ratio characterizes the noise of the elastographic system at which a value of strain is estimated. SNR_e can be defined by following expression,

$$SNR_e = \frac{m_{\hat{\varepsilon}}}{\sigma_{\hat{\varepsilon}}} \quad \text{..... (3.2)}$$

where $m_{\hat{\varepsilon}}$ denotes the statistical mean strain estimate and $\sigma_{\hat{\varepsilon}}$ denotes the standard deviation of the strain noise estimated from the elastogram.

3.13 RESOLUTION OF ELASTOGRAM

In more specific language it is called spatial resolution .Though a unique definition of resolution is hard to find as its measurement may vary according to the definition. The spatial resolution of a image is the number of distinct pixels (smallest addressable screen element or smallest unit of a picture that can be controlled) in each dimension that can be displayed. One of the fields in which resolution has been explicitly defined is optics. It is one of the primary parameters utilized to characterize the performance of an imaging system. In an optical system resolution is regarded as a measure of the ability of the system to distinguish between two closely spaced point sources and it is related to point spread function of a system. In sonography, the instrumental ability of resolving two closely spaced reflecting boundaries in the axial direction. A simplified theoretical expression for the sonographic axial resolution (R) for a spherical radiator focus is given by:

$$R = \frac{(Q_f \times \lambda)}{4} \quad \text{..... (3.3)}$$

here Q_f represents the quality factor of the transducer and λ is the wavelength. From equation it is clear that by higher transducer fractional bandwidth (Q=1/fractional bandwidth) at a constant wavelength, improved sonographic axial resolution is possible. Another way to improve it to increase the frequency that means decreasing the wavelength (λ) at a given Q_f.

3.14 NOISE IN ELASTOGRAM

In general, elastograms exhibit good spatial and parametric resolution. The elastograms of phantoms with homogeneous elastic properties exhibit a noisy appearance. Since this noisy appearance is

not directly related to ultrasonic speckle in conventional B-scans, we refer to it as elastographic noise. At least two factors contribute to the noisy appearance of elastograms. First, while the elasticity of synthetic foam phantoms we have used is globally homogeneous, some real local variability is expected. Second, errors in the time shift correlation estimations result in a temporal uncertainty that causes random noise in the local strain estimates, and ultimately noise in the elastogram [112].

3.15 CHAPTER SUMMARY

Fundamental concepts in Elastography have been introduced and discussed in this chapter. Different types of excitation methods and their comparative discussion have been incorporated. Estimation of Time delay from the strain information obtained through cross-correlation technique has been discussed with necessary details. Especially, the effect of decorrelation in elastogram which is the ultimate product of any elastographic methodology has been pointed out in a brief manner. Explanation of Data widow and its importance in estimating the time delay has been discussed thoroughly. In addition to that, different elastographic methods and their relative comparisons have been incorporated. Lastly, various performance parameters and their effect on Elastogram have been introduced too.

CHAPTER IV

STRAIN IMAGING, TECHNIQUES AND PARAMETERS RELATED TO IT

4.1 INTRODUCTION

The relative stiffness of soft biological tissues, as described by strain images, has the potential to be a sensitive indicator of some pathological growth inside human body. Strain images are formed from measurements of local displacements induced by compressive forces applied to tissue surfaces. The displacement fields are estimated using correlation techniques that track echo delays in segmented waveforms recorded before and after static compression. Several techniques use signals from imaging systems to form diagnostic images that describe the spatial and temporal distributions of tissue elasticity, in vivo. Already in literature, a vivid description of several strain estimation techniques does exist namely: 2D Companding, Doppler US imaging, Temporal Stretching, Adaptive Stretching, Speckle Tracking etc. We will try to extract the gist of these strain imaging techniques. The parameters which influence the overall elastographic method will be introduced in a concise form too.

4.2 STRAIN IMAGING

Strain imaging concept stands on the process of compressing the tissue and this is the solution to have strain. The compression technique inherently related to the decorrelation between the RF signals. Though decorrelation itself is used for the finding of the delay & strain but it is also a fact that it is the cause of degradation of performance of delay and strain estimators.

If we express pre and post compression signals as following expression,

$$y_1(t) = x_1(t) + r_1(t) = x(t) * h(t) + r_1(t) \quad \text{.....(4.1)}$$

and

$$y_2(t) = x_2(t) + r_2(t) = x(t/a - D) * h(t) + r_2(t) \quad \text{.....(4.2)}$$

The strain $\hat{\varepsilon}$ can be estimated for small strains using the following expression

$$\hat{\varepsilon} \approx 1 - \rho_{12} \quad \text{.....(4.3)}$$

ρ_{12} in eq^{n} (4.3) is the correlation coefficient between the pre- and post-compression signals.

Here $x_1(t)$ and $x_2(t)$ are the signal of interest , $x(t)$ is the one-dimensional scattering distribution of elastic target, $h(t)$ is the impulse response of ultrasonic system or point spread function (PSF), $r_1(t)$ and $r_2(t)$ are the independent zero mean white noise sources (uncorrelated radiation of random noise). $a = 1 - \varepsilon$ is related to strain ε. D is the differential time delay.

A well-established method to calculate the differential time delay, D is to compute the cross-correlation function.

$$R_{x_1x_2}(\tau) = E\{x_1(t)x_2(t+\tau)\} = aR_{xx}(\tau - D) + R_{r_1r_2}(\tau) \quad \text{.....(4.4)}$$

where τ is a variable time , $E\{\bullet\}$ is expectation, $R_{xx}\{\bullet\}$ is autocorrelation function of $x(t)$ and $R_{r_1r_2}\{\bullet\}$ is the cross-correlation of noise. If $r_1(t)$ and $r_2(t)$ are mutually independent processes then $R_{r_1r_2}(\tau) = 0$ .The time delay D can be estimated when the maximizing function $R_{x_1x_2}(\tau)$ with respect to the parameter τ.

$$D = \arg\max_{\tau} R_{x_1x_2}(\tau) \quad \text{.....(4.5)}$$

By the Fourier transformation of $R_{x_1x_2}(\tau)$, the cross-spectral density (CSD) function $G_{x_1x_2}(\omega)$ can be obtained. Here it is the fact that $R_{x_1x_2}(\tau)$ and $G_{x_1x_2}(\omega)$ are the Fourier transform pair. The computation of the cross-correlation function is simpler in the frequency domain.

$$F\{R_{x_1x_2}(\tau)\} = G_{x_1x_2}(\omega) = aG_{xx}(\omega)e^{j\omega D} + G_{r_1r_2}(\omega) \quad \text{.....(4.6)}$$

If $r_1(t)$ and $r_2(t)$ are non-correlated, then $G_{r_1r_2}(\omega)=0$ .In these case, the cross-spectral density spectrum CSD, $G_{x_1x_2}(\omega)$, becomes the scaled version of $G_{xx}(\omega)$,multiplied by a complex exponential function. In practice, only the estimates $\hat{G}_{x_1x_2}(\omega)$ of $G_{x_1x_2}(\omega)$ and $\hat{R}_{x_1x_2}(\tau)$ of $R_{x_1x_2}(\tau)$ can be obtained from the finite number of observations of signals $x_1(t)$ and $x_2(t)$ .The Generalized Cross-Correlation function(GCC) is obtained by the inverse Fourier transformation of (4.2) that is:

$$\hat{R}_{x_1x_2}(\tau)=\int_{-\infty}^{\infty} W(\omega)G_{x_1x_2}(\omega)e^{-j\omega\tau}d\omega \qquad \text{.....(4.7)}$$

where $W(\omega)$ is a weight or window function. In order to smooth the estimated cross-correlation, various window functions can be used to make possible a more accurate estimation of time delay between signals. The argument τ which maximizes the estimated $\hat{R}_{x_1x_2}(\tau)$ is ideally equal to the time delay D. Under ideal conditions, it is easy to exactly determine the location of dominant peak of the differential delay between the signals of the sane source. When a good number of delays are contained by the cross-correlation function, it becomes difficult as we try to extract one peak.

4.3 VARIOUS STRAIN ESTIMATORS

4.3.1 2D COMPANDING

Companding process is used mainly in signal processing applications to have better precision where we do time delay measurements on correlation basis. This technique is applied to minimize decorrelation errors, which are the dominant source of noise in the way of generating strain image. Companding includes both expansion and compression. The word refers to a spatially variable signal scaling that compresses and expands waveforms acquired in an ultrasonic scan plane or volume [113]. 2D companding described by Chaturvedi et al. is based on a sum-absolute-difference (SAD) algorithm for blood velocity estimation.

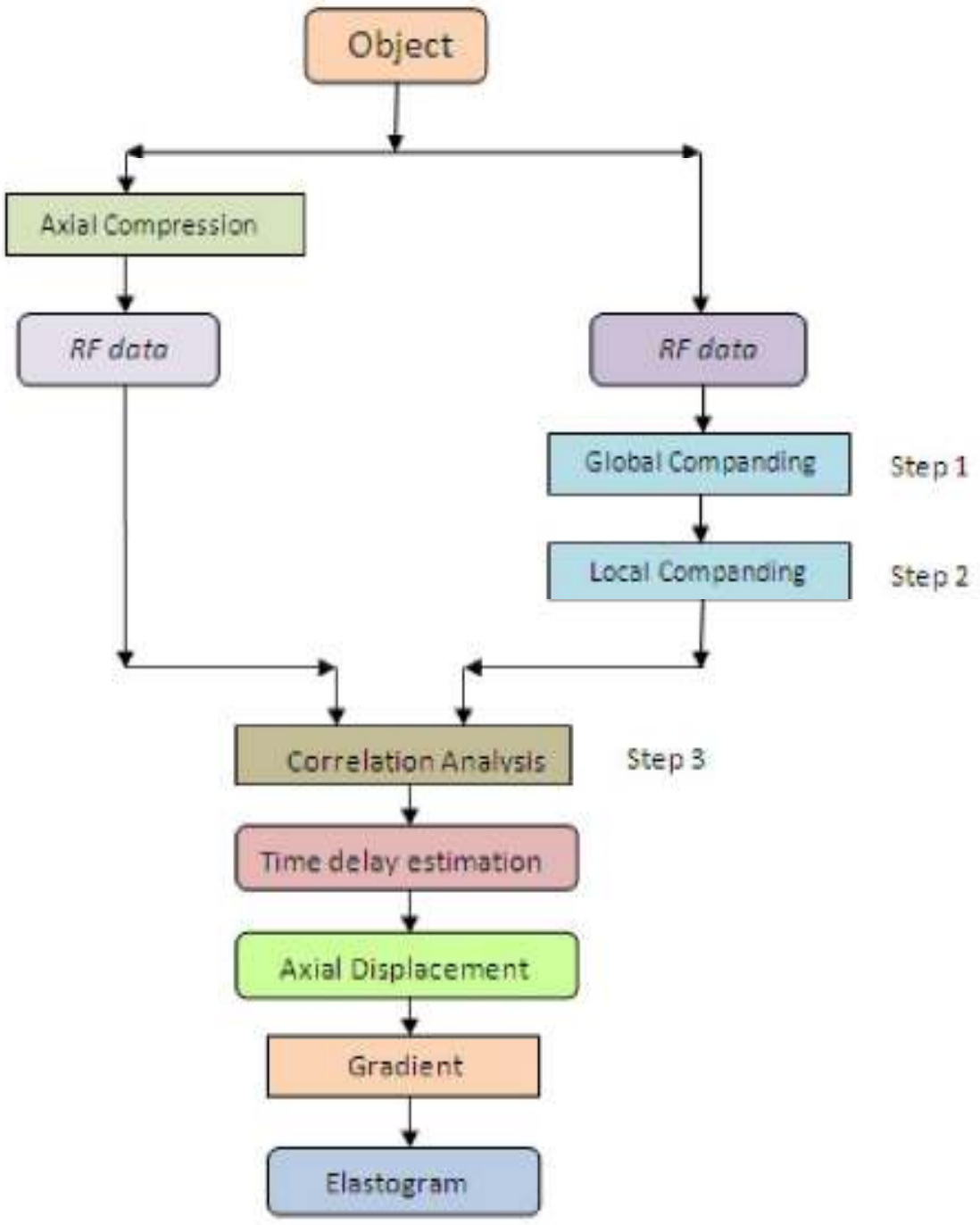

Figure4.1: Flow chart summarizing the algorithm of strain imaging by 2D-Companding.

4.3.2 SHEAR STRAIN COMPANDING

It is relatively a new imaging technique which can provide information on the bonding between a tumor and the surrounding tissue. The definitions of shear strain in general can be illustrated as the sum of the axial and lateral shear strain.

$$\varepsilon_{x,y} = \left(\frac{\partial x}{\partial v} + \frac{\partial y}{\partial u} \right)$$

where (y, x) are the lateral and axial displacement components along the v (lateral direction) and u (axial direction) axes, respectively. The degree of bonding between a tumor and the surrounding tissue influence the shear strain magnitude and pattern which may carry additional information. For a given amount decorrelation, the noise in the lateral shear strain estimates is approximately six times worse than that of noise in the axial shear strain estimates.

4.3.3 DOPPLER ULRTRASOUND IMAGING

Doppler ultrasound is based on the reflected sound waves to observe pattern of blood flow through a blood vessel. It gives the physicians to track the motion of blood flow through major arteries and veins, such as those of arms, legs and neck. A hand-controlled transducer is gently crossed over the skin above the blood vessel. The transducer sends and receives sound waves that are amplified through a microphone. Tissue deformation can also be assessed by the Ultrasound Doppler technique. The strain rate, i.e., the rate of deformation, of a tissue segment can be estimated from the issue Doppler data by calculating the spatial velocity gradient. Color Doppler uses standard ultrasound methods to produce a picture of a blood vessel. Also, a computer converts the Doppler sounds into colors that are overlaid on the image of the blood vessel and that represent the speed and direction of blood flow through the vessel.

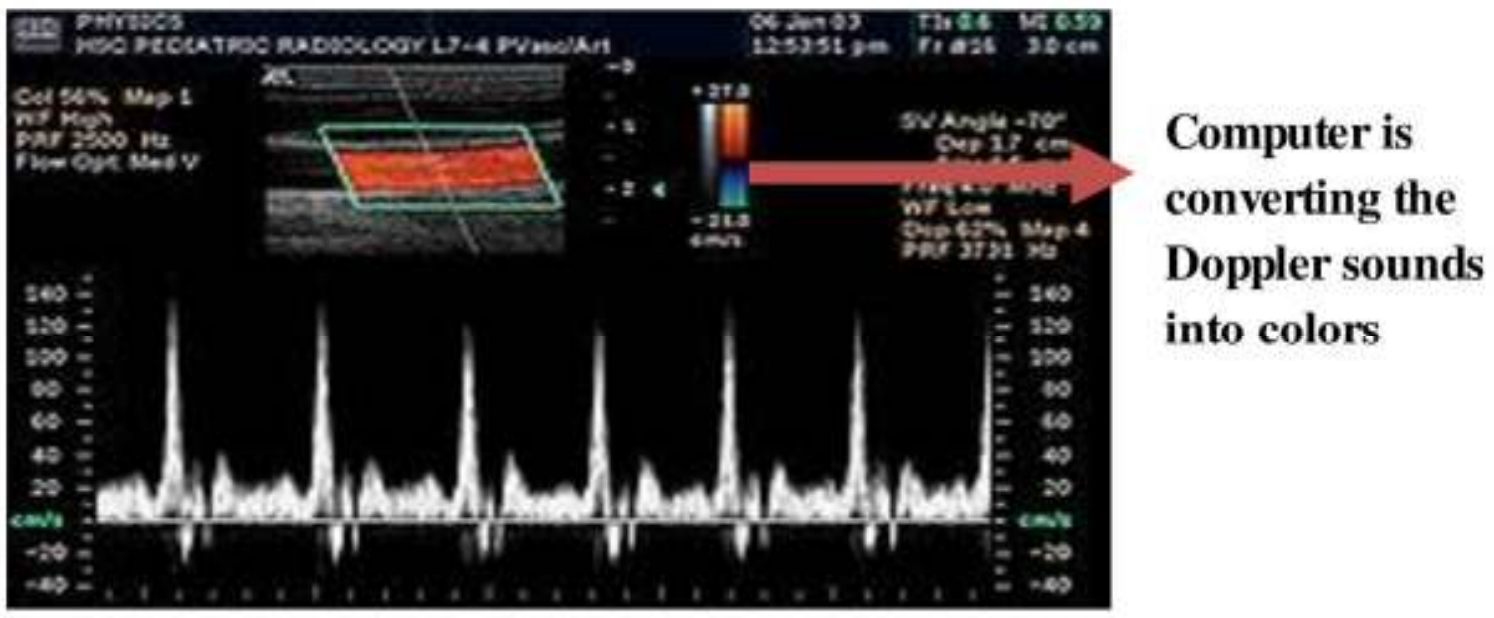

Figure 4.2: Doppler ultrasound imaging.

4.3.4 TEMPORAL STRETCHING

When tissue is compressed, unresolved scatters generally move closer together along the axial direction, resulting in a signal that can be quite different from that obtained in the post-compression state. Additionally, scatters move in the lateral and elevational directions, resulting in further signal decorrelation. Alam et al. discussed and assumed that the lateral and elevational decorrelation is small compared to the axial decorrelation when the target compared to the transducer [114]. The prime purpose of the temporal stretching technique of the post-compression signal is to align the two RF peaks with the pre-compression signal, which reduces signal decorrelation.

4.3.5 ADAPTIVE STRETCHING

Stretching the post-compression A-lines improves the correlation between the pre- and post-compression A-lines and reduces the strain noise. However, the use of a constant stretch factor (global stretching) is not optimal in the presence of strain contrast and an accurate prediction of the required stretch factor is difficult in practice. Adaptive time domain cross-correlation techniques overcome these difficulties by estimating strain in localized regions in the tissue. Adaptive stretching is mainly based on temporal stretching of the post-compression echo signals. Here the stretching factor is varied iteratively which is applied to the post-compression RF echo signal until the correlation coefficient function between the pre and post-compression signal is maximized. The gradient operation introduces significant amount of noise into the strain estimates. But no gradient method is associated with the adaptive stretching method.

4.3.6 STRAIN IMAGING BY SPECKLE TRACKING

Speckle is the natural characteristics of ultrasound images. It is caused by local variations in intensity in an ultrasound image. The texture of the speckle pattern does not correspond to the underlying structure that is being imaged. Speckle is a random, deterministic interference pattern generated by the reflected ultrasound signal. The reflected ultrasound beams creates irregular interference patterns in the ultrasound image. The interference pattern depends on the frequency and the shape of the transmitted pulse and it depends on the beam width of the pulse.

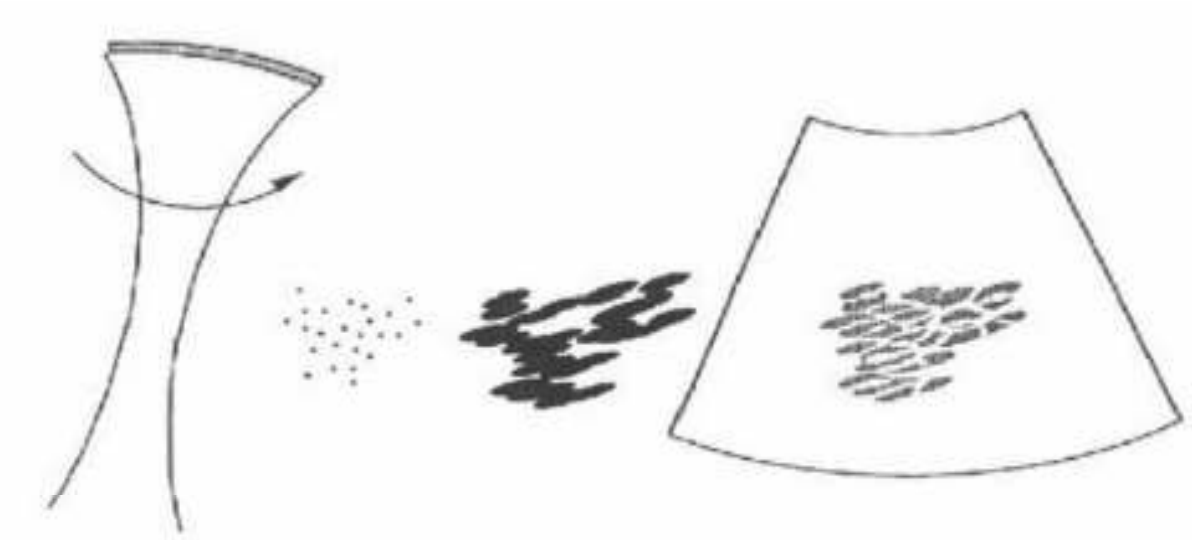

Figure 4.3: Interference between the signals from many close point targets is creating speckle in the image as seen to the right [115]

Speckle tracking is a method that is being used by cardiologists to visualize the left ventricle wall movement during a heart cycle. By examining the wall movement in the ultrasound image, it is possible to determine how large an area is affected by myocardial infarction. Now a day's speckle tracking method

is used for strain imaging which is done mainly on heart. This processing can produce high resolution maps of the time derivative of the strain magnitude. Such images complement tissue velocity images (TVI), providing a more complete description of cardiac mechanics.

4.3.7 SPECTRAL STRAIN ESTIMATION

In general, the goal of spectral estimation is to determine the spectral content of a stationary random process based on a finite sequence of data. In spectral elastography, strain is directly related to the shift between a set of pre- and post-compressed spectral signals. It is assumed that by maximizing the spectral estimation accuracy, we can do the same for the subsequent strain estimates.

4.4 DIFFERENT PARAMETERS IN THE OVERALL ELASTOGRAPHIC METHOD

- Ultrasonic parameters
  - ✓ Transducer center frequency, f_c
  - ✓ Bandwidth, B
  - ✓ sampling frequency
- DSP parameters
  - ✓ window size, W
  - ✓ window overlap/shift ,ΔW
- Mechanical parameters
  - ✓ Applied Strain
  - ✓ Elastic Modulus
  - ✓ effective Poisson's ratio and boundary conditions

4.5 INTERPOLATION

Interpolation is the construction of a function that matches given data values $\mathbf{y_i}$, at given data sites x_i, in the sense that $f(x_i)=y_i$, all i. The interpolant f is usually constructed as the unique function of the form

$$f(x) = \sum_j f_j(x) a_j$$

That matches the given data, with the f_j chosen 'appropriately'. Many considerations might enter the choice .One of these considerations is sure to be that one can match in this way arbitrary data. For example, polynomial interpolation is popular because, for arbitrary **n** data points (x_i, y_i) with distinct data sites, there is exactly one polynomial of order n-1 that matches these data. Explicitly choosing the f_j in the above "model" to be

$$f_j(x) = \prod_{i \neq j} (x - x_i)$$

which is an **n-1** degree polynomial for each **j.** $f_j(x_i) = 0$ for every $i \neq j$ but $f_j(x_i) \neq 0$ as long as the x_i are all distinct. Set $a_j = y_j / f_j(x_i)$ so that

$$f(x_i) = f_j(x_i) a_j = y_j \text{ for all } j$$

4.5.1 LINEAR INTERPOLATION

Linear interpolation is the simplest method of getting values at positions in between the data points. The points are simply joined by straight line segments. Each segment (bounded by two data points) can be interpolated independently.

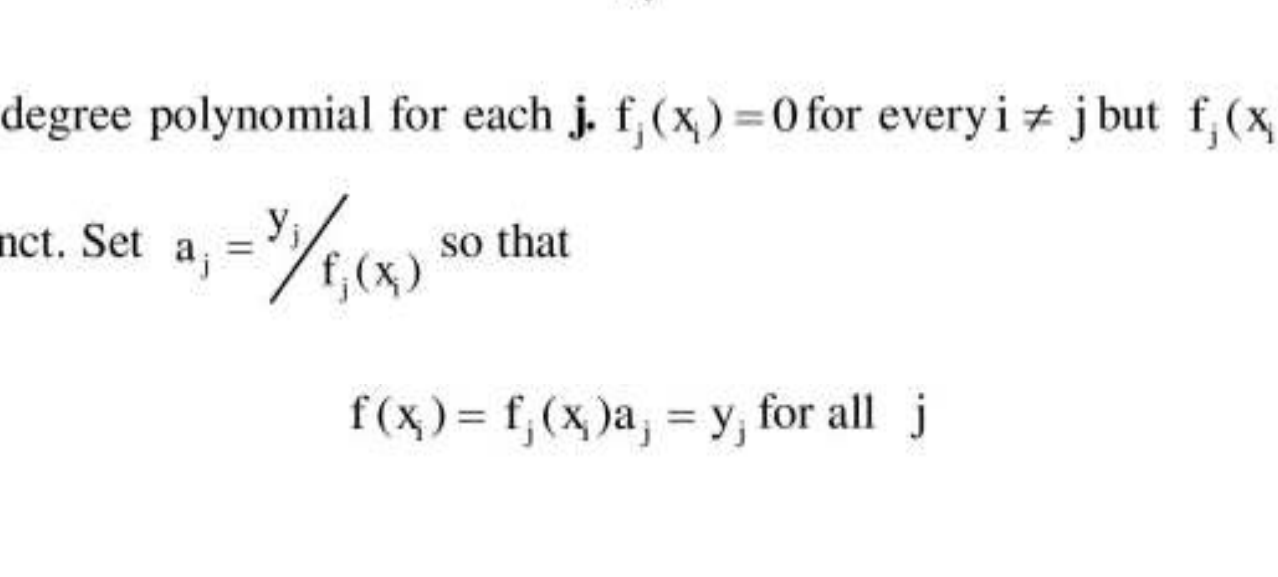

Figure 4.4: Linear Interpolation

4.5.2 PARABOLIC INTERPOLATION

Let us consider a triplet (*a, b, c*) that brackets a minimum, we approximate the objective function in the interval (*a, c*) with the parabola fitting the triplet. Then we find the minimum of this parabola with the formula .If we want to find the abscissa we have to apply *inverse parabolic interpolation.*

$$x = b - \frac{1}{2} \times \frac{(b-a)^2[f(b)-f(c)] - (b-c)^2[f(b)-f(a)]}{(b-a)[f(b)-f(c)] - (b-c)[f(b)-f(a)]}$$

This method is useful only when the function is quite smooth in the interval, but it has the advantage that the convergence is almost quadratic, and it is perfectly quadratic when the function to be optimized is a quadratic form.

4.6 CHAPTER SUMMARY

In this chapter, we have introduced strain imaging concept and computation of strain from that. Relationship between pre and post-compressed RF-echo signals has been established quantitatively. Various strain estimators such as: Companding, Stretching, Speckle tracking etc. have been introduced and discussed briefly. Additionally, different parameters in the overall elastographic method have been incorporated concisely. Lastly, a brief discussion has been presented the use of Interpolation in strain imaging technique.

CHAPTER V

MATERIALS AND METHODS

5.1 INTRODUCTION

Robust strain estimation is important in elastography. We will try to discuss a novel strain estimation approach that reduces noise in strain images while maintaining good resolution. A strain image is formed by estimating strain throughout a tissue cross correlation by segmenting echoes along each scan line into overlapping temporal windows. Strain is usually estimated by computing the local gradient of displacement estimates due to external compression; local tissue displacements are estimated using cross correlation analysis between gated pre and post compressed RF echo data sets. However, the gradient operation is noisy inherently. To eliminate noise from gradient operations, several methods have been developed namely LSQSE (Least-Squares Strain Estimator), Adaptive Stretching, Temporal Stretching etc. Although these methods have provided reduced noise in Elastogram, but they suffer from resolution problem. We have developed a method based on the least-squared-error-based 2D plate smoothing-spline, which does not suffer from the limitations of the above methods. Results from data generated by finite element simulation and phantom experiments show that the smoothing-spline-based strain estimator produces low-noise strain estimates without degrading the resolution.

5.2 SPLINES

This spline consists of weights attached to a flat surface at the points to be connected. A flexible strip is then bent across each of these weights, resulting in a pleasingly smooth curve. The mathematical spline is similar in principle. The points, in this case, are numerical data. The weights are the coefficients on the cubic polynomials used to interpolate the data. These coefficients 'bend' the line so that it passes through each of the data points without any erratic behavior or breaks in continuity. Spline interpolation is preferred over polynomial interpolation because the interpolation error can be made small even when using low degree polynomials for the spline.

Suppose we are considering a set $S := \Pi^{\mu}_{\xi,k}$ of all (scalar-valued) piecewise-polynomials of order k with breaks $\xi_1 < ..... < \xi_{l+1}$ that, for $i=2.....l$, may have a jump across ξ_i in its μ_i th derivative but have no jump there in any low order derivative. This set is a linear space, in the sense that any scalar multiple of a function in S is again in S, as is the sum of any two functions in S.

Accordingly, S contains a basis (in fact many bases), that is, a sequence $f_1 ..... f_n$ so that every f in S can be written uniquely in the following form :

$$f(x) = \sum_{j=1}^{n} f_j(x) a_j \text{ for suitable } a_j$$

The number n appearing here is the dimension of the linear space S. The coefficients $\mathbf{a_j}$ are often referred to as the coordinates of **f** with respect to the basis.

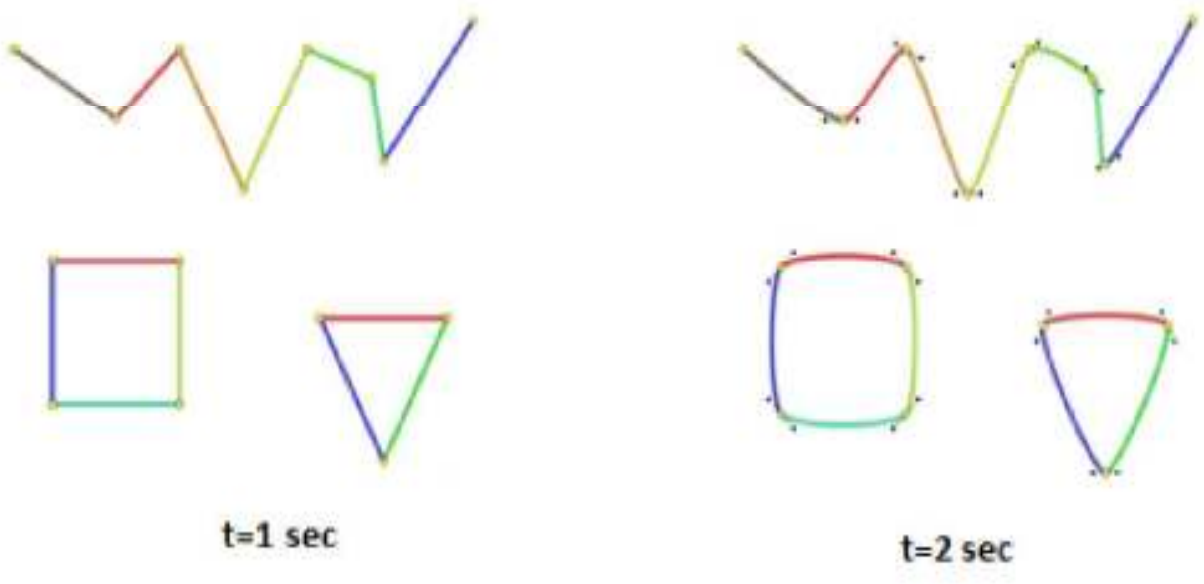

Figure 5.1: Position of the spline knots in smoothing a function

5.3 SMOOTHING SPLINE

If the data is noisy, we may try to fit it using a smoothing spline. The smoothing spline s is constructed for the specified smoothing parameter p and the specified weights w_i . The smoothing spline minimizes

$$p\sum_i w_i(y(x_i)-\hat{y}(x_i))^2+(1-p)\int\left(\frac{d^2\hat{y}}{dx^2}\right)^2 dx$$

Here w_i is the specified weight. $\hat{y}$ is a piecewise, three times differentiable, cubic polynomial. Strain is estimated by computing the gradient of the smoothing spline $\hat{y}$. A smoothing spline is also called a natural spline in numerical analysis literature. If the weights are not specified, they are assumed to be 1 for all data points.pis defined between 0 and 1. p = 0 produces a least-squares straight-line fit to the data, while p = 1 produces a cubic spline interpolant. If the smoothing parameter is not specified, it is automatically selected in the range near $1/(1+h^3/6)$ where h is the average spacing of the data points, and it is typically much smaller than the allowed range of the parameter.

5.4 THIN PLATE SMOOTING SPLINE

The thin plate spline (TPS) is an effective tool for modeling coordinate transformations that has been applied successfully in several computer vision applications. The thin plate spline (TPS) is a commonly used basis function for representing coordinate mappings from $R^2 \rightarrow R^2$. The thin plate spline is the 2D generalization of the cubic spline.

Thin Plate Smoothing Spline mainly used in 3D Image Recovery, Finger Print Analysis, Image Warping, Medical Image Analysis, Data Mining.

Let v_i denote the target function values at locations (x_i, y_i) in the plane with i=1, 2…..,p. In particular, we will set v_i equal to the target coordinates (x_i', y_i') in turn to obtain one continuous transformation for each coordinate .We assume that the locations (x_i, y_i) are all different and are not collinear. The TPS interpolant $f(x, y)$ minimizes the bending energy

$$I_f=\iint_{R^2}(f_{xx}^2+2f_{xy}^2+f_{yy}^2)dxdy$$

And has the form

$$f(x, y) = a_1 + a_x x + a_y y + \sum_{i=1}^{p} w_i U(\|(x_i, y_i) - (x, y)\|)$$

where $U(r)=r^2 \log r$. In order for f(x,y) to have square integrable second derivatives, we require that

$$\sum_{i=1}^{P} w_i = 0$$

and

$$\sum_{i=1}^{P} w_i x_i = \sum_{i=1}^{P} w_i y_i = 0$$

Together with the interpolation conditions, $f(x_i, y_i) = v_i$ this yields a linear system for the TPS coefficients:

$$\begin{bmatrix} K & P \\ P^T & O \end{bmatrix} \begin{bmatrix} w \\ a \end{bmatrix} = \begin{bmatrix} v \\ o \end{bmatrix}$$

where $K_{ij} = U(\|(x_i, y_i) - (x_j, y_j)\|)$,the i^{th} row of P is $(1, x_i, y_i)$ .O is 3×3 matrix of zeros. o is a 3×1 column vector of zeros, w and v are column vectors formed from w_i and v_i ,respectively and a is column vector with element a_1,a_x,a_y.We will denote the $(p+3)\times(p+3)$ matrix of this system L. L is nonsingular. If we denote the upper left $p \times p$ block of L^{-1} by L_p^{-1} .then it can be shown that

$$I_f \alpha v^T L_p^{-1} v = w^T K w$$

When there is noise in the specified values v_i , one may wish to relax the exact interpolation requirement by means of regularization. This is accomplished by minimizing

$$H|f| = \sum_{i=1}^{n} (v_i - f(x_i, y_i))^2 + \lambda I_f$$

The regularization parameter λ, a positive scalar, controls the amount of smoothing; the case of $\lambda=0$ reduces the exact interpolation.

5.5 SIMULATION AND ANALYSIS OF THE DATA

We've use the Finite Element Model Analysis simulation phantom for checking the performance of different salient features of the proposed methods. A rectangular phantom of 20 mm × 20 mm was simulated using the software named Algor (Algor, Inc., Pittsburgh, PA) by FEM method. It has a homogeneous background with the stiffness of 60 KPa with two circular inclusions. We have chosen 60 KPa as stiffness because it is close to the average stiffness of normal glandular tissue in the breast [116]. Both the circular inclusions are 7.5 millimeter (mm) in diameter which is embedded in the phantom. The stiffness of these four inclusions are also different from each other; top inclusion is +10 dB (10 times) and the bottom inclusion is +40dB (10,000 times) stiffer than their background. The bottom of the phantom was placed on a planar surface and the phantom was in full free-slip condition (allowed to expand) at top and bottom surfaces. During the simulation, the Poisson's ration was used as 0.495. The phantom was compressed from the top using a larger-width planar compressor.

An ultrasonic transducer was used to scan the phantom from the top (center frequency, f_o= 5 MHz, band-width = 60%). A non-directing transducer beam was simulated with a beam width of 1.5 mm. The total number of A-lines was 128. Random white noise was added to simulate a sonographic SNR of 40 dB. Despite the uniform stiffness background, the strain variations occur in the back ground region due to interaction between lesions. With the increase of the percentage applied strain there will be distortion which is sometimes almost random in case of the inclusions compared to their background.

For the numerical analysis and all kinds of computation was done using MATLAB (The Mathworks™ Inc.).

Variable Editor - Data

File Edit View Graphics Debug Desktop Window Help

Stack: Base | No valid plots for: Data(1,1)

Data <1891x128 double>

	1	2	3	4	5	6	7	8	9	10	11
1	138	1	1	1	1	1	1	1	1	1	1
2	130	1	1	1	1	1	1	1	1	1	1
3	140	1	1	1	1	1	1	1	1	1	1
4	125	1	1	1	1	1	1	1	1	1	1
5	110	1	1	1	1	1	1	1	1	1	1
6	114	0	0	0	0	0	0	0	0	0	0
7	98	196	239	231	234	237	224	201	168	165	196
8	86	190	246	262	260	253	256	268	262	260	220
9	81	186	227	271	245	222	230	233	230	245	262
10	65	202	244	258	271	277	267	246	243	237	246
11	59	188	240	262	256	251	238	237	248	246	238
12	48	190	207	221	200	184	184	170	145	168	195
13	39	197	241	247	249	235	241	247	235	222	214
14	37	152	220	248	240	236	224	224	236	211	221
15	25	154	150	165	144	133	140	111	86	92	112
16	20	162	188	187	189	168	174	187	177	179	171
17	14	118	163	189	190	186	181	192	202	186	182
18	3	105	119	131	127	118	113	96	74	69	97
19	11	95	107	108	108	98	93	93	89	93	92
20	-2	83	97	96	80	72	71	87	111	112	98
21	-47	69	85	99	101	91	87	74	56	53	69
22	6	53	60	66	64	53	55	54	44	43	49
23	22	55	56	47	35	28	25	36	60	61	46
24	-64	43	57	65	62	59	50	39	22	21	34
25	-19	28	37	41	39	25	28	21	8	12	17
26	32	24	25	20	16	15	13	19	37	36	19
27	-43	15	15	20	24	22	16	14	0	-5	16
28	-37	20	15	-2	-18	-28	-31	-21	6	-11	-15
29	-14	15	48	56	70	82	92	55	27	72	53
30	-11	-56	-41	-6	18	-7	-34	-28	-67	-75	-48
31	-34	-37	-91	-141	-208	-234	-222	-196	-122	-166	-158
32	-39	64	71	74	87	138	162	120	97	175	165
33	-21	-50	13	79	122	99	53	57	31	0	-6
34	-22	-91	-143	-202	-274	-273	-291	-279	-234	-282	-256
35	-35	69	41	0	-19	0	63	91	96	142	147
36	-34	-21	31	100	164	157	130	122	96	79	52
37	-23	-63	-80	-100	-130	-139	-181	-213	-216	-224	-208
38	-31	-25	-51	-79	-118	-136	-104	-73	-54	-41	-35
39	-37	-1	-11	-16	-3	9	25	28	22	21	15
40	-27	-23	-13	-1	19	9	-22	-34	-42	-45	-52
41	-27	-45	-52	-66	-90	-94	-94	-96	-89	-92	-87
42	-36	-24	-42	-55	-74	-80	-64	-55	-57	-60	-41
43	-34	-18	-20	-21	-7	-19	-31	-31	-23	-15	-42

Figure 5.2: A snapshot of data from the MATLABs variable editor, There are 1891 rows and 128 columns where 128 indicates RF A lines

Our target is to get a better result on the Elastographic data. As stated before we used smoothing spline method to analyze the data. We have varied the percentage strain tried to figure out the output on the basis of that .We varied he strain like 1%, 2%, 4%, 6% and 8% and so on.

5.6 CHAPTER SUMMARY

In this chapter, we have discussed about Splines and its application in strain estimation. We have also discussed why Spline function is advantageous over Interpolation function. Different spline functions and their application have been incorporated concisely. We have also discussed about the simulation and data analysis and the use of Finite Element Model Analysis simulation phantom for checking the performance of different salient features of the proposed methods. With the variation of strain percentage, the resulting elastograms using smoothing spline function and their noise performance has also been shown.

CHAPTER VI

RESULT: PERFORMANCE OF ELASTOGRAM BY 2D PLATE SMOOTING SPLINE

6.1 INTRODUCTION

In Elastographic application, accurate and precise information regarding TDE is of profound importance. TDE is typically performed on sampled signals and delay estimates are usually desired over a continuous domain time delay estimator performance should be considered in conjunction with associated interpolation. In this particular chapter, we present our result which we have obtained employing the 2D plate smoothing method. How the variation of strain affects the performance of signal to noise ratio of in an elastogram that we will try to explore. Since, signal to noise ratio parameter is one of the important parameters which quantify the quality of an elastogram; therefore, our target is to maximize SNR_e by reducing Noise as much as possible. The effect of two important parameters related to spline mathematics on SNR_e will be depicted. We will also try to demonstrate another important parameter Contrast to Noise Ratio i.e. CNR_e which influences the performance of an elastogram.

6.2 RESULT BY VARIATION OF SIGNAL TO NOISE RATIO WITH THE VARIATION OF STRAIN

The transducer center frequency was 5 MHz as we have previously mentioned. After having the data digitally we can sample data according to our necessity .after that further processing is possible by changing the window length and then calculating the resolution value. In the following figure a plot is seen with two different sampling frequencies. Actually here f_o indicates the sampling frequency of the data used. We have taken sampling frequency of 20 MHz and the 30 MHz and then a resolution plot is generated where the intensity of resolution is calculated in millimeter (mm) scale .Obviously the higher sampling frequency will give us better resolution result which is clearly comprehensible from the Figure. 6.1 The maximum and the minimum ranges of the variation of error are also shown in the graph.

We will vary the resolution by changing the sampling frequency of data:

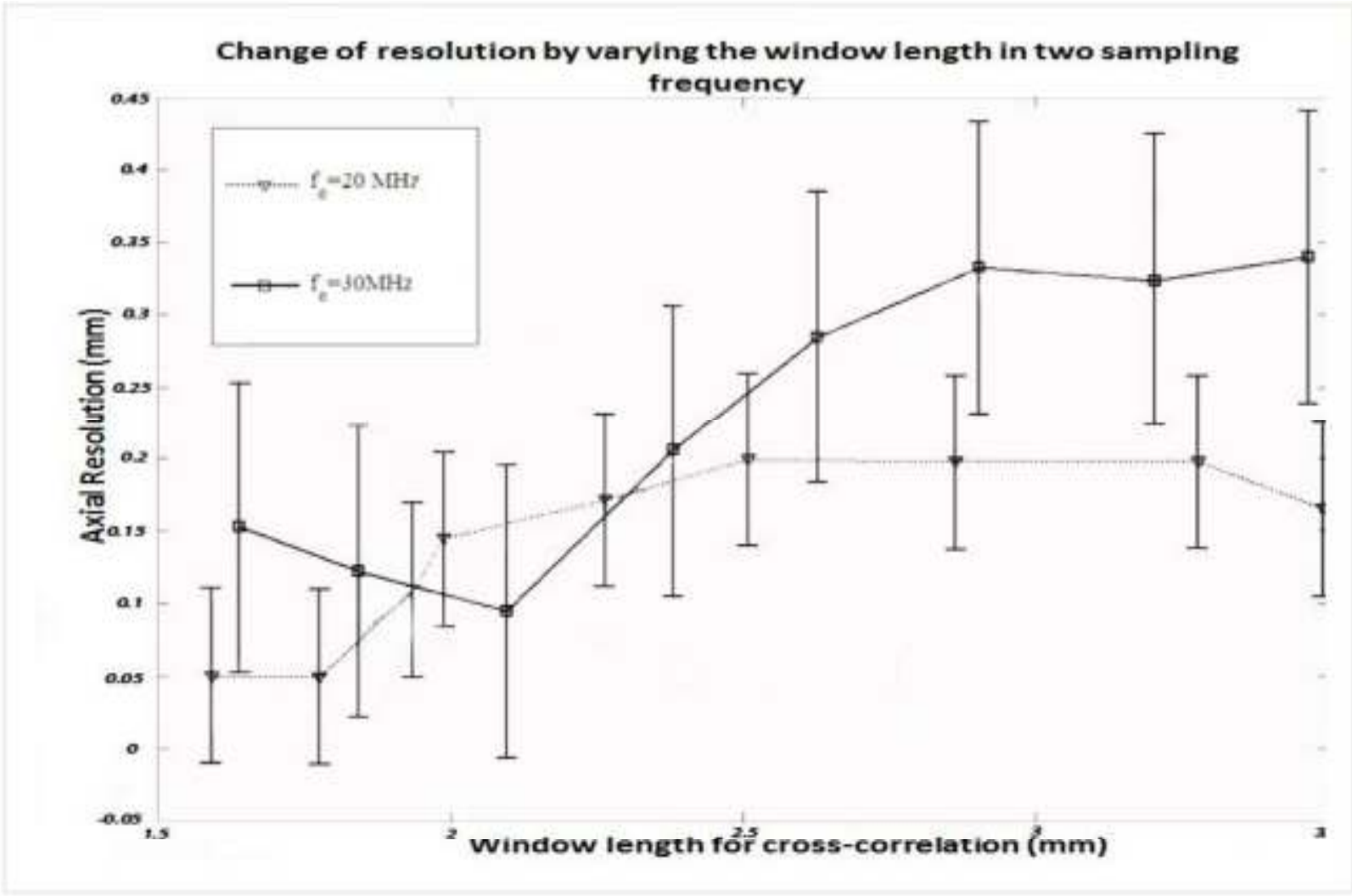

Figure 6.1: Change of resolution by varying the window length in two sampling frequency

Throughout this experiment the size of the window seems very much important analyzing the data and removing noise .We know that spreaded window means accepting more data that means in the frequency domain the leakage will be less. There was 192 A-lines and it was possible to manipulate all the data by upsampling or downsampling. We have shown the comparison taking the transducer center frequency being 20 MHz and 30 MHz (where bandwidth 50%). Then each case we have varied the window length in different ranges from 1.5 mm to 3.5 mm. Resolution is improved when the center frequency is improved.

6.3 VARIATION OF SNR_e WITH THE VARIATION OF APPLIED STRAIN:

We already explained earlier about the signal-to-noise ratio parameter which is one of the parameter to measure the quality of Elastogram. Here it is visible from the graph that the 2D spline showing better result in the lower strain where in the higher percentage values it is not showing as good performance as the adaptive stretching method.

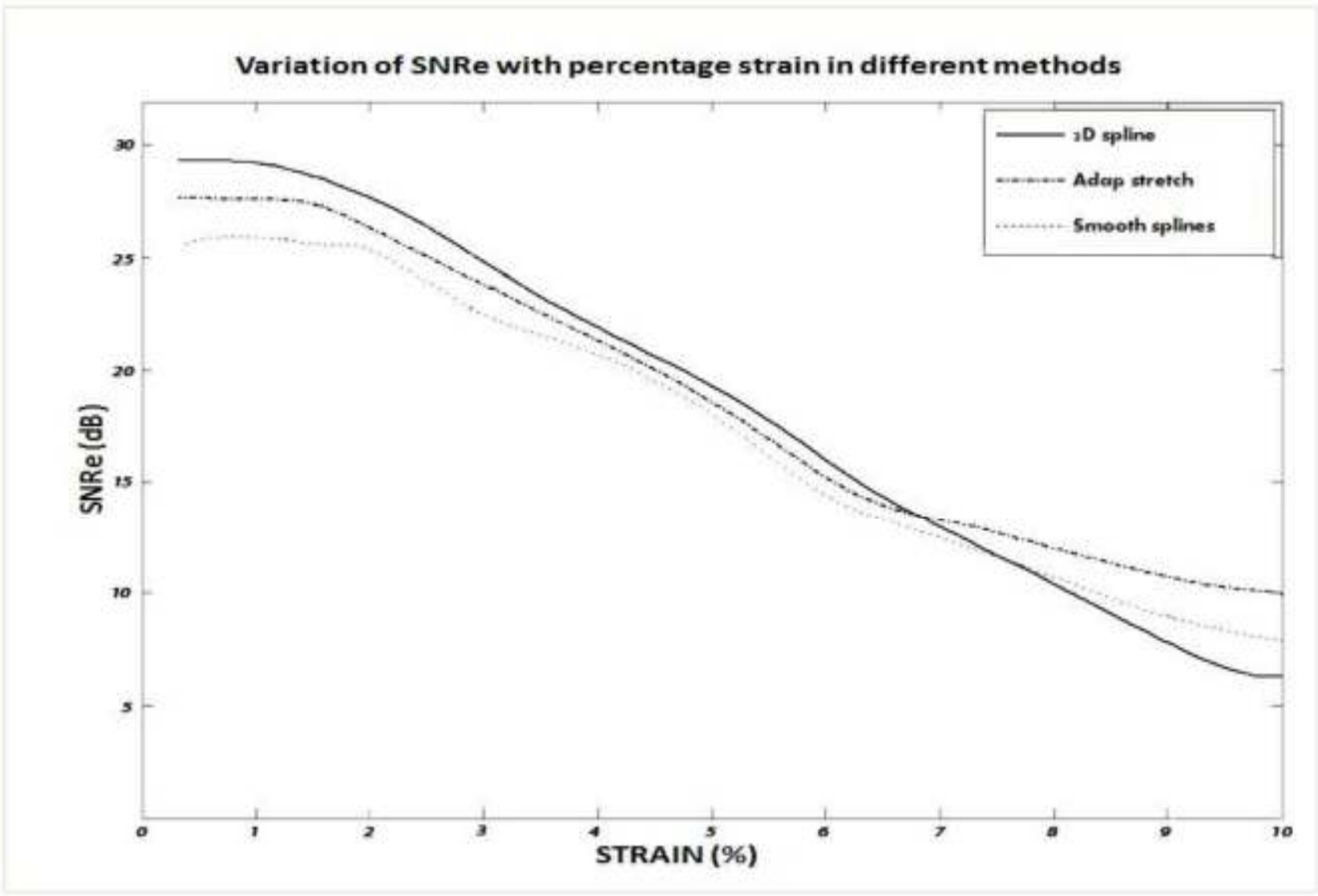

Figure 6.2: variation of signal-to-noise ratio with percentage strain in different methods

6.4 EFFECT OF SMOOTHING PARAMETER ON SNR_e

We have already mentioned about the following spline mathematics,

$$p\sum_i w_i\left(y(x_i)-\hat{y}(x_i)\right)^2+(1-p)\int\left(\frac{d^2\hat{y}}{dx^2}\right)^2 dx$$

in the MATLAB's tpaps function there was a specific parameter , p ,we changed that parameter and then observed the output and it looks like the following. Though we are not actually that much focused on the intricate mathematics which is related and manipulating the spline functions used in MATLAB, we are just using it and as input we are just giving the parameter as input. According to the spline mathematics lower p means more smoothing. More smoothed data means less noisy approximation which leads to the increases signal-to-noise ratio.

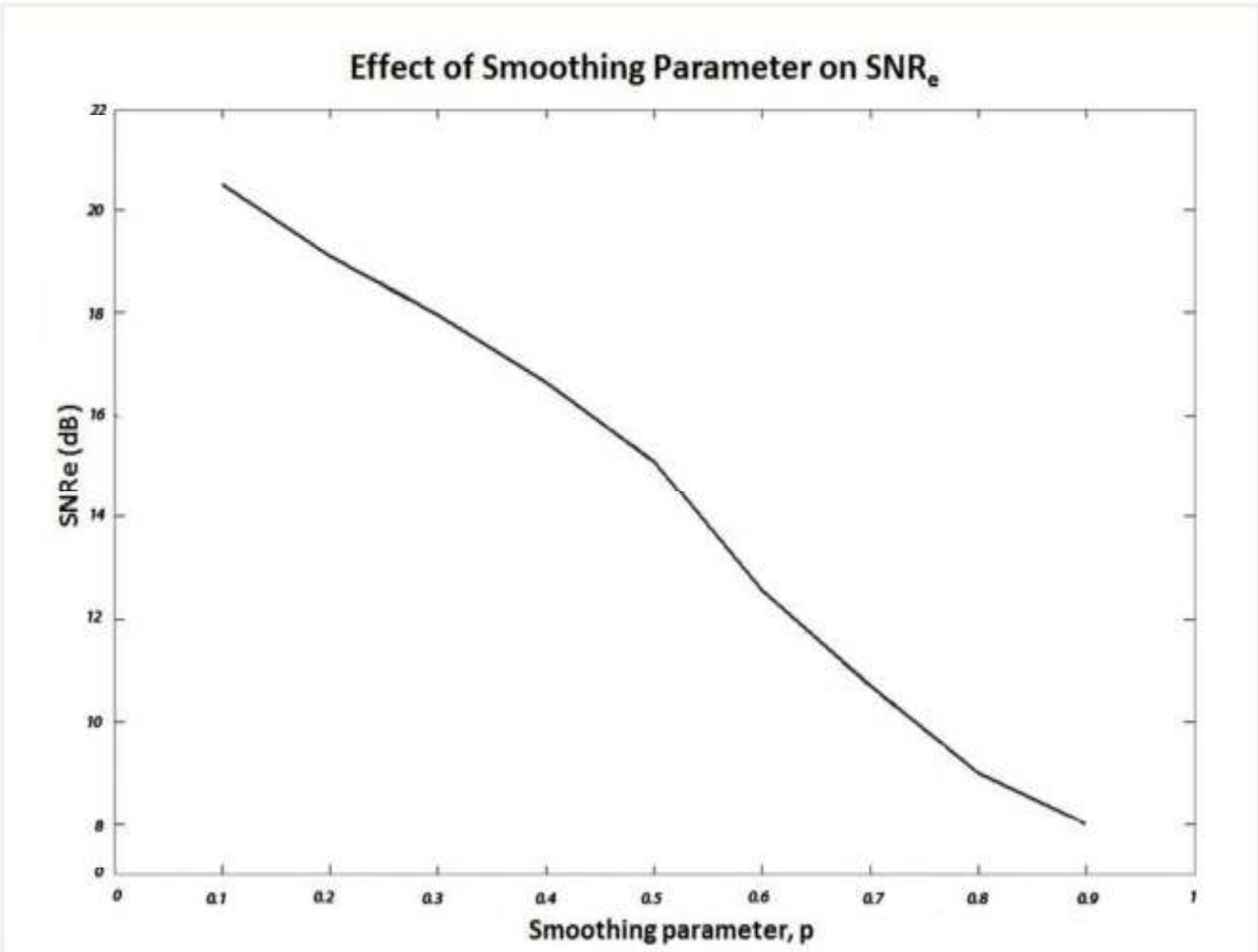

Figure 6.3: Effect of Smoothing Parameter on SNR_e

6.5 CHANGE IN CNR_E WITH VARIATION OF WEIGHT

We have option to vary the weight, w_i(of the spline equation mentioned in previous topics)and then see the variation of the CNR_e and the SNR_e. If we define c as the correlation value corresponding to the displacement estimate then w_i is expressed as $w_i=c^i$ where i=0, 1, 2, 3, 4, 5.....etc. So $w_i=1$, c, c^2,c^3 and so on. We know for displacement estimate we need information of time delay estimation and for that correlation technique is necessary.

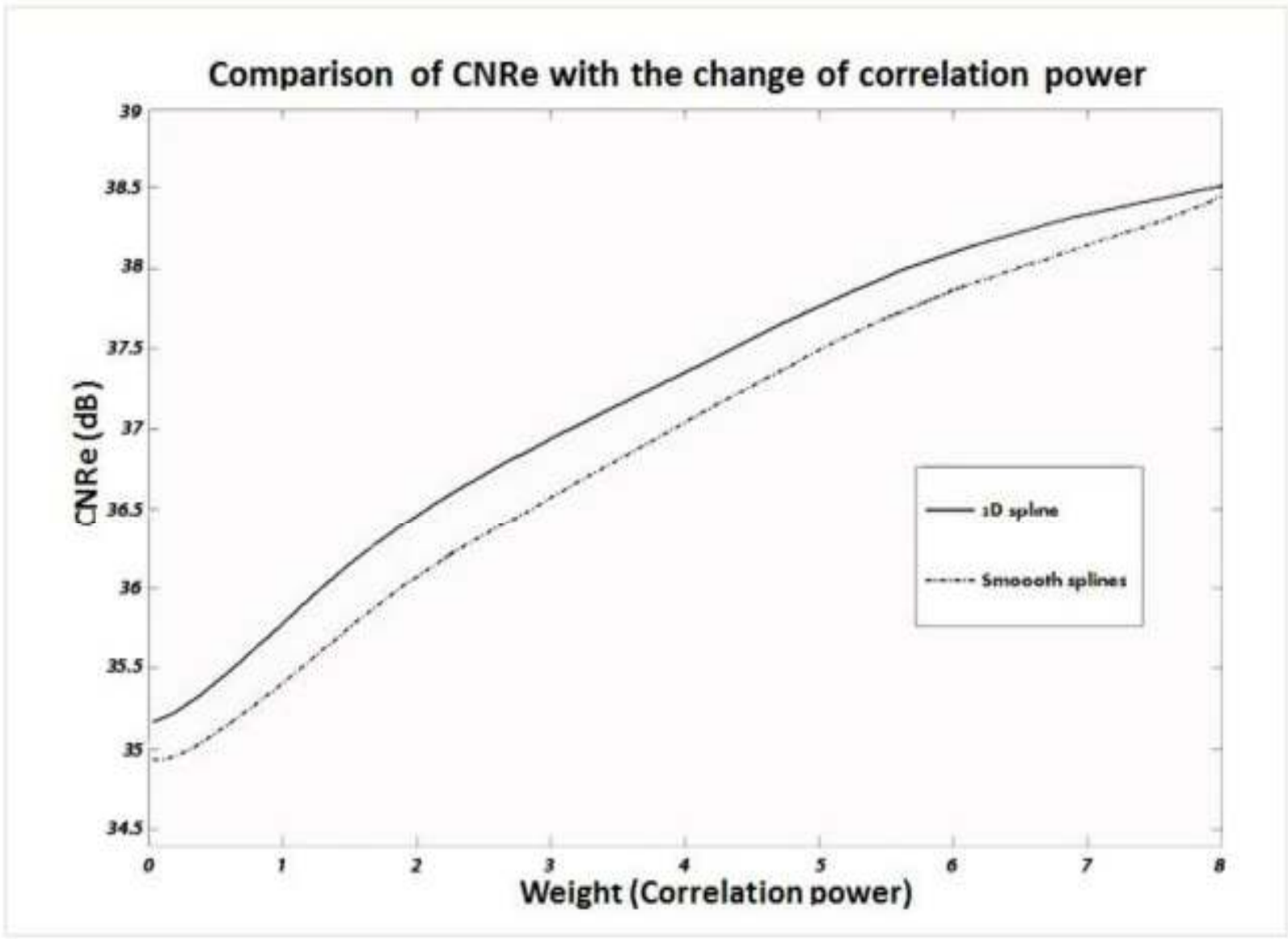

Figure 6.4: Comparison of contrast -to-noise ratio with the change of correlation power

Displacement of the tissue in the axial direction which is a resulting effect of the application of an external quasi-static compression can be computed using the cross-correlation technique.

$$E(k) = \frac{\Delta t(k) - \Delta t(k-1)}{\Delta T}$$

Here E(k) is the average strain which is calculated from the k^{th} and $(k-1)^{th}$ RF echo segments , ΔT is the time interval between the k^{th} and $(k-1)^{th}$ segments; $\Delta t(k)$ and $\Delta t(k-1)$ respectively, are the estimated time shifts of the k^{th} and $(k-1)^{th}$ echo segments due to compression. The time shift $\Delta t(k)$ can be determined by locating the maximal peak of the cross-correlation function,

$$F_{12}(t) = \frac{1}{T_k} \int_{T_k} x_1(t) x_2(\tau + t) dt$$

Where x_1 and x_2 are corresponding to pre and post-compression echo signals, T_k is the length of k^{th} tracing echo segment. In Elastography following correlation coefficient is widely used.

$$c_{12}(m) = \frac{\sum_{n=1}^{N} y_1(n)\, y_2(n+m)}{\sqrt{\sum_{n=1}^{N} y_1^{\,2}(n) \sum_{n=1}^{N} y_2^{\,2}(n+m)}}$$

where $y_1$and y_2 signals are digitized form of $x_1$and x_2,N is the sampling number in the tracking segment T_k.

CNR_e increases with the increase of correlation power in the both cases (smooth splines and 2D plate spline)

6.6 PERFORMANCE COMPARISONS OF THE STRAIN IMAGES ACQUIRED BY SEVERAL TECHNIQUE

The following figure gives us a comparative idea regarding the performance of the 2D plate smoothing spline estimator with the 1D spline the adaptive stretching method. We have applied percentage strain of 1%, 2%, 4% and 8% .We used a standard window length of 2mm and window overlap of 2mm , which is actually same as the window length. We have applied the strain operation on the displacement values and after the smoothing operation we have taken the gradient operation finally. Median filtering was done to make the elastograms smoother. With the lower applied strain they are showing a better result in comparison with the result at higher applied strain. Higher strain introducing unwanted noise and thus as a resultant effect there is introduction of the artifacts degrading the comprehensibility of the malignant targeted lesions with its background. Our experiment with our introduced technique of the 2D spline is quite satisfactory at least compared with the smoothing spline method. But it should be mentioned about the unavoidable trade-off related with this is the manipulation and the calculation time.

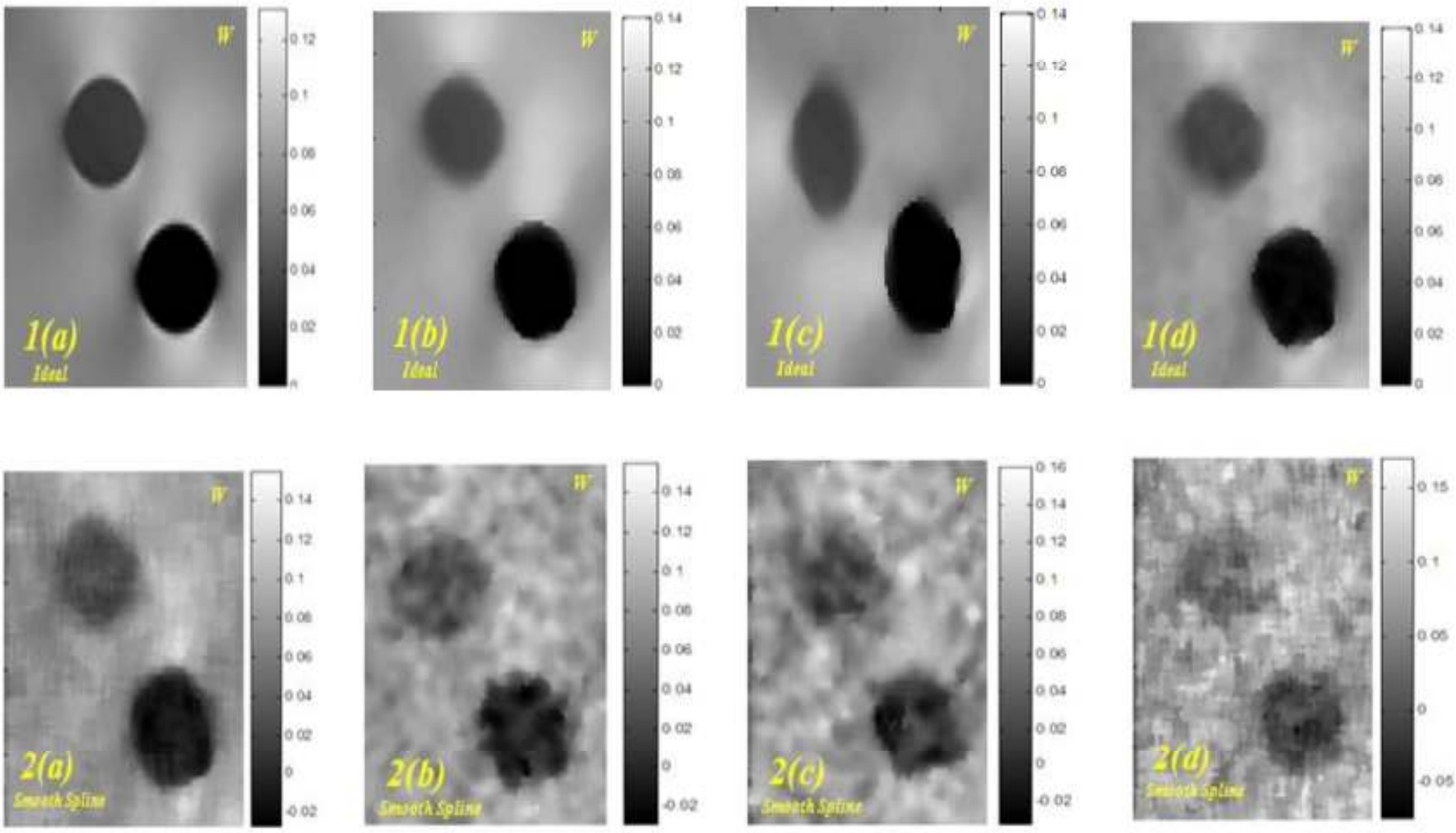

Applied strain, 1% Applied strain, 2% Applied strain, 4% Applied strain, 8%

Figure 6.5: Strain images of the FEM simulation phantom generated by different methods:
1(a)-1(d) are produced using ideal data (Simulated)
2(a)-2(d) are produced by smoothing spline technique
3(a)-3(d) are produced by 2D plate spline technique

6.7 CHAPTER SUMMARY

In this chapter, we have discussed about the variation of SNR_e with varying strain. The change in resolution due to the variation in data window length has been shown. From the plot of SNR_e vs. Strain, we have shown that using 2D plate smoothing spline method at lower strain values yields better resolution in the elastogram while at the same time, maintaining the noise in a reduced level. Effect of smoothing parameter on SNR_e & CNR_e also been incorporated in this chapter. In addition to these, we have discussed about relative comparisons regarding performance of strain images acquired by several techniques.

CHAPTER VII

DISCUSSIONS

7.1 FINDINGS OF THE THESIS

An axial smoothing spline based strain imaging technique was found to be a good estimator of axial strain in ultrasound scans. A technique based on smoothing curve to a set of noisy observations, using a spline function on one dimensional data is developed on 1D data sets. This technique was tested on data sets acquired from 1D scanning of phantom test subjects, and it was found that in most cases the results contained many good images, from which a hard inclusion could be segmented out. A "ghost image" artifact was noted, but it was found that this could be suppressed by applying logarithmic compression to the signal amplitude.

An efficient search algorithm was copied from the work of a leading elastography research group. It was found that considerable speed optimization was possible, so the algorithm operated in genuine real-time. This was made possible because it was found that a high down-sampling factor could be used without seriously reducing the accuracy of the displacement estimation.

Our target was to use 2D RF data and apply thin plate smoothing spline method to have better elastograms. The algorithm was applied to 2D data sets acquired from a rectangular phantom of 20 mm x 20 mm. This phantom was simulated using the software named Algor (Algor, Inc., Pittsburgh, PA) by FEM method. The results were highly promising, with higher performance in the human tissue, which was actually found to have low susceptibility to one of the main sources of error in the phantom scans (dropouts).

Mainly SNR_e and CNR_e have been used to evaluate the performance of the generated elastograms. Result by variation of SNRe with the variation of strain has been incorporated to show the feasibility of 2D plate smoothing spline method. It has shown better performance in the lower strain where in the higher percentage values it is not showing as good performance as the adaptive stretching method. But as we have discussed earlier that adaptive stretching is computation intensive because many iterations may be required at each window location. Again, we also have checked the feasibility of our developed algorithm by comparing with other conventional strain estimators. And 2D plate smoothing spline

produces elastograms with high SNR_e and CNR_e without significant loss of resolution at higher strain than the other strain estimators.

7.2 PROBLEMS FACED

Selecting homogenous area from the region of interest is a very important issue while calculating Elastographic signal-to-noise ratio (SNR_e) and contrast-to-noise ratio (CNR_e). If this selection of homogenous area is wrong then wrong conclusion might be drawn from the graphs. Moreover, one should define the strain value above which a tissue will be considered stiff and below it will be healthy. This setting of strain limit is a vital step and should be done with extra care to get better result. Apart from these, an efficient algorithm for 2D plate smoothing spline based strain estimator was also a difficult job to accomplish. Because it is inherently a problematic task to fit a smoothing curve to a set of noisy observations, applying a thin plate smoothing spline method on two dimensional data. Again, due to higher decorrelation phenomenon, this becomes increasingly difficult at higher percentage of applied strain.

7.3FUTURE WORKS

Some undesired motions always exist in freehand elastography, which cannot be ignored applications and we need robust strain estimators that can estimate in the presence of these decorrelations. 2D spline might be one way to reduce the noise. We have previously discussed to locate a malignant area with a finer accuracy we need to take into account all the directions axial, lateral and elevational. But with freehand scanning there are so many limitations mainly uniform scanning of the portion is not feasible. Here we need more sophisticated setup of the whole ultrasound scanning system which is fully automated by the use of computers. A special design of the ultrasound transducer is also necessary. If we can take in to account the entire dimension axial, lateral and elevational and then apply 2D spline with pairs, after that superimposition of all the combinations are expected to produce better results. In this experiment we have mainly worked on the simulated phantom, but it is possible to extend this research in practical cases. We optimize the whole processing steps and techniques in practical applications such as breast, kidney, prostate, liver etc.

7.4 CONCLUSION

The dreaming of mankind to live longer was definitely indomitable and the history verified the truth. Human civilization experienced lots of technological breakthroughs which changed the world in such a way which was beyond its thinking sometimes with a difference of 10 years hardly. Advancement in Biomedical Engineering to lessen the curse of the age-old killer diseases are worth of mentioning. Cancer is one of those diseases for which human failed to make an impervious shield which was possible in other cases. We dream for a day when all the human diseases will be identified just by the scanning without biopsy even touching the organ. Elastography is not a solution to cure a malignant tumor or a cancerous tissue it emphasizes on the art of its accurate detection. We used a mathematical interpolation technique which utilizes two separate dimensions and then analyzes data according to the algorithm. In the strain imaging technique a trade-off inescapable. If we want to detect a lesion more accurately then the well-established algorithms take are time- consuming calculations. Opposite is also true, the methods which produce quick strain images seems to be misleading with artifacts and the unwanted noises. Though 2D plate spline can be defined in the first category but it has immense possibility for having a improved contrast-to-noise ratio compared to the smoothing spline method. It should be mentioned that resolution is one of the parameters to determine the image quality; it has been found that for accurate detection it is proved that better CNR_e has more potential than the resolution. In this point our method is successful and in future there remains a lot of scope to extend the research for optimizing the time constraint.

BIBLIOGRAPHY

1. Adams, F. (ed.) 1849 The genuine works of Hippocrates. London, UK: Adlard.
2. http://ww2.cancer.org/downloads/STT/CPED2002PWSecured.pdf (Page 25)
3. Iatridis JC, Kumar S, Foster RJ, Weidenbaum M, Mow VC. Shear mechanical properties of human lumbar annulus fibrosus. J Orthop Res. 1999 Sep;17(5):732-7.
4. Fung YC. Biomechanics: Mechanical properties of living tissues, 2nd edition, Springer-Verlag, New York, 1993.
5. Krouskop TA, Wheeler TM, Kallel F, Garra BS, Hall T. Elastic moduli of breast and prostate tissues under compression. Ultrasonic Imaging 20: 260-274, 1998.
6. Miyanaga, N., Akaza, H., Yamakawa, M., Oikawa, T.,Sekido, N., Hinotsu, S., Kawai, K., Shimazui, T. &Shiina, T. 2006 Tissue elasticity imaging for diagnosis of prostate cancer: a preliminary report. Int. J. Urol.13, 1514–1518. (doi:10.1111/j.1442-2042.2006.01612.x)
7. Douglas Christensen, Ultrasonic Bioinstrumentation, John Wiley & Sons, 1988
8. hroy, Jr., Robert E. (1995). "X-Ray equipment". In Bronzino, J.D. The Biomedical Engineering handbook. CRC Press and IEEE Press. pp. 953–960. ISBN 0-8493-8346-3.
9. Herman, Gabor T. (2009). Fundamentals of Computerized Tomography: Image Reconstruction from Projections (2nd ed.). Springer. ISBN 978-1-85233-617-2.
10. Szabo TL. Diagnostic ultrasound imaging: inside out, Acedemic Press, New York, 2004.
11. Hendee, William R; Morgan, Christopher J (1984). "Magnetic Resonance Imaging Part I—Physical Principles". West J Med. 141 (4): 491–500.
12. Kollman C, New sonographic techniques for harmonic imaging – underlying physical principles. Eur J Radiol 64 (2007) 164–72.
13. Tranquart F, Grenier N, Eder V, Pourcelot L. Clinical use of ultrasound tissue harmonic imaging. Ultrasound Med Biol 1999; 6: 889-4.
14. Mark J. Shumate MJ, Kooby DA, Alazraki NP: A Clinician's Guide to Nuclear Oncology: Practical Molecular Imaging and Radionuclide Therapies. Society of Nuclear Medicine, January 2007. ISBN 978-0-9726478-8-5.
15. Ell P, Gambhir S: Nuclear Medicine in Clinical Diagnosis and Treatment. Churchill Livingstone, 2004. (1950 pages). ISBN 978-0-443-07312-0.
16. Céspedes I, Ophir J, Ponnekanti H, Yazdi Y, Li X. Elastography: elasticity imaging using ultrasound with application to muscle and breast in vivo. Ultrasonic Imaging 1993;15:73 88

17. Sarvazyan AP, Rudenko OV, Swanson SD, Fowlkers JB, Emelianov SY. Shear wave elasticity imaging: a new ultrasonic technology of medical diagnostics. Ultrasound Med. Biol. 24: 1419-1435, 1998.

18. Ophir, Jonathan, MD. "New Medical Imaging Technique Improves Chances of Early Cancer Detection." Algor. June 16, 1998. http://www.algor.com/news_pub/cust_app/cancer/cancer.asp

19. "Elastography reduces unnecessary Breast Biopsies." Science Daily. November 30, 2009. http://www.sciencedaily.com/releases/2009/11/091130084716.htm

20. "Elastogram' instantly diagnoses breast cancer." MSNBC.com. Dec. 1, 2006. http://www.msnbc.msn.com/id/15990645/

21. Oestricher H L 1951 Field and impedance of an oscillating sphere in a viscoelastic medium with an application to biophysics J. Acoust. Soc. Am. 23 707–14

22. Dickinson R J and Hill C R 1982 Measurement of soft tissue motions using correlation between A-scans Ultrasound Med. Biol. 8 263–71

23. Birnholz J C and Farrell E E 1985 Fetal lung development: compressibility as a measure of maturity Radiology 157 495–8

24. Krouskop T A, Dougherty D R and Levinson S F 1987 A pulsed Doppler ultrasonic system for making noninvasive measurements of the mechanical properties of soft tissues J. Rehabil. Res. Biol. 24 1–8

25. Lerner R M and Parker K J 1987 Sonoelasticity images derived from ultrasound signals in mechanically vibrated targets Proc. 7th European Communities Workshop (Oct 1987, Nijmegen, The Netherlands)

26. Ophir J, Cespedes I, Ponnekanti H, Yazdi Y and Li X 1991 Elastography: a quantitative method for imaging the elasticity of biological tissues Ultrason. Imaging 13 111–34

27. Parker KJ, Fu D, Graceswki SM, Yeung F, Levinson SF, "Vibration sonoelastography and the detectability of lesions," Ultrasound Med Biol, 1998 Nov;24(9):1437-47.

28. K.J. Parker, M.M. Doyley, and D.J. Rubens, "Imaging the elastic properties of tissue: the 20 year perspective," Physics in Medicine and Biology, vol. 56, 2011, pp. R1-R29.

29. Moran PR, "A flow velocity zeugmatographic interlace for NMR imaging in humans," MagnReson Imaging. 1982; 1(4):197-203.

30. Dijk P Van. Direct cardiac NMR imaging of heart wall and blood flow velocity. J Comput Assist Tomogr. 1984 Jun; 8(3) :429-36

31. Lewa CJ, De Certaines JD. Viscoelastic property detection by elastic displacement NMR measurements. J MagnReson Imaging. 1996 Jul-Aug; 6(4):652-6

32. Muthupillai R, Lomas D J, Rossman P J, Greenleaf J F, Manduca A and Ehman R L 1995 Magnetic resonance elastography by direct visualization of propagating acoustic strain waves Science 269 1854–7

33. Nightingale K R, Palmeri M L, Nightingale R W and Trahey G E 2001 On the feasibility of remote palpation using acoustic radiation force J. Acoust. Soc. Am. 110 625–34

34. Schmitt J M 1998 OCT elastography: imaging microscopic deformation and strain of tissue Opt. Express 3 199–211

35. Fung YC. Biomechanics: Mechanical properties of living tissues, 2nd edition, Springer-Verlag, New York, 1993.

36. Fung YCB. Elasticity of soft tissues in simple elongation. American J. Physiology 213(6): 1532-1544, 1967.

37. Krouskop TA, Wheeler TM, Kallel F, Garra BS, Hall T. Elastic moduli of breast and prostate tissues under compression. Ultrasonic Imaging 20: 260-274, 1998

38. Mridha M, Ödman S. Characterization of subcutaneous edema by mechanical impedance measurements. J. Invest. Dermatology 85(5): 575-578, 1985.

39. Chou PCC, Pagano NJ. Elasticity: Tensor, dyadic and engineering approaches, Dover, New York, 1967.

40. Levinson SF. Ultrasound propagation in anisotropic soft tissue: the application of linearelastic theory. J. Biomech. 20: 251-260, 1987.

41. Truong XT, Jarrett SR, Rippel DV. Longitudinal pulse propagation characteristics in striated muscle. J. Acoust. Soc. Am. 64(5): 1298-1302, 1978.

42. Timoshenko SP, Goodier JN. Theory of elasticity, 3rd edition, McGraw-Hill, NewYork, 1970.

43. Parker KJ, Huang SR, Musulin RA, Lerner RM. Tissue response to mechanical vibrations for "sonoelasticity imaging". Ultrasound Med. Biol. 16(3): 241-246, 1990.

44. L. D. Landau & E. M. Lifshitz. Theory of Elasticity, 1st edition, Pergamon Press Ltd. , 1959.

45. Joseph C. Kolecki. An Introduction to Tensors for Students of Physics and Engineering, NASA/TM—2002-211716.

46. Knight MG, de Lacerda LA, Wrobel LC, Henshall JL. Parametric study of the contactstresses around spherical and cylindrical inclusions. Comp. Mat. Science 25: 115-121, 2002.

47. Bilgen M, Insana MF. Elastostatics of a spherical inclusion in homogeneous biological media. Phys. Med. Biol. 43: 1-20, 1998.

48. Hoyt, Spectral Strain Estimation Techniques for Tissue Elasticity Imaging, 2005.

49. Ophir J, Cespedes I, Ponnekanti H, Yazdi Y, Li X. 1991. Elastography: a quantitative method for imaging the elasticity of biolog-icaltissues.Ultrason. Imag.13:111–34

50. Garra BS, Céspedes EI, Ophir J, Spratt SR, Zuurbier RA, Magnant CM, Pennanen MF. Elastography of breast lesions: initial clinical results. Radiology 202: 79-86, 1997.

51. PesaventoA, Lorenz A. Real time strain imaging and in-vivo applications in prostate cancer. Proc. IEEE Ultrason. Sympos. 2: 1647-1652, 2001.

52. Righetti R, Kallel F, Stafford RF, Price RE, Krouskop TA, Hagle JD, Ophir J. Elastographic characterization of HIFU-induced lesions in canine livers. Ultrasound Med. Biol. 25(7): 1099-1113, 1999.

53. Varghese T, Zagzebski JA, Lee FT. Elastographic imaging of thermal lesions in the liver in vivo following radiofrequency ablation: preliminary results. Ultrasound Med. Biol. 28(11): 1467-1473, 2002.

54. Konofagou EE, Harrigan T, Ophir J. Shear strain estimation and lesion mobility assessment in elastography. Ultrasonics 38: 400-404, 2000.

55. Ophir J, Alam SK, Garra B, Kallel F, Konofagou E, Krouskop T, Varghese T. Elastography: ultrasonic estimation and imaging of the elastic properties of tissues. Proc. Instn. Mech. Engrs. 213 Part H: 203-233, 1998.

56. Kellel F, Ophir J. Three-dimensional tissue motion and its effect on image noise in elastography, IEEE Trans. Ultrason. Ferroel. Freq. Cont. 44(6): 1286-1296, 1997.

57. Konofagou EE, Harrigan T, Ophir J. Shear strain estimation and lesion mobility assessment in elastography. Ultrasonics 38: 400-404, 2000.

58. Dickinson RJ, Hill CR. 1982. Measurement of soft tissue motion using correlation between A scans. Ultrasound Med. Biol.8:263–71

59. Wilson LS, Robinson DE. 1982. Ultra-sonic measurement of small displacements and deformations of tissue.Ultrason. Imag. 4:71–82

60. Mai JJ, Insana MF. 2002. Strain imaging of internal deformation. Ultrasound Med. Biol.28:1475–84

61. Bjaerum S, Torp H, Kristoffersen K. 2002. Clutter filters adapted to tissue motion in ultrasound color flow imaging. IEEE Trans. Ultrason. Ferroelec. Freq. Contr.49:693–704

62. Ophir J, Cespedes I, Ponnekanti H, Yazdi Y, Li X. 1991. Elastography: a quantitative method for imaging the elasticity of biolog-icaltissues.Ultrason. Imag.13:111–34

63. Ophir J, Alam SK, Garra B, Kallel F, Konofagou E, Krouskop T, Varghese T. Elastography: ultrasonic estimation and imaging of the elastic properties of tissues. Proc. Instn. Mech. Engrs. 213 Part H: 203-233, 1998.

64. O'Donnell M, Skovoroda AR, Shapo BM, Emelianov SY. Internal displacement and strain imaging using ultrasonic speckle tracking. IEEE Trans. Ultrason. Ferroel. Freq. Cont. 41(3): 314-325, 1994.

65. Céspedes I, Huang Y, Ophir J, Spratt S. Methods for estimation of subsample time delays of digitized echo signals. Ultrasonic Imaging 17: 142-171, 1995.

66. Ponnekanti H, Ophir J, Céspedes I. Axial stress distributions between coaxial compressors in elastography: an analytical model. Ultrasound Med. Biol. 18(8): 667-673, 1992.

67. De Korte CL, Céspedes EI, van der Steen AFW, Pasterkamp G. Intravascular ultrasound elastography: assessment and imaging of elastic properties of diseased arteries and vulnerable plaque. European J. Ultrasound 7(3): 219-224, 1998.

68. Kellel F, Ophir J. Three-dimensional tissue motion and its effect on image noise in elastography, IEEE Trans. Ultrason. Ferroel. Freq. Cont. 44(6): 1286-1296, 1997.

69. Varghese T, Ophir J. Characterization of elastographic noise using the envelope of echo signals. Ultrasound Med. Biol. 24(4): 543-555, 1998.

70. Bamber JC, Bush NL. Freehand elasticity imaging using speckle decorrelation rate. Acoustical Imaging 22: 285-292, 1996.

71. Talhami HE, Wilson LS, Neale ML. Spectral tissue strain: a new technique for imaging tissue strain using intravascular ultrasound. Ultrasound Med. Biol. 20(8): 759-772, 1994.

72. Konofagou EE, Varghese T, Ophir J, Alam SK. Power spectral strain estimators in elastography. Ultrasound Med. Biol. 25(7): 1115-1129, 1999.

73. Hoyt K, Forsberg F, Ophir J. Investigation of parametric spectral estimation techniques for elasticity imaging. Ultrasound Med. Biol. (In press), 2005a.

74. Oppenheim AV, Willsky AS. Signals and systems, 2nd edition, Prentice Hall, New Jersey, 1997.

75. Kremkau FW, Diagnostic ultrasound: principles and instruments, 6th edition, Saunder, Pennsylvannia, 2002.

76. Lerner RM, Huang SR, Parker KJ. "Sonoelasticity" images derived from ultrasound signals in mechanically vibrated tissues. Ultrasound Med. Biol. 16(3): 231-239, 1990.

77. Huang SR, Lerner RM, Parker KJ. On estimating the amplitude of harmonic vibration from the Doppler spectrum of reflected signals. J. Acoust Soc. Am. 88(6): 2702-2712,1990.

78. Parker KJ, Huang SR, Musulin RA, Lerner RM. Tissue response to mechanical vibrations for "sonoelasticity imaging". Ultrasound Med. Biol. 16(3): 241-246, 1990.

79. Parker KJ, Fu Dongshan, Gracewski SM, Yeung F, Levinson SF. Vibration sonoelastography and the detectability of lesions. Ultrasound Med. Biol. 24(9): 1437-1447, 1998.

80. Rudenko OV, Sarvazyan AP, Emelianov SY. Acoustic radiation force and streaming induced by focused nonlinear ultrasound in a dissipative medium. J. Acoust. Soc. Am. 99(5): 2791-2798, 1996.

81. Sarvazyan AP, Rudenko OV, Swanson SD, Fowlkers JB, Emelianov SY. Shear wave elasticity imaging: a new ultrasonic technology of medical diagnostics. Ultrasound Med. Biol. 24: 1419-1435, 1998.

82. Fatemi M, Greenleaf JF. Ultrasound-stimulated vibro-acoustic spectrography. Science 280: 82 85, 1998.

83. R.F. Wagner, M.F. Insana and D.G. Brown, "Statistical propertiesof radio-frequency and envelope-detected signals with applications to medical ultrasound," J. Opt. Soc. Am. A, Vol. 4, No. 5, May 1987.

84. Ruey J. Sung and Michael R. Lauer (2000). Fundamental approaches to the management of cardiac arrhythmias. Springer. p. 153. ISBN 978-0-7923-6559-4.

85. Melvin A. Shiffman, Sid J. Mirrafati, Samuel M. Lam and Chelso G. Cueteaux (2007). Simplifie Facial Rejuvenation. Springer. p. 157. ISBN 978-3-540-71096-7.

86. C. Ifeachor& W. Jervis. Digital Signal Processing A practical Approach, 1st edition, Addison-Wesley Publishers Ltd., 1993.

87. S. Kaisar Alam and J. Ophir. Reduction of Signal Decorrelation from Mechanical Compression of Tissues by Temporal Stretching: Applications to Elastography. Ultrasound in Med. & Biol., Vol. 23, No. 1 pp. 95-105, 1997.

88. Céspedes I, J. Ophir & S. Kaisar Alam. The Combined Effect of Signal Decorrelation and Random Noise On The Variance of Time Delay Estimation. IEEE Transactions on Ultrasonics, Ferroelectrics & Frequency Control, Vol. 44, No. 1, January 1997.

89. Alam S.K., Ophir J., Céspedes I., Varghese T., A deconvolution filter for improvement of time-delay estimation in elastography, IEEE Trans. Ultrason. Ferroel. Freq. Cont. 45 (6) (1998) 1565–1572

90. Céspedes I., Ophir J., Reduction of image noise in elastography, Ultrasonic Imag. 15 (2) (1993) 89–102.

91. Alam S.K., Ophir J., Reduction of signal decorrelation from mechanical compression of tissues by temporal stretching: applications to elastography, Ultrasound Med. Biol. 23 (1997) 95–105.

92. Alam S.K., Ophir J., Konofagou E.E., An adaptive strain estimator for Elastography, IEEE Trans. Ultrason. Ferroelec. Freq. Cont. 45 (1998) 461–472.

93. Ophir J. Céspedes I. Ponnekanti H. Yazdi Y. Li X. Elastography: a quantitative method for imaging the elasticity of biological tissues. Ultrasonic Imaging 1991; 13:111–134. [PubMed: 1858217]

94. Céspedes I. Huang Y. Ophir J. Spratt S. Methods for estimation of subsample time delays of digitized echo signals. Ultrasonic Imaging 1995; 17:142–171. [PubMed: 7571208]

95. Zhu Y. Hall T.J. A modified block matching method for real-time freehand strain imaging. Ultrasonic Imaging 2002; 24:161–176. [PubMed: 12503771]

96. A. H. Gee, R. W. Prager, G. M. Treece, and L. Berman. Engineering a freehand 3D ultrasound system. Pattern Recognition Letters, 24(4–5):757–777, 2003.

97. J. E. Lindop, G. M. Treece, A. H. Gee, and R. W. Prager. 3D elastography using freehand ultrasound. Ultrasound in Medicine and Biology, 32(4):529–545, April 2006.

98. Walker, C.L., et. al. "Magnetic resonance imaging of ultrasonic fields." Ultrasound in Medicine & Biology, 1998. 24(1): p. 137-42.

99. Kruse, S.A., et al. "Tissue characterization using magnetic resonance elastography: preliminary results." Physics in Medicine and Biology, 2000. 45: p. 1579-1590.

100. Bhutani MS, et al. A comparison of the accuracy of echo features during endoscopic ultrasound (EUS) and EUS-guided fine-needle aspiration for diagnosis of malignant lymph node invasion. GastrointestEndosc, 1997; 45(6):474-479.

101. Lindop, J. E., Treece, G. M., Gee, A. H., Prager, R. W., 2007a. Estimation of displacement location for enhanced strain imaging. In press for IEEE Transactions on Ultrasonics, Ferroelectrics and Frequency Control.

102. Lindop, J. E., Treece, G. M., Gee, A. H., Prager, R. W. "An intelligent interface for freehand strain imaging". Tech. Rep. CUED/F-INFENG/TR 578, Cambridge University Department of Engineering.

103. D'hooge, J., Bijnens, B., Thoen, J., Van de Werf, F., Sutherland, G. R. &Suetens, P. 2002 Echocardiographic strain and strain-rate imaging: a new tool to study regional myocardial function. IEEE Trans. Med. Imag. 21, 1022–1030. (doi:10.1109/TMI.2002.804440)

104. Muthupillai, R., Lomas, D. J., Rossman, P. J., Greenleaf, J. F., Manduca, A. &Ehman, R. 1995 Magnetic resonance elastography by direct visualization of propagating acoustic strain waves. Science 269, 1854–1857.

105. S. Diridollou, M. Berson, V. Vabre, D. Black, B. Karlsson, F. Auriol, J. M. Gregoire, C. Yvon, L. Vaillant, Y. Gall, and F. Patat, "An in vivo method for measuring the mechanical properties of the skin using ultrasound," Ultrasound Med. Biol., vol. 24, no. 25, pp. 215–224, 1998.

106. S. Diridollou, F. Patat, F. Gens, L. Vaillant, D. Black, J. M. Lagarde, Y. Gall, and M. Berson, "In vivo model of the mechanical properties of the human skin under suction," Skin Res. Technol., vol. 6, no. 4, pp. 214–221, 2000.

107. L. Pan, L. Zan, and F. S. Foster, "In vivo high frequency ultrasound assessment of skin elasticity," in Proc. IEEE Ultrason. Symp., 1997, pp. 1087–1091.

108. P. Altmeyer, S. el-Gammal, and K. Hoffmann, Eds. Ultrasound in Dermatology. Berlin: Springer, 1992.

109. R. C. Chan, A. H. Chau, W. C. Karl, S. Nadkarni, A. S. Khalil, N. Iftimia, M. Shishkov, G. J. Tearney, M. R. Kaazempur-Mofrad, B. E. Bouma, "OCT-based arterial elastography: Robust estimation exploiting tissue biomechanics," Opt. Express 12, 4558–4572 (2004).

110. J. Rogowska, N. A. Patel, J. G. Fujimoto, M. E. Brezinski, "Optical coherence tomographic elastography technique for measuring deformation and strain of atherosclerotic tissues," Heart 90, 556–562 (2004).

111. H. J. Ko,W. Tan, R. Stack, S. A. Boppart, "Optical coherence elastography of engineered and developing tissue," Tissue Eng. 12, 63–73 (2006).

112. Cespedes I, Ophir J. Reduction of image noise in elastography. Ultrason. Imaging 1993;15:89–102.

113. P. Chaturvedi, M. F. Insana, and T. J. Hall. 2-D companding for noise-reduction in strain imaging. IEEE Transactions on Ultrasonics, Ferroelectrics, and Frequency Control, 45(1):179–191, January 1998.

114. S. K. Alam and J. Ophir, "Reduction of signal decorrelation from mechanical compression of tissues by temporal stretching: applications to elastography," Ultrason. Med. Biol., vol. 23, pp. 95-105, 1997.

115. Angelsen, Bjørn A.J. & Hans G. Torp (2000), Forelesningsnotater TTK4160/TTK4165, NTNU

116. Krouskop TA, Wheeler TM, Kallel F, et al. Elastic moduli of breast and prostate tissues under compression, Ultrasonic Imaging. 20, 260-274 (1998).